# A Comparison of Mitochondrial Heat Shock Protein 70 and Hsp70 Escort Protein 1 Orthologues from *Trypanosoma brucei* and *Homo sapiens*

By

Francis B. Hand

A THESIS

Submitted in fulfilment of the requirements for the degree of

MASTER OF SCIENCE

RHODES UNIVERSITY

November 2022

# Table of Contents

# List of Figures

# List of Tables

# Acknowledgements

I would like to acknowledge and give my heartfelt thanks to my supervisor Professor Boshoff whose guidance and support made this work possible. Her assistance was imperative during the trying times that this research was undertaken in.

I would also like to give my undying thanks to my parents for their continuous support and understanding throughout the duration of the research.

Finally, I would like to thank Tazmin, her constant support and drive throughout this period gave me the impetuous to keep going in these trying times. I adore you.

# List of Abbreviations

| Abbreviation | Full name |
|---|---|
| % | Percentage |
| ~ | Approximately |
| µg | Micrograms |
| µl | Microlitre |
| µM | MicroMolar |
| A | Absorbance |
| *A. thaliana* | *Arabidopsis thaliana* |
| $A_{595}$ | Absorbance at 595 nm |
| $A_{600}$ | Absorbance at 600 nm |
| AAT | Animal African Trypanosomiasis |
| AD | Alzheimer's disease |
| ADP | Adenosine diphosphate |
| APS | Ammonium persulphate |
| ATP | Adenosine triphosphate |
| BLAST | Basic Local Alignment Search Tool |
| Bp | Base pairs |
| BSA | Bovine serum albumin |
| BSF | Bloodstream form |
| ℃ | Degree Celsius |

| | |
|---|---|
| *C. reinhardtii* | *Chlamydomonas reinhardtii* |
| CD | Circular dichroism |
| CNS | Central nervous system |
| Da | Daltons |
| DMSO | Dimethyl sulfoxide |
| DNA | Deoxyribonucleic Acid |
| DnaK | Prokaryotic Hsp70 |
| DTT | Dithiothreitol |
| *E. coli* | *Escherichia coli* |
| EDTA | Ethylene diamine tetra-acetic acid |
| EEVD motif | Glutamate-Glutamate-Valine-Aspartate (Glu-Glu-Val-Asp) motif |
| ER | Endoplasmic Reticulum |
| G | Grams |
| *G* | Gravitational force |
| G/F rich region | Glycine-phenylalanine rich region |
| g/mol | Grams per mole |
| gHAT | *T. b. gambiense* Human African Trypanosomiasis |
| *H. sapiens* | *Homo sapiens* |
| HAT | Human African Trypanosomiasis |
| HCl | Hydrochloric acid |
| Hep1 | Hsp70 escort protein 1 |
| His-Tag | Histidine-tag (6x) |

| | |
|---|---|
| HPD motif | Histidine-proline-aspartic acid motif |
| HPLC | High-performance liquid chromatography |
| Hr(s) | Hour(s) |
| HRP | Horse radish peroxidase |
| Hsp | Heat shock protein |
| Hsp110 | Heat shock protein (110 kDa) |
| Hsp70 | Heat shock protein (70 kDa) |
| IPTG | Isopropyl-β-D-thiogalactopyranoside |
| ITC | Isothermal titration calorimetry |
| JDP(s) | J-domain containing protein(s) |
| $Kan^R$ | Kanamycin resistance gene |
| Kbp | Kilo base pairs |
| kDa | Kilo Daltons |
| *L. braziliensus* | *Leishmania braziliensus* |
| M | Molar |
| MDH | Malate dehydrogenase |
| MEGA | Molecular Evolutionary Genetic Analysis |
| Mg | Miligram |
| $MgCl_2$ | Magnesium chloride |
| Min(s) | Minute(s) |
| MMPT | Mitochondrial membrane permeability transition pore |
| MSA | Multiple sequence alignment |

| | |
|---|---|
| mtDNA | Mitochondrial DNA |
| mtHsp70 | Mitochondrial Hsp70 |
| NaCl | Sodium chloride |
| NBD | Nucleotide binding domain |
| NCBI | National Center for Biotechnology Information |
| NEF | Nucleotide exchange factor |
| NMR | Nuclear magnetic resonance |
| NTD | Neglected tropical diseases |
| OD | Optical density |
| P | Proline |
| PAM | Presequence translocase-associated motor |
| PBS | Phosphate buffered saline |
| PD | Parkinson's Disease |
| Pf | *P. falciparum* |
| PfHep1 | *P. falciparum* Hsp70 escort protein 1 |
| PI3K | Phosphatidylinositol 3-kinase |
| PMSF | Phenylmethylsulfonyl fluoride |
| PQC | Protein quality control system |
| rHAT | *T. b. rhodesiense* Human African Trypanosomiasis |
| RNS | Reactive nitrogen species |
| ROS | Reactive oxygen species |
| RT | Room temperature |

| | |
|---|---|
| *S. cerevisiae* | Saccharomyces cerevisiae (Yeast) |
| SBD | Substrate binding domain |
| SDS | Sodium Dodecyl Sulphate |
| SDS-PAGE | Sodium Dodecyl Sulphate - Polyacrylamide Gel Electrophoresis |
| SIF | Stumpy induction factor |
| SMART | Simple Modular Architecture Research Tool |
| SSU-rRNA | Small subunit ribosomal ribonucleic acid |
| *T. b. brucei* | *Trypanosoma brucei brucei* |
| *T. b. gambiense* | *Trypanosoma brucei gambiense* |
| *T. b. rhodesiense* | *Trypanosoma brucei rhodesiense* |
| *T. brucei* | *Trypanosoma brucei* |
| TbHep1 | *T. brucei* Heat shock protein escort protein 1 |
| TbHsp | *Trypanosoma brucei* Heat shock protein |
| TbmtHsp | *Trypanosoma brucei* mitochondrial Heat shock protein |
| TBS | Tris-buffered saline |
| TBS-T | Tris-buffered saline with Tween |
| TEMED | N,N,N,N-tetramethylene diamine |
| TIM | Translocase of the inner membrane |
| V | Volts |
| v/v | Volume per volume |
| VDAC | Voltage-dependent anion channel |
| VSG(s) | Variable surface glycoprotein(s) |

| | |
|---|---|
| w/v | Weight per volume |
| WHO | World Health Organization |
| YT | Yeast Tryptone media |
| zf-DNL | Zinc-finger domain |
| ZR | Zinc ribbon protein |
| A | Alpha |
| Aβ | Amyloid-beta |
| B | Beta |

# Abstract

The causative agent of African trypanosomiasis, *Trypanosoma brucei* (*T. brucei*), has an expanded retinue of specialized heat shock proteins, which have been identified as crucial to the progression of the disease. These play a central role in disease progression and transmission through their involvement in cell-cycle pathways which bring about cell-cycle arrest and differentiation. Hsp70 proteins are essential for the maintenance of proteostasis in the cell. Mitochondrial Hsp70 (mtHsp70) is a highly conserved molecular chaperone required for both the translocation of nuclear encoded proteins across the two mitochondrial membranes and the subsequent folding of proteins in the matrix. The *T. brucei* genome encodes three copies of mtHsp70 which are 100% identical. MtHsp70 self-aggregates, a property unique to this isoform, and an Hsp70 escort protein (Hep1) is required to maintain the molecular chaperone in a soluble, functional state. This study aimed to compare the solubilizing interaction of Hep1 from *T. brucei* and *Homo sapiens* (*H. sapien*). The recently introduced Alphafold program was used to analyze the structures of mtHsp70 and Hep1 proteins and allowed observations of structures unavailable to other modelling techniques. The GVFEV motif found in the ATPase domain of mtHsp70s interacted with the linker region, resulting in aggregation, the Alphafold models produced indicated that the replacement of the lysine (K) residue within the KTFEV motif of DnaK (prokaryotic Hsp70) with Glycine (G), may abrogate bond formation between the motif and a region between lobe I and II of the ATPase domain. This may facilitate the aggregation reaction of mtHsp70 orthologues and provides a residue of interest for future studies. Both TbHep1 and HsHep1 reduced the thermal aggregation of TbmtHsp70 and mortalin (*H. sapien* mtHsp70) respectively, however, TbHep1 was ~ 15 % less effective than HsHep1 at higher concentrations (4 uM). TbHep1 itself appeared to be aggregation-prone when under conditions of thermal stress, Alphafold models suggest this may be due to an N-terminal α-helical structure not present in HsHep1. These results indicate that TbHep1 is functionally similar to HsHep1, however, the orthologue may operate in a unique manner which requires further investigation.

# Chapter 1: Literature Review

## 1.1 Molecular chaperones

Folding newly synthesized proteins from the nascent polypeptide form into the native conformation is imperative for a protein to attain functionality (Lumry & Eyring, 1954). However, when being extruded from a ribosome into the cellular environment, a nascent polypeptide is subject to an unstable environment with high concentrations of nascent preproteins, biomolecules and other interfering factors that can deleteriously alter the folding process, leading to the misfolding of proteins and the generation of protein aggregates (Ellis, 2001). This is particularly important when producing organelle proteins exposed to these conditions upon extrusion from the ribosome, as these require transport to their respective compartments in an unfolded form to allow translocation across membranes (Dierks et al., 1993). To allow the correct folding of nascent proteins, the actions of molecular chaperones are often required (Ellis, 1987); these proteins act as catalysts in the folding process, protecting the vulnerable preproteins from the cellular environment and facilitating the correct folding without being incorporated into the final protein product (Hartl, 1996).

The molecular chaperone family predominantly consists of heat shock proteins (Hsps), with a litany of Hsp subfamilies being classified based on structure, function, and expression (Craig & Schlesinger, 1985). The Hsp subfamilies are varied in their operations, with many acting directly as chaperones while others work as co-chaperones, assisting the functions of other chaperones (Balch et al., 2008). These are considered vital to maintaining proteostasis within the cell (Powers et al., 2009), and were termed Hsps due to the discovery of these genes via the induction of expression in response to heat shock within the salivary glands of *Drosophila* and the subsequent identification of the protein products (Ritossa, 1962; Tissiéres et al., 1974). Mammalian Hsps have been divided into different subfamilies based on domains and functions, including: HSPC (Hsp90), JDP (Hsp40/DNAJ), HSPH (Hsp110), HSPA (Hsp70), HSPD/E (Hsp60/chaperonin) and HSPB (small Hsps) (Kampinga et al., 2009). Attention has been directed towards the activities of the largest

subfamily, Hsp70, due to the importance of the subfamily in many pathways and processes that play direct roles in cell functioning and disease development.

## 1.2 The Hsp70 family

The Hsp70 family has high evolutionary conservation and displays great ubiquity, with orthologues being found in every organism currently studied and isoforms within all major cellular compartments (Rohde et al., 2005; Daugaard et al., 2007). The functions of Hsp70 are numerous and varied; however, the most prevalent functions include folding proteins, the repair of misfolded proteins, the disassembly of aggregates, and the designation of irreparable proteins towards proteolytic degradation, as well as intracellular transport and translocation across membranes (Mayer & Bukau, 2005). These varied activities are accommodated by the formation of complexes with other chaperones, the actions of co-chaperones and the use of short hydrophobic stretches as target motifs which allows Hsp70 to interact with a variety of different targets (Rüdiger et al., 1997; van den Ussel et al., 1999; Czarnecka et al., 2006). The Hsp70 chaperone system is responsible for an estimated 10 – 20 % of all protein folding in prokaryotes, where it is referred to a DnaK and 20 – 30 % within eukaryotic cells (Bukau et al., 2000).

### 1.2.1 The structure of Hsp70

The structure of the highly conserved Hsp70 consists of an N-terminal nucleotide-binding domain (NBD) (~ 44 kDa) followed by a short, conserved linker region. This is followed by the C-terminal substrate binding domain (SBD) divided into the β-sandwich peptide binding subdomain (SBDβ) (~18 kDa), consisting of two pairs of parallel β-sheets localized around the peptide binding pocket followed by the variable α-helical subdomain (SBDα) (~10 kDa), known as the lid, which covers the SBDβ (Flaherty et al., 1990; Zhu et al., 1996; Bertelsen et al., 2009).

The NBD consists of two lobes known as lobes I and II with a distinct cleft separating the two; these are further divided into four subdomains: Ia, Ib and IIa, IIb; these subdomains are located around the central binding pocket with the bound nucleotide forming a complex with contacts on every subdomain (Figure 1.1) (Flaherty et al., 1990). The structure of the NBD is highly flexible, and the operations involve tilting a subdomain and shearing action between lobes to disrupt the bound nucleotide and transmit binding signals (Liu et al., 2010; General et al., 2014). However, this flexibility is often restricted by the SBD, and an allosteric mechanism is required to bring about efficient NBD subdomain movement and activity (Kityk et al., 2015).

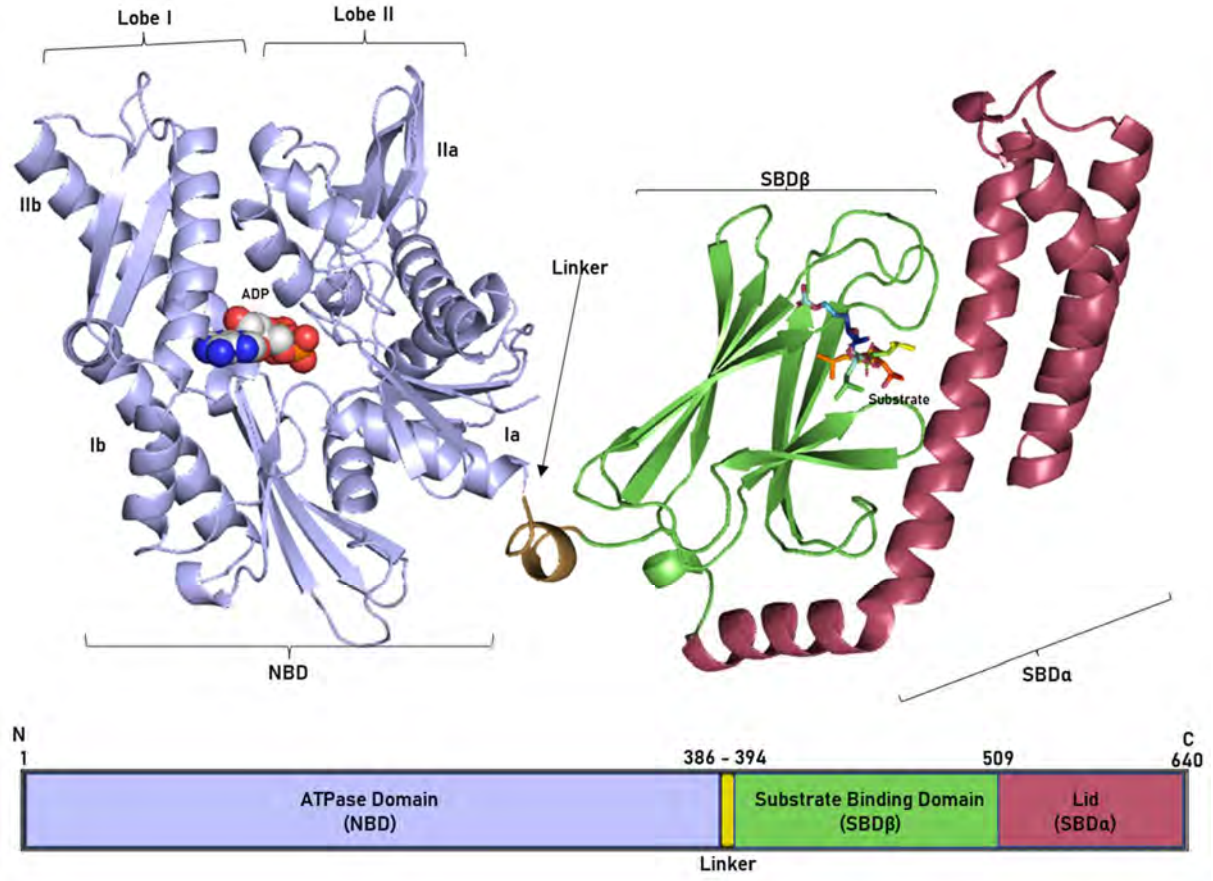


Figure 1.1: The structure of human cytosolic Hsp70: (A) The structure of Hsp70 with ADP bound in the NBD (Light blue) (3AY9) and the subdomains indicated. The SBD domain (2KHO) is indicated with the SBDβ binding domain (green) containing a sample peptide and the SBDα lid indicated (maroon). The two domains are connected by the linker region displayed in brown. (B) The schematic diagram of Hsp70 with the domains displayed in a similar colour to the model apart from the linker region which is yellow.

The C-terminal SBD consists of two subdomains, the SBDβ (~ 18 kDa) followed by the SBDα (~ 10 kDa), referred to as the lid (Figure 1.1). The SBDβ consists of two β-sheet regions arranged

parallel to one another which form the peptide binding pocket (Zhu et al., 1996). This subdomain is not only responsible for peptide binding but is also crucial to interdomain communication and co-chaperone interaction (Bukau & Horwich, 1998). The SBDα is primarily involved in substrate trapping and release in response to nucleotide cycling (Moro et al., 2003; Qi et al., 2013). The Hsp70s found in the cytosol of eukaryotes have an EEVD motif at the C-terminus which is required for co-chaperone interactions (Freeman et al., 1995). However, the structure and function of the SBDα is highly variable depending on the Hsp70, with DnaK exhibiting a significantly diminished functional role of the SBDα (Zhu et al., 1996). The SBDα tends to consist primarily of α-helices with some isoforms introducing a 'hinge' loop structure which causes the SBDα to fold, allowing for increased substrate trapping (Zhang et al., 2014).

The structure of Hsp70 makes it highly versatile and capable of carrying out several different functions with a wide range of substrates. It achieves this using an allosteric mechanism centred around nucleotide cycling and interdomain communication (Buchberger et al., 1995). However, the basal catalytic rate of Hsp70 is low (Schmid et al., 1994), and for it to achieve a viable catalytic rate, the actions of co-chaperones are required (Liberek et al., 1991).

### 1.2.2 Hsp70 Co-chaperones

There are a wide range of Hsp70 co-chaperones that differ depending on the Hsp70 homologue, the cellular localization and the operation being performed. The two families of co-chaperones that are crucial to Hsp70 operations and have the most influence over the catalytic cycle are known as J-domain containing proteins (JDPs) which stimulate the NBD, allowing for rapid ATP hydrolysis and nucleotide exchange factors (NEFs) which are responsible for the subsequent dissociation of ADP, and in some cases the reintroduction of ATP (Liberek et al., 1991).

**J-domain containing proteins**

J-domain containing proteins (JDPs) are also known as J-proteins or Hsp40s. JDPs are defined by the presence of a J-domain, a highly conserved, "J" shaped domain consisting of four α-helices

which contain a histidine-proline-aspartate (HPD) motif required to stimulate the ATPase activity of Hsp70 (Pellecchia et al., 1996; Cheetham & Caplan, 1998). The co-chaperoning activities of JDPs play a role in the determination of the cellular function to be carried out by the Hsp70 via the delivery of the substrate to the SBD as well as the subsequent mediation of substrate specificity through the stimulation of the NBD (Kampinga & Craig, 2010). JDPs can also act independently of Hsp70 and have functions such as holdase activities and protein transportation (Dekker et al., 2015).

The JDP family is large and has been divided into four subtypes based on their structural layout. Type I JDPs contain an N-terminal J-domain followed by a glycine and phenylalanine (G/F) rich domain, a zinc-finger (zf-DNL) domain and finally a variable C-terminal. Type II JDPs lack the zinc-finger domain but maintain the type-I structure. The type I and II proteins can bind substrates, facilitating an increase in Hsp70 activity via substrate delivery and stimulation of the NBD (Walsh et al., 2004; Hennessy et al., 2005). However, type I and II JDPs have differences in structure and can vary considerably in function (Langer et al., 1992; Lu & Cyr, 1998; Fan et al., 2004). Type III JDPs have a J-domain that is not located on the N-terminal and can be found anywhere in the sequence. This leads to substantial differences in structure within this type and a high level of specialization (Cheetham & Caplan, 1998). Finally, Type IV JDPs are defined by the presence of a J-domain with an altered HPD motif (Botha et al., 2007). Due to the lack of this motif, type-IV JDPs may operate via a unique mechanism of action and with different proteins relative to other JDPs (Tsai & Douglas, 1996; Botha et al., 2007). Due to the large number of JDPs and the diversity of their structures, it is theorized that there are multiple mechanisms of action however most studies have described the DnaK – DnaJ interaction from *E. coli* (Kityk et al., 2018).

**Nucleotide Exchange Factors**

Nucleotide exchange factors (NEFs) are more varied in structure and mechanism than JDPs. Rather than a single conserved domain being a defining feature, NEFs are defined by their function in allowing ADP or GDP dissociation (Goody & Hofmann-Goody, 2002), with several domains being identified as capable of imparting this ability. NEFs are therefore placed into types depending on the domain used; these are known as Bag-domain proteins, Grp170s and Sil1 proteins with organelles like chloroplasts and mitochondria having NEF proteins which resemble the GrpE NEF

found within prokaryotes (Bracher & Verghese, 2015). Of these, the DnaK-GrpE interaction from *E. coli* is the most well documented.

The structure of a GrpE-like NEF consists of a short, disordered N-terminal followed by one long and one short α-helix stretch, encompassing most of the structure with the C-terminal end consisting of a small β-sheet domain. These operate as long dimers in which the two pairs of α-helices are arranged into two parallel lines with the β-sheet domains protruding from either side (Harrison et al., 1997). The dimerized structure is necessary for binding as GrpE cannot operate in monomer form although only one β-sheet domain is used in the interaction with DnaK (Wu et al., 1996; Harrison, 2003). GrpE returns to monomer form under stressful cellular conditions, and it has been hypothesized that this occurs to allow for an increase in Hsp70-substrate complexes and the sequestering of a more significant number of vulnerable preproteins (Harrison, 2003; Bracher & Verghese, 2015).

### 1.2.3 Hsp70 Catalytic Cycle

The catalytic cycle of Hsp70 operates using an allosteric mechanism in which the enzyme shifts between two states; the first is an open state in which ATP is bound, and peptide substrates may interact with the SBD; however, affinity is low, and these interactions are transient. The closed state occurs when ADP is bound in the NBD, this state has high substrate affinity, and any bound peptide is tightly enclosed within the SBD (Bukau & Horwich, 1998). Basal Hsp70 catalytic rates are significantly low, and the JDPs and NEFs facilitate ATP hydrolysis and ADP dissociation, respectively, to maintain a viable rate (Figure 1.2) (Liberek et al., 1991; McCarty et al., 1995).

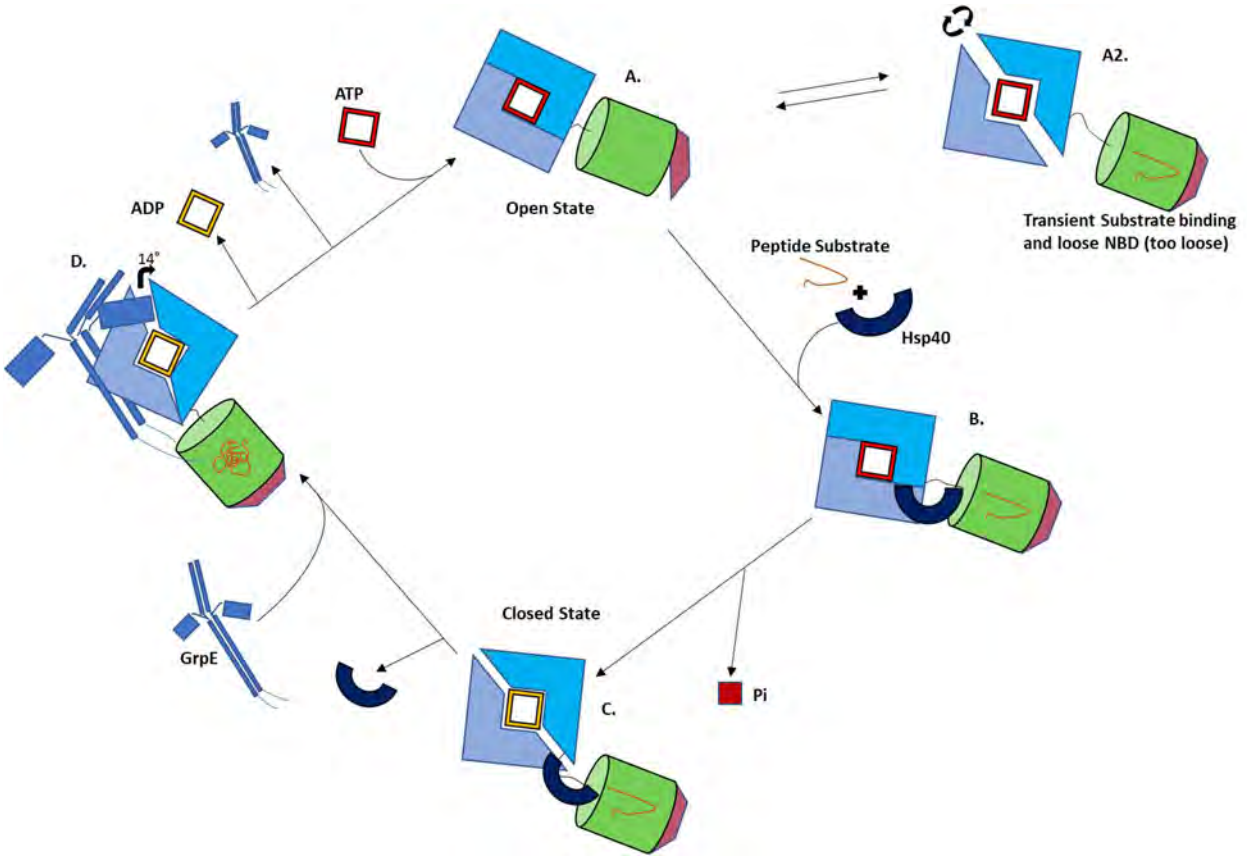


Figure 1.2: The catalytic cycle of Hsp70: (A) The open state of Hsp70 with ATP (Red) bound in the NBD (Blue) and the SBDβ (Green) and SBDα (Pink) docked to the NBD. (A.2) Hsp70 with ATP bound in the NBD and a substrate transiently bound in the SBD, which is undocked but loosely connected to the NBD, preventing efficient ATP hydrolysis. (B) Hsp70 with ATP bound in the NBD and both a JDP and substrate bound, immediately prior to ATP hydrolysis. (C) Hsp70 in a closed state with ADP bound in the NBD and a peptide substrate locked into the SBD. (D) Hsp70 in a closed state with GrpE bound, immediately prior to the release of ADP and the folded peptide product.

The catalytic cycle of Hsp70 begins in the open state with ATP bound in the NBD and no peptide substrate within the SBD (Figure 1.2). In this state, ATP forms a complex with two $K^+$ ions and one $Mg^{2+}$ ion in the lower portion of the NBD binding site (Flaherty et al., 1990). While the NBD has a highly flexible structure, the binding of ATP causes the lobes to rotate into a position incompatible with γ-phosphate cleavage and the SBDβ docks to the NBD; this prevents the lobes from rotating, arresting movement and effectively locking the nucleotide in place (Kityk et al., 2012). In this open state, the NBD is tightly closed; however, the SBD can transiently interact with peptide substrates. If this occurs, the SBDβ dissociates and allows NBD lobe rotation, this can result in ATP hydrolysis; however, the binding sites are inopportunely placed, and the interactions are short, resulting in a relatively small increase in the rate of ATP hydrolysis of approximately 10-fold (Figure 1.2.A2). A

JDP is required to provide the interdomain communication necessary to facilitate efficient ATP hydrolysis and substrate trapping (Benaroudj et al., 1996; Karzai & McMacken, 1996).

ATP hydrolysis is initially stimulated by a JDP via the delivery of a peptide substrate to the SBD. Upon substrate delivery, an interface between the JDP C-terminal and the SBDβ is formed. Simultaneously, the highly conserved HPD motif interacts with multiple sites in the linker region of DnaK, and the J-domain interacts with the NBD and SBDβ via an extensive network of interactions (Kityk et al., 2015, 2018). In this way, the JDP stimulates ATP hydrolysis and substrate binding by allowing efficient signal transmission from the SBDβ to the NBD and via the movement of the linker region into the space between NBD lobes. This effectively prevents excessive movement of the NBD subdomains and allows the correct positioning of the catalytic residues (Kityk et al., 2018). This positioning and the J-domain interactions allow for rapid ATP hydrolysis with a JDP and peptide substrate producing catalytic rates approximately 1000-fold greater than the basal rate of Hsp70 (Karzai & McMacken, 1996; Barouch et al., 1997). Upon ATP hydrolysis, the substrate is effectively bound in the SBD binding pocket, the JDP dissociates, and Hsp70 is left in the closed state with ADP bound in the NBD (Figure 1.2.C) (Schmid et al., 1994). The duration of this DnaK-substrate complex varies depending on several factors, such as the function being undertaken and the cellular conditions present (Brehmer et al., 2001; Groemping & Reinstein, 2001).

The dissociation of ADP from DnaK and the reintroduction of ATP to the NBD binding cleft are required to allow product release and a return to the open state. This process varies considerably depending on the Hsp70 and the interacting NEF; in *E. coli*, this process is facilitated by the NEF GrpE (Harrison, 2003). The GrpE dimer allows ADP dissociation by binding across the length of DnaK with the N-terminal regions of GrpE interacting with the SBD domain while the remainder of the structure forms an extensive interface with the NBD (Figure 1.2.D) (Wu et al., 2012). One of the distal β-sheet domains of GrpE is inserted between the IB and IIB subdomains of the NBD, acting as a wedge and bringing about the rotation of the IIB subdomain 14˚ outwards from the binding cleft (Harrison et al., 1997).

This rotation displaces multiple residues previously coordinating ADP within the cleft. This displacement and simultaneous interactions with a hydrophobic patch and salt bridges at the top of the NBD binding cleft open the domain and allow ADP to dissociate (Harrison et al., 1997). ATP is

often in high concentration in the surrounding environment and rapidly associates with the NBD, returning DnaK to the closed state; in *E. coli,* this is facilitated by GrpE in *E. coli*, which remains in the complex until ATP reintroduction (Packschies et al., 1997).

## 1.3 The role of mitochondrial Hsp70

The Hsp70 known to localize to the mitochondrial matrix was first identified in 1993 during rat cell-fusion studies, while searching for markers of mortal and immortal fibroblast cell phenotypes (Wadhwa et al., 1993a). Two isoforms were identified in the study, MOT-1 and MOT-2, with only two amino acid differences within the SBD differentiating the two but a significant difference in activity as the overexpression of MOT-1 induced senescence in NIH3T3 cells while MOT-2 overexpression resulted in the development of malignancy (Kaul et al., 1998; Wadhwa et al., 1999). The name for mtHsp70 found in higher eukaryotes, mortalin, has since been derived from this initial mouse study. Sequencing has shown that the one human mortalin isoform is more closely related to MOT-2 than MOT-1 and exhibited the ability to induce malignancy in cancer cells (Wadhwa et al., 1993b; Kaul et al., 2007).

The translocation of preproteins and their subsequent folding in the mitochondrial matrix is of particular importance, more than 98 % of mitochondrial proteins are encoded within the nucleus, and their translocation and assembly are crucial to mitochondrial viability (Pfanner & Geissler, 2001; Young et al., 2001). Mortalin is primarily involved with the pre-sequence pathway, which is responsible for most free-floating mitochondrial matrix proteins, making up approximately 60 % of all protein imports (Bolender et al., 2008; Wiedemann & Pfanner, 2017). Mortalin is recruited to the translocase of the inner membrane-44 (TIM-44) and operates as part of the PAM complex, facilitating the import of preproteins into the mitochondrial matrix (Neupert & Brunner, 2002). In yeast, a mtHsp70 paralogue Ssc1 operates in concert with the membrane-bound type-III JDP, the translocase of the inner membrane 14 (Tim14) and the NEFs Mge1/Yge1 to facilitate ATP hydrolysis and provide the energy for the translocation of preproteins (Szklarz et al., 2005; Sichting et al., 2005; Blamowska et al., 2010). After translocation, mtHsp70 then facilitates the transfer of

the preprotein to the chaperone systems of Hsp60 or free-floating mortalin, which subsequently fold the preprotein into the native form (Kang et al., 1990; van der Laan et al., 2010; Mokranjac, 2020). These chaperone systems often work in concert, forming complexes to complete folding operations that are vital to the mitochondria (Wadhwa et al., 2005). High levels of reactive oxygen and nitrogen species (ROS and RNS) are generated by the electron transport chain, and the inactivation of chaperone systems has been shown to lead to their accumulation, damaging critical mitochondrial components and ultimately resulting in the loss of mitochondrial and cellular viability (Deocaris et al., 2006a; Williamson et al., 2008).

Mitochondrial Hsp70 undertakes several important functions in the mitochondrial membrane. These include the assembly and maintenance of complexes and supercomplexes of the electron transport chain (Herrmann et al., 1994; Böttinger et al., 2015). MtHsp70 also plays a critical role in the alteration of mitochondrial cristae shape as well as the maintenance of mitochondrial membrane permeability and potential (Orsini et al., 2004). Inter-organelle communication is also facilitated, with mtHsp70 being involved in endoplasmic reticulum-mitochondrial communication via involvement in the mitochondria-associated membranes (Raeisossadati & Ferrari, 2020), as well as the formation of the mitochondrial membrane permeability transition pore (MMPT). This is done through interactions with the voltage-dependent anion channel (VDAC) and the mitochondrial permeability transition pore (Honrath et al., 2017). MtHsp70 is therefore critical to mitochondrial membrane maintenance and functionality along with roles involved in apoptotic pathways. Mitochondrial DNA (mtDNA) also relies on mtHsp70 for chromosomal maintenance and via its ATP hydrolysis to provide energy during mitochondrial protein expression (Herrmann et al., 1994).

The Hsp70 family structural layout is conserved in mortalin as well as the nucleotide centered allosteric mechanism of action, with sequencing studies indicating that mortalin has greater similarity to bacterial DnaK than cytosolic Hsp70s and the C-terminal EEVD motif is replaced by a conserved KEDQKEEKQ motif (Falah & Gupta, 1994; Deocaris et al., 2006b; Wiedemann & Pfanner, 2017). Mitochondrial Hsp70 is constitutively expressed and makes up ~ 1 % of all mitochondrial proteins. Mortalin has been observed throughout the cell, with approximately 30 % being found in other cellular compartments where it is suspected to play a role in a number of cell-cycle pathways, although the amount varies depending on the levels of cellular stress (Wadhwa et

al., 1993b; Ran et al., 2000). It is a central component of the protein quality control system (PQC), a collection of chaperones, co-chaperones and proteases that maintain mitochondrial proteostasis via the control of protein synthesis, iron-cluster biogenesis, repair, and degradation (Bukau & Horwich, 1998; Dutkiewicz et al., 2003; Uzarska et al., 2013; Böttinger et al., 2015). Overexpression is induced by most forms of cellular stress with an increased reaction to oxidative conditions and stress brought about by resource depletion (Liu et al., 2005; Jin et al., 2006).

Mortalin has also been identified playing a number of additional roles in the cell; these include centrosome duplication (Ma et al., 2006), cytoskeleton organization (Wakula et al., 2020), vesicle transportation (Kaul et al., 2007), immune response via antigen presentation (Pilzer & Fishelson, 2005) and the regulation of inflammatory cascades including the formation of the membrane attack complex (MAC) (Ray et al., 2014; Honrath et al., 2017). These functions are essential to regular cell functionality; however, the most significant impact mortalin has in any given organism may be an involvement in the regulation of several cell cycle pathways, particularly in response to oxidative stress (Bahr et al., 2022).

### 1.3.1 Mortalin as an oncogene

MOT-2 overexpression was seen to induce malignancy as a result of binding to the tumour suppressor protein p53, preventing migration to the cytosol and nucleus in times of oxidative stress, thereby preventing its transcriptional activity and delaying apoptosis (Wadhwa et al., 2002). Several studies have since identified mortalin as a critical regulator in other cell cycle pathways, such as the formation of a complex with tumour necrosis factor receptor-associated protein 1, preventing both the activation of apoptosis-inducing factor and c5b-9 formation in the complement system at multiple steps (Sinha & D'Silva, 2014; Fishelson & Kirschfink, 2019). Mortalin has also been shown to play a role in other pathways such as the inhibition of the apoptotic inducing protein *P66SHc* activation via the formation of a complex with mortalin recruited by TIM (Orsini et al., 2004). Activation of *P66SHc* under conditions of mild oxidative stress is inhibited until oxidation levels reach an unknown threshold and *P66SHc* is released (Bhat et al., 2015). Investigations are ongoing

into the role mortalin plays in the phosphorylation of cancer-related proteins. Recent studies have provided invaluable information regarding these interactions with the unrestricted phosphorylation of the signal protein phosphatidylinositol 3-kinase (PI3K)/Akt, shown to induce malignancy via multiple pathways regulating NF-κβ activation and stimulating angiogenesis (Yang et al., 2021).

### 1.3.2 Mortalin in neurodegenerative disease

Due to the actions of mortalin in the translocation and folding of preproteins entering the mitochondria, it would inevitably play a role in the development of diseases characterized by misfolded proteins, particularly neurodegenerative diseases such as Parkinson's and Alzheimer's Disease (PD and AD) (Priyanka & Seth, 2022). These diseases are often related to the effects of ageing, typically described as an increase in oxidative stress leading to DNA and mtDNA damage, a corresponding reduction in respiratory rates and a collapse of proteostasis brought about by the inability of chaperone systems to cope with the increase in damage (Frankowska et al., 2022; Margulis et al., 2020). This process can be further exacerbated by a mutation or improper post-translational modification of proteins within the chaperone system (Santra et al., 2019; Macario & de Macario, 2002). While this can occur in all ageing cells, it is more prevalent within the brain due to the relatively large amount of RNS and ROS generation brought about by high energy turnover rates in human neurons (Meriin & Sherman, 2005). Mortalin is usually defined as a glial protector which is vital for signaling between neurons and astrocytes as well as maintenance of the mitochondria adjacent to synaptic clefts with upregulation being observed in brain ischemia studies indicating that it acts to reduce ROS and mitigate the response from signal pathways (Calvillo et al., 2013; Volobоueva et al., 2013). In many cell lines and clinical studies, the overexpression of mortalin has been shown to rescue cells; however, mutant mortalin genes and post-translational modifications to it and its chaperone system have also been linked with the development of early onset neurodegenerative diseases (Havalová et al., 2021).

In Parkinson's Disease, which is characterized by the loss of dopaminergic cells primarily brought about by the accumulation of α-synuclein and other aggregates (Jankovic, 2008), mortalin has been

shown to co-localize and interact with most of the associated aggregates and proteomic data has demonstrated that mortalin expression is significantly reduced in astrocyte cells within the brains of PD patients (Macario & de Macario, 2002; Jin et al., 2006). A negative correlation has also been observed between mortalin expression and α-synuclein levels within PD patient serum samples and mouse models (Singh et al., 2018) with studies providing evidence that the overexpression of mortalin in neuronal and astrocyte cells can prevent inflammation and cell-death mediated by dysfunctional astrocytes (Priyanka et al., 2020).

Alzheimer's disease is characterized by senile plaques of amyloid-beta (αβ) aggregates primarily located in the extracellular space. However, these plaques are also found within the cell, associated with the mitochondrial membrane, and the amount localized there correlates with an increase in mitochondrial damage and disease severity in mice (Dragicevic et al., 2010). These plaques appear to induce mitochondrial morphology changes brought about by cristae damage and a reduction in energy production due to αβ-aggregates interacting directly with complexes of the electron transport chain (Baloyannis, 2006; Manczak et al., 2010; Xie et al., 2013). The role of mortalin in AD is still unknown; it appears to play a similar protective role as in PD, preventing inflammatory cascades and delaying apoptosis via multiple pathways, such as the prevention of MMPT formation, with the overexpression of mortalin being documented to mitigate and, in some cases, reverse the damage done to the mitochondria (Wang et al., 2015; Jia & Du, 2021).

The potential of mortalin as a drug target has been documented from its initial discovery in 1993; however, *in vitro* research into this Hsp70 isoform was delayed by more than a decade due to an inability to express it in a soluble form as mortalin was found to rapidly self-aggregate when recombinantly expressed (Szklarz et al., 2005; Bohnert et al., 2007). Research has shown that this is unique to mortalin with cytosolic Hsp70s localized to the mitochondria remaining soluble and thermal unfolding studies showing an association event in mortalin that is not evident in cytosolic Hsp70 (Blamowska et al., 2010; Dores-Silva et al., 2015). This may be the result of an off-pathway conformational change within the catalytic cycle which is aggregation-prone with the absence of a nucleotide being a significant driver of this outcome (Blamowska et al., 2012). The prevention of this self-aggregation and maintenance of mtHsp70 in a soluble and functional state is critical to

cellular viability and a Hsp70 escort protein (Hep1) is required to attain this within a cellular environment.

## 1.4 Mitochondrial Hsp70 Escort Protein (Hep1)

In 2005 a protein interacting with a mtHsp70 within yeast (Ssc1) was identified and initially named Zim17 and Tim15 due to the presence of a zinc finger domain and its suspected inclusion in the translocase of the inner membrane (TIM) complex respectively, although it was later found to only have a transitory interaction with TIM (Sichting et al., 2005; Yamamoto et al., 2005). Deletion mutants of Zim17 were shown to induce the arrest of mitochondrial protein translocation, protein folding and iron-sulfur cluster biogenesis, which lead to alterations of mitochondrial morphology and cell death when under conditions of stress for extended periods (Burri et al., 2004; Szklarz et al., 2005; Sichting et al., 2005). Identifying these results as possible markers of mortalin non-functionality rather than the direct result of Zim17 loss, researchers went on to confirm that Zim17, also known as Hep1, was needed to keep mtHsp70 in a soluble and functional state (Szklarz et al., 2005).

Since its initial characterization, several Hep1 orthologues have been identified in various eukaryotes, including plants, where it is classified as a zinc ribbon protein (ZR1,2,3) with plastidic isoforms being categorized as Hep2s (Kluth et al., 2012). However, no orthologue has been identified in prokaryotic cells (Yamamoto et al., 2005). *De novo* studies carried out in Hep1 minus yeast cells have shown that Hep1 is needed to fold mtHsp70 upon its entry to the mitochondria with no other chaperone systems involvement (Blamowska et al., 2012). The minimum binding entity is the NBD and the linker region; this correlates with folding studies, which suggest that mtHsp70 aggregation occurs around the NBD/linker region with the SBD being able to fold independently of Hep1 when expressed attached to a cytosolic linker/NBD (Zhai et al., 2008; Blamowska et al., 2010, 2012).

Hep1 proteins are zinc-finger proteins with one tertracysteine motif that is part of the zinc finger domain. They are small (~ 20 kDa), L-shaped proteins with a conserved zinc-finger binding domain (zf-DNL) (shown in green), with the structure outside of the zf-DNL showing significant variation between orthologues (Figure 1.3) (Dores-Silva et al., 2013; Nyakundi et al., 2018). The zf-DNL binding site consists of a zinc-ion localized between a pair of β-sheets by a tetra-cysteine motif formed by two CXXC pairs (shown in yellow). Experiments involving the replacement of the binding pocket cysteine residues with glycine have been shown to collapse Hep1 structure and remove the functionality of the protein (Momose et al., 2007). Similar results are brought about when the zinc-ion of the zf-DNL is chelated via the use of EDTA and has shown that the zinc ion is crucial to Hep1 functionality and structure (Zhai et al., 2011).

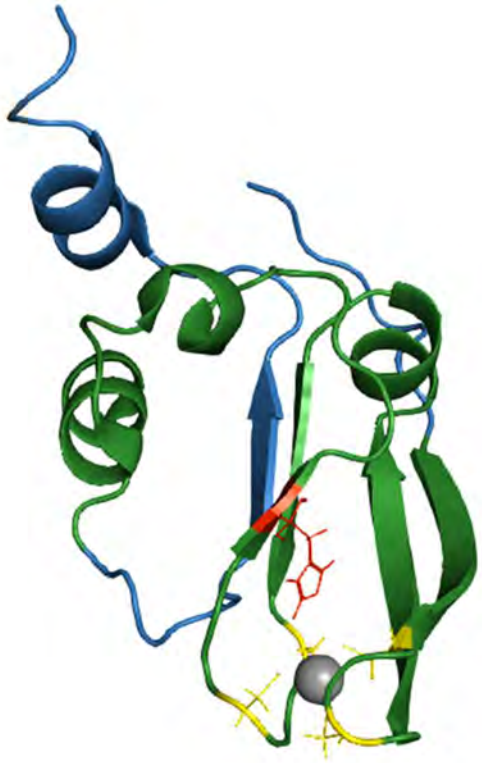

Figure 1.3: The structure of Tim15c: The structure of *S. cerevisiae* Tim15c (Momose et al., 2007) with the zinc finger binding domain displayed in green and conserved histidine in red. The tetra-cysteine motif is displayed in yellow with the zinc-ion in grey. The areas of low confidence are shown in blue.

Outside of the zf-DNL there is considerable variation between orthologues. The orthologue found within *P. falciparum*, has a number of asparagine (N) repeats which is characteristic of the organism and causes the orthologue to aggregate, a property unique among Hep1 orthologues (Nyakundi et

al., 2016). Alterations of sequence and structure outside of the zf-DNL are suspected to impart differing functions on Hep1, currently a number of these have been documented with the yeast orthologue exhibiting only the ability to solubilize mtHsp70 (Momose et al., 2007). Human Hep1 displays the ability to suppress the aggregation of client proteins such as rhodanese, MDH and luciferase (Goswami et al., 2010; Dores-Silva et al., 2021). Human Hep1 and the orthologue belonging to the protozoan parasite *L. braziliensis* have also exhibited co-chaperoning functions, resembling the ability of a JDP by stimulating the ATPase activity of their respective mtHsp70, a conserved histidine has been identified as necessary for this stimulation (Zhai et al., 2008; Dores-Silva et al., 2017). This may correspond with previous theories that Hep1 may act as a fractured JDP, providing the zf-DNL region for type-III JDPs although this has yet to be confirmed (Burri et al., 2004).

Recent microscopy studies have also concluded that Hep1 is not limited to the mitochondria and has been observed interacting with liposome membranes as well as being identified within the nucleus (Dores-Silva et al., 2021). The study also found that human Hep1 could interact with and stimulate the activity of human cytosolic Hsp70 (HSPA1A) (Dores-Silva et al., 2021). These studies indicate that Hep1 may have a litany of functions around the cell, whether these only pertain to mtHsp70s operations is still unknown but the arrest of Hep1 has been shown to reduce cellular viability in yeast models (Szklarz et al., 2005). The most deleterious effects of Hep1 loss are those brought about by the subsequent aggregation of mtHsp70, these include a drop in the rate of protein import and the generation of Fe/S cluster proteins as well as reduced genome stability which ultimately results in cell death (Szklarz et al., 2005; Sichting et al., 2005; Uzarska et al., 2013). The critical role that Hep1 plays in the operations of mtHsp70 may allow it to be targeted in the treatment of diseases caused by protozoan parasites such as *Trypanosoma brucei* which are known to rely on a single mitochondrion for all mitochondrial operations.

## 1.5 Trypanosomatida

The Trypanosomatida order is a collection of corkscrew-shaped protozoa which are exclusively parasitic, of which two genera are dixenous and represent a danger to humans, Trypanosoma and Leishmania (Lopes et al., 2010). Both genera are the causative agents of different trypanosomiases; Leishmania species cause Chagas disease and leishmaniasis endemic to Southern America, and the Trypanosoma subspecies of *Trypanosoma brucei* cause Trypanosomiasis. The tsetse fly is the vector of *Trypanosoma brucei* subspecies; however, the hosts they infect can differ and Trypanosomiasis can be further divided into Human African Trypanosomiasis (HAT) and Animal African Trypanosomiasis (AAT), otherwise known as nagana, with *Trypanosoma brucei rhodesiense* and *Trypanosoma brucei gambiense* being responsible for HAT and the subspecies *Trypanosoma brucei brucei* causing AAT.

### 1.5.1 African Trypanosomiasis

HAT currently affects 37 countries, primarily within sub-Saharan Africa, with most cases reported in the Democratic Republic of the Congo (Kennedy, 2019). As part of the initiative targeting neglected tropical diseases, the disease was initially targeted to be under control by 2020, with the complete elimination of new transmissions by 2030. Significant progress has been made, and sustained control efforts have resulted in a drop in new cases from below 10,000 in 2009 to below 1000 cases in 2020 (Kennedy, 2019). These containment methods have primarily been directed towards both detection of cases and the control of the insect vector responsible for the transmission of the parasites, the tsetse fly; these efforts include the reduction of tsetse fly populations and the reduction of opportunities for tsetse-human contact (Simarro et al., 2008). The lifecycle of *T. brucei* parasites is digenetic and oscillates between the insect vector and the mammalian host. Mammalian reservoirs are expected to be a significant hinderance in attaining the 2030 goal as non-symptomatic human carriers, wild animals such as antelope and domesticated animals, primarily pigs, are suspected to be effective reservoirs for the subspecies of parasites which are capable of infecting humans (Njiokou et al., 2006, 2010).

Two forms of the disease exist depending on the subspecies of *T. brucei* involved; the most prevalent is the chronic form brought about by *T. b. gambiense* (85-90 % of cases), with the remainder accounted for by an acute form of the disease brought about by the *T. b. rhodesiense* subspecies, while different time scales are present both forms share similar stages and disease progression (Kennedy, 2013). After transmission through the bite of the tsetse fly, the first of two stages of the disease begins, the haemolymphatic stage, in which the parasite multiplies and spreads via the patient's bloodstream, infecting multiple tissues and the lymphatic system. Common symptoms experienced in this stage can be easily misdiagnosed as they resemble the common cold, with joint pain, headaches, and fever commonly encountered. Misdiagnosis is especially problematic as trypanosome parasites are hard to detect unless blood samples are taken for direct visualization, and serological tests or specially engineered rapid diagnostic tests are used (Bouteille & Buguet, 2012). Stage 2 of the disease is known as the encephalitic stage and is initiated when the parasites pass the blood-brain barrier and enter the central nervous system. The name of the disease is derived from this stage as chronic encephalopathy develops, causing severe disruption to the sleep-wake cycle of the patient as well as various neurological and cognitive issues (Romero-Meza & Mugnier, 2020). Once stage 2 is reached, the infection steadily progresses and ultimately leads to the patient succumbing to coma and death. If untreated, the disease is fatal and will lead to the patient's death (Brun et al., 2010).

### 1.5.2 The current state of human African trypanosomiasis medications

The treatments for HAT are relegated to pharmacological medications, which are administered based on the progression of the disease and the stage experienced by the patient. Vaccine development has been hampered due to a mechanism of defense employed by *T. brucei* and other trypanosomes in which variable surface glycoproteins (VSGs) are implemented to avoid the patient's immune system resulting in vaccines being relatively ineffective (Rios et al., 2019). Recent research on *T. vivax* may have identified a flagellum-membrane protein as a viable target with

consistent long-term results; however, further investigation is required into whether this development applies to other trypanosome species (Autheman et al., 2021). The treatments currently administered are less than ideal due to several negative aspects, such as severe side effects, the requirement of a professional to administer the treatment and an inability to cross the blood-brain barrier, thereby failing to treat both stages of the disease. These negative aspects must be viewed with the knowledge that those primarily affected by this disease are located in rural areas far from hospitals and undertake laborious work in their day-to-day lives (Bouteille & Buguet, 2012). Stage 1 treatments include Pentamidine and Suramin, while stage 2 treatments include Melarsoprol, Eflornithine and Nifurtimox, with the latter administered in combination (Bouteille & Buguet, 2012). A promising new treatment, Fexinidazole, has been identified as effective against both stages of *T. b. gambiense* HAT (gHAT) and is currently undergoing clinical trials for *T. b. rhodesiense* HAT (rHAT) (Imran et al., 2022).

Pentamidine is an IV-administered treatment which requires daily doses over seven days; it is used to treat the first stage of gHAT. The side effects are relatively mild and can include hypotension, hypoglycaemia, cardiac arrhythmia and acute pancreatitis (Charney et al., 2022). Suramin is an IV-administered treatment which requires five weekly doses; it is primarily used to treat stage 1 of rHAT. The side effects are severe and can include renal and bone-marrow toxicity, anaemia, peripheral neuropathy and the possible induction of anaphylactic reactions (Brun et al., 2010; Wiedemar et al., 2020). These treatments are administered to slow the disease's progression as they significantly reduce the dissemination of *T. brucei* into new tissues; however, they are most effective in the bloodstream, with a reduction in effectiveness based on the tissues infected by the parasite (Brun et al., 2010). These treatments represent an ongoing expense; they cannot pass the blood-brain barrier and can only affect stage 1 of the disease.

Melarsoprol is an arsenic-derived, IV-administered treatment requiring three to four sets of daily doses with approximately seven days between each; it is used to treat the second stage of rHAT and gHAT. The side effects are very severe, and it is the least preferred of all treatments as it can induce a litany of adverse effects, culminating in encephalopathic syndrome, which may result in death, with between 1 – 5 % of patients treated dying as a result. The drug is only administered in severe cases where no other stage 2 treatment is available (Fairlamb & Horn, 2018). Eflornithine is an IV-

administered treatment which requires daily doses over 14 days; it is used to treat the second stage of gHAT. The side effects are numerous, including convulsions, gastrointestinal disruptions, and bone marrow toxicity with the accompanying anaemia, leukopenia, and thrombocytopenia (Jobanputra et al., 2007). Eflornithine is often administered in combination with Nifurtimox as this has shown to be more effective, cheaper and produces less severe side effects than each treatment administered individually. Nifurtimox is an orally administered treatment which is given in combination with Eflornithine or Melarsoprol treatments as this has shown to be more effective, cheaper and produces less severe side effects than either treatment administered individually (Fairlamb & Horn, 2018; Hidalgo et al., 2021). Nifurtimox-Eflornithine combination therapy is the preferred treatment due to the similar effectiveness and lower risk associated with Eflornithine relative to Melarsoprol. Side effects of Nifurtimox are negligible when administered orally; however, disruptions to appetite and weight loss can occur (Hidalgo et al., 2021).

Fexinidazole is an orally administered drug taken over ten days; it is used to treat both stages of HAT infection as it can pass the blood-brain barrier. To date, only the second phase of clinical trials has been undertaken, and the common side effects are uncharacterized; however, they tend to include gastrointestinal disruptions, insomnia, tremors and headaches (Mesu et al., 2018; Hidalgo et al., 2021). The drug has been approved for use in the Democratic Republic of the Congo and by the United States Food and Drug Administration despite the lack of phase 3 trial completion due to the promising results of initial studies indicating only a slight reduction in effectiveness relative to Nifurtimox-Eflornithine combination therapy (~ 6.3 %) and the urgent need for a non-IV based treatment which can be used to combat both stages of the disease (Mesu et al., 2018).

### 1.5.3 The life cycle of *T. brucei*

The life cycle of *T. brucei* is described as a progression from the metacyclic trypomastigote form which is injected by a tsetse fly bite. The parasite then differentiates into the bloodstream or ‘slender’ trypomastigote form which spreads via the bloodstream, infiltrating mammalian tissues and multiplying via binary fission. The trypomastigotes are then ingested upon the bite of the tsetse fly

and taken into the midgut of the insect vector where they transform to the procyclic trypomastigote form and multiply via binary fission. Transformation into the epimastigote form then occurs as the parasites exit the midgut. The epimastigotes move to the salivary glands and multiply via binary fission before returning to the metacyclic trypomastigote form where the life cycle begins again (Figure 1.4) (Büscher et al., 2017).

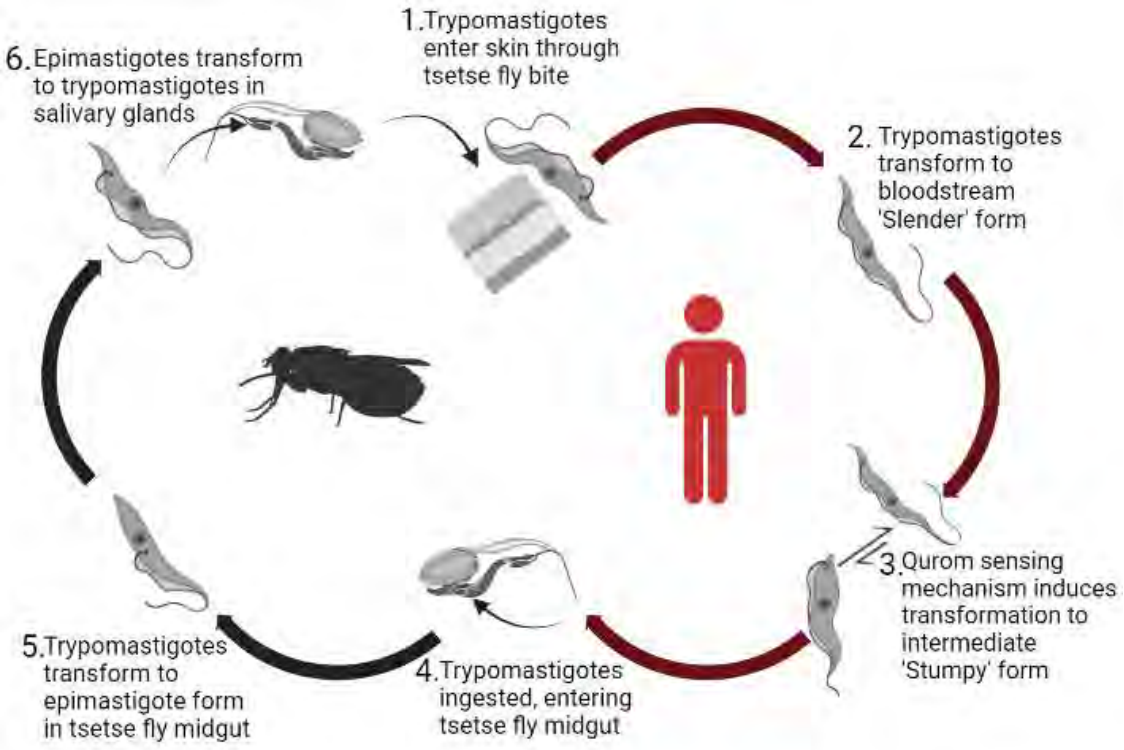


Figure 1.4: The life cycle of *T. brucei*: (1) Following the bite of a tsetse fly *T. brucei* parasites enter the bloodstream of the mammalian host (Red). (2-3) *T. brucei* then spreads through the bloodstream and infects multiple tissues with a quorum sensing mechanism causing cell-cycle arrest and differentiation to a quiescent 'stumpy' form to allow spread and transmission without killing the host. (4) The trypomastigote form is ingested by the tsetse fly once more (Black), entering the midgut. (5) The trypomastigotes transform into the epimastigote form and multiply. (6) The epimatigotes transform back to the trypomastigote form as they move to the salivary glands to begin the cycle again. The figure was created using BioRender.com.

One of the most effective mechanisms of response which makes the control of *T. brucei* difficult is quorum sensing, this can bring about differentiation from the 'slender' form to the quiescent 'stumpy' form of the parasite within mammals. This has been shown to evade the immune system and medications such as suramin more efficiently and allow preadaptation of the parasite to the tsetse fly vector (Wiedemar et al., 2020; Quintana et al., 2021). This preadaptation is seen via several strategies such as a switch from a focus on glycosome-based glucose metabolism, which is advantageous in human tissues, to mitochondrial-based metabolism of alternate carbon sources such

as amino acids, particularly proline, a resource which is far more abundant in the tsetse fly (Lopes et al., 2010). This mechanism was initially thought to be the product of a parasite-derived stumpy induction factor (SIF); however, recent research indicates that SIF may be a collection of short, host-derived oligopeptides which are the product of peptidase enzymes secreted by the parasite. The oligopeptide receptor GRP89 is central to detecting these and the subsequent activation of pathways which bring about cell-cycle arrest and differentiation (Rojas et al., 2019).

### 1.5.4 The heat shock proteins of Trypanosomatida

Research undertaken on *T. brucei*, *T. cruzi* and *L. braziliensis* have provided evidence that Hsps play crucial roles throughout the life cycle of parasitic protozoa and is integral to disease progression and transmission. High-throughput RNA interference studies carried out on *T. brucei* which used phenotypic observations indicate that a variety of Hsp70s and JDPs are involved in protein secretion and glycolysation including the production of VSGs with the majority of *T. brucei* Hsp70s identified as crucial to cellular viability (Subramaniam et al., 2006; Field et al., 2010; Alsford et al., 2011). Few of these proteins have been biochemically examined in detail, however, the type I JDP Tbj2 has been shown to be essential for cellular viability within all life stages and RNAi knockdown studies targeting the protein resulted in severe growth defects (Alsford et al., 2011). Biochemical studies have also indicated that Tbj2 functionally co-operates with Hsp70.4, an Hsp70 located in the *T. brucei* cytosol (Bentley & Boshoff, 2019).

The most accepted theory regarding how these adaptations were initially brought about is that of an expanded heat shock response (Quintana et al., 2021). This is displayed in the extensive proliferation of proteins involved in the heat shock response, with 12 putative Hsp70 proteins being identified and approximately 67 putative JDPs (Bentley et al., 2019). Given the central role that mtHsp70 plays in the formation of mitochondrial complexes and supercomplexes, as well as post-translational modifications and the activation of cell-cycle pathways (Matthews, 2021), an investigation into the role of mtHsp70 and the interacting co-chaperones is warranted. This would assist in combatting infections originating from the Trypanosoma order and may provide a helpful model to expand our

knowledge of mtHsp70 in cell processes within other diseases such as various cancers and neurodegenerative diseases (Folgueira et al., 2007).

## 1.6 Knowledge Gap and motivation

Heat shock proteins are crucial to the survival of protozoan parasites, including *T. brucei*, and play a central role in cell-cycle pathways involved in the differentiation of the parasites. Hep1 may provide a viable avenue for controlling *T. brucei* and could allow a new strategy in eliminating the parasites within reservoir species as well as targeting the metabolism of the quiescent 'stumpy' form which can reduce cases of remission. To begin research into this there is the need to characterize this orthologue and confirm that the structure and characteristics resemble those of other orthologues, as currently it has only been identified in proteomic studies. Comparative analysis against the well characterized *H. sapien* orthologues is of particular importance in identifying differences between host and parasite Hsp machinery. This is especially important regarding the ability of the *T. brucei* Hep1 (TbHep1) to maintain the mtHsp70 of *T. brucei* (TbmtHsp70) in a soluble and functional state as mtHsp70 may have a role in cell-cycle pathways, which are critical to multiple survival strategies employed by *T. brucei*. The ability of HsHep1 to act as a J-protein will also be investigated. The recent release of the folding program Alphafold may also provide a new method of bioinformatic analysis that could provide insight into the structure of Hep1 orthologues outside of the zf-DNL which was previously the only modellable area. These developments call for an analysis of these structures using the new technology as well as a comparison of the ability of TbHep1 to prevent the aggregation of the TbmtHsp70 relative to the *H. sapien* orthologues HsHep1 and HSPA9 (mortalin).

## 1.7 Hypothesis

TbHep1 can facilitate the expression of soluble and functional TbmtHsp70 and suppress aggregation when placed under thermal stress in a similar manner to that of the *H. sapien* orthologue.

## 1.8 Aims and objectives

To analyze, using *in silico* tools, the mitochondrial Hsp70 chaperone system in *T. brucei* in comparison to HSPA9. This study will investigate the phylogenetic relationship TbHep1 has with mitochondrial JDPs found within *T. brucei*. The program Alphafold will also be used to analyze models of Hep1 and mtHsp70 orthologues to allow comparisons of the models with those produced using other methods and to investigate if the new method provides insights into how structures alter the properties of different orthologues.

This study will biochemically characterize TbHep1 and TbmtHsp70 to investigate the properties of TbHep1 and confirm if it shares the property to prevent TbmtHsp70 aggregation upon expression and when placed under thermal stress. These characterizations will be made in comparison with the previously studied *H. sapien* orthologues HsHep1 and HSPA9 (mortalin)

### 1.8.1 Specific objectives

The specific objectives of this study are:

- Bioinformatic analysis of mtHsp70 and Hep1 orthologues

This study aimed to undertake comparative sequence and phylogenetic analysis of TbHep1 and TbmtHsp70 to infer their properties and identify unique structures which may influence their

structures and functions. Domains and relationships between analyzed orthologues of these proteins will be examined.

- A phylogenetic analysis of TbHep1 with the extensively developed network of JDPs from *T. brucei*.

This study aims to identify if the extensive development of JDPs with *T. brucei* may provide insight into the cladistic relationship of Hep1 to JDP operations as previously hypothesized in other studies (Burri et al., 2004).

- Comparisons between Hep1 models derived from NMR and Alphafold

This study aimed to examine Hep1 models created using the Swissmodel program and the NMR-derived TIM15c template (Momose et al., 2007). Comparisons could then be made with those made using the AI-driven Alphafold program in an effort to identify differences between the modelling techniques.

- Analysis of critical residues in mtHsp70 models generated using Alphafold

This study aimed to use Alphafold to produce models of aggregating mtHsp70 orthologues in an effort to identify the significance of residues previously identified as critical to the aggregating properties.

- The expression and purification of TbmtHsp70 and TbHep1 *H. sapien* orthologues mortalin and HsHep1

This study aimed to examine the efficacy of overexpressing TbmtHsp70 and TbHep1 using a bacterial expression system and purification of the recombinant proteins. Analysis of expression and solubility will be carried out using an SDS-PAGE and various solubilization approaches used to determine the ideal method to produce soluble and functional TbmtHsp70.

The study also aimed to investigate the ability of TbHep1 to solubilize TbmtHsp70 when expressed and allow the purification of the chaperone in a soluble and functional state.

- The examination of the ability of TbHep1 to suppress the aggregation of TbmtHsp70 and malate dehydrogenase.

The ability of TbHep1 to suppress the aggregation of TbmtHsp70 when placed under thermal stress will be also analyzed by comparing the effects of this orthologue with the one found within *H. sapien*. The specificity of TbHep1 will also be preliminarily examined by observing the ability to suppress the thermally induced aggregation of MDH. The role the $Zn^{2+}$ localized in the zf-DNL plays in the structural integrity of TbHep1 will also be investigated.

# Chapter 2: Bioinformatic analysis of Hsp70 escort protein 1

## 2.1 Introduction

The collection and repository of biological data into online databases has revolutionized how protein research is approached, making it convenient to access information regarding most species and providing the ability to identify and categorize proteins based on sequence identity, localization and domain organization (Krogh et al., 2001; Hugenholtz, 2002; Letunic et al., 2006, 2021) This bioinformatic approach provides a platform with consolidated data about any documented target sequence, allowing for easy acquisition, storage, analysis, and visualization (Tatusov et al., 2003; Manichaikul et al., 2010). There are several databases which pertain specifically to tropical diseases such as the Tropical Disease Research site or PlasmoDB which provide broad information on multiple tropical disease and the *Plasmodium* species respectively (Bahl et al., 2003).

The successful sequencing of the genomes of various Trypanosoma species has allowed the creation of TritrypDB, an online database which consolidates the data collected on the Trypanosoma genus (Aslett et al., 2009). This provides extensive information on a variety of Trypanosoma species such as *T. b. brucei, T. b. gambienses* and *T. b. rhodesiense*, allowing access to their entire genome sequences as well as any computationally predicted gene suites, proteins, and protein features such as domains and motifs, these can be further annotated manually following practical experimentation. Information is also provided regarding expression data and the alteration of gene suites under different lifecycle stages collected via proteomic studies (Aslett et al., 2009). These features make TritrypDB an invaluable resource which integrates relevant data and allows access, providing the ability to make queries into data relevant for any given study pertaining to the Trypanosoma subfamily and a collection of other kinetoplasts (Aslett et al., 2009).

The use of these databases allows predictions about proteins to be further improved by modelling software, such as Swissmodel, which allows homology modelling, the creation of a 3D structure of a putative protein based on a template of an orthologue or highly conserved segment which has been

previously elucidated using NMR or X-ray crystallography (Waterhouse et al., 2018). This is advantageous as it allows for the analysis of protein structure and arrangement without the need for intensive and expensive techniques with studies indicating that proteins with greater than 25 % sequence identity are likely to share structural features (Pearson, 2013).

This field of research has recently been enhanced with the addition of the AI-driven Alphafold modelling program which does not require a template model to operate and has been shown to have exceptional accuracy in the prediction of protein structures (Jumper et al., 2021). This is of particular interest in studies of the Hep1 proteins due to the lack of a complete protein model, currently the zinc-finger binding domain (zf-DNL) region of the *Saccharomyces cerevisiae* (*S. cerevisiae*) Hep1 protein (Tim15c) is the only available structure (Momose et al., 2007). This restricts homology modelling to the conserved domain and studies have indicated that Tim15c has large differences in activity and sequence similarity in comparison to other Hep1 orthologues. Due to the methodology of Alphafold the examination of areas outside of the zf-DNL has been made available without the need for a new template model. This is done through a specially designed neural network from the company Deepmind (USA) which incorporates previously accumulated data regarding protein structures, physical chemistry, and the incorporation of multiple sequence alignments (Jumper et al., 2021).

TbmtHsp70 and TbHep1 have been identified and documented on TritrypDB with one TbHep1 protein identified and three identical TbmtHsp70s (A, B and C). The TbmtHsp70 sequences bare the GVFEV motif within the NBD which have been observed in other mtHsp70 orthologues. Previously, mutation studies carried out on the aggregating paralogue Ssc1 from yeast cells indicated that when this motif is replaced by that found in cytosolic Hsp70 the aggregation property was abrogated (Blamowska et al., 2010). Studies of the kinetoplast orthologue *L. braziliensis* have also indicated that the motif is needed for communication between domains and with co-chaperones (Dores-Silva et al., 2017). Hep1 orthologues were previously identified by localization and the highly conserved zinc-finger domain, multiple mutation and zinc-chelating studies using Hep1 orthologues have indicated that the tetra-cysteine motif as well as the zinc-ion localized between them within the zf-DNL are required for the solubilizing interaction with mtHsp70 (Zhai et al., 2008; Blamowska et al., 2012).

Studies conducted on human Hep1 have indicated three residues involved in the stimulation of the ATPase activity of HSPA9, these are R81, H107 and D111. Alterations of the R81 and D111 residues to glycine resulted in reduced stimulation and binding efficiency while a complete abrogation of ATPase stimulation occurred with alterations to H107 (Zhai et al., 2011). TbHep1 and TbmtHsp70 have not been previously analyzed and the presence of these sequence features must be investigated. Observations on the extensive network of JDPs which operate in concert with the mitochondrial Hsp machinery and how they relate to TbHep1 may provide insight into the operations of JDP machinery in other organisms. This would be of particular interest as it may provide insight into the fractured JDP theory, put forward by Burri et al. (2004), which suggests that Hep1 may functionally interact with type-III JDPs, providing the zinc-finger domain and possibly playing a role in substrate delivery to the co-chaperone. The use of the new modelling software Alphafold may allow analysis of the structures of mtHsp70 and Hep1 orthologues without the cumbersome generation of new models. Motifs and residues have been analyzed within *S. cerevisiae* orthologues and the properties they bring about have been documented, the AI-driven approach may provide further insight into these residues of interest.

## 2.2 Objectives

The aim of this study was to use bioinformatic tools to examine the mtHsp70 machinery of *T. brucei* and discern if similarities between previously described orthologues of mtHsp70 and Hep1 are maintained in *T. brucei*.

### 2.2.1 Specific objectives:

- Sequence alignments to analyze the degree of conservation between domains and residues involved in the interaction of mtHsp70 and Hep1 of *T. brucei* using previously defined eukaryotic orthologues of both proteins.

- A phylogenetic analysis between TbHep1 and the extensive collection of JDPs in the mitochondria of *T. brucei* which may be involved in mtHsp70 operations.

- The modelling and analysis of TbHep1 and TbmtHsp70 using the AI-driven protein folding program Alphafold.

- The consolidation of mitochondrial *T. brucei* proteins previously identified in genomic and proteomic studies which may be involved in the actions of *T. brucei* mtHsp70 (TbmtHsp70).

- A phylogenetic analysis into the relationship between TbHep1 and the extensive network of *T. brucei* mitochondrial JDPs.

- A comparison of results produced by the modelling software Swissmodel and Alphafold using TbHep1 and TbmtHsp70 models against cytosolic paralogues.

## 2.3 Methodology

### 2.3.1 Sequence Acquisition and analysis

The nucleic and amino acid sequences of *T.brucei* mitochondrial Hsp70, Hep1 and identified mitochondrial JDPs were obtained from the TritrypDB database (Amos et al., 2022) and the remaining sequences were obtained from the National Center for Biotechnology Information

(NCBI) (https://www.ncbi.nlm.nih.gov/) and UniProt (Bateman et al., 2021) (https://www.uniprot.org/). JDPs were collected from previous proteomic studies: (Ashburner et al., 2000; Acestor et al., 2009; Niemann et al., 2013; Güther et al., 2014; Bentley et al., 2019). Sequence alignments and percentage identity were carried out using T-COFFEE for Hep1 alignments and Clustal Omega for mtHsp70 (Dric Notredame et al., 2000; Sievers et al., 2011). The shading of residue conservation was done using Jalview (Waterhouse et al., 2009) and annotations were manually performed on Microsoft Office (Microsoft Corporation, USA).

### 2.3.2 Phylogenetic analysis

Phylogenetic analyzes were carried out using Molecular Evolutionary Genetics Analysis 11 (Mega 11) (Tamura et al., 2021). The primary amino acid sequences were the input in a multiple sequence alignment (MSA) using the inbuilt MUSCLE aligning program and the resulting MSA was used in the construction of a phylogenetic tree carried out using a maximum likelihood statistical method following a poission distribution substitution model (Tamura et al., 2021). A consensus tree was produced via 1000 bootstrap replicates with the branch swap filter capped at strong. The final tree was imaged using Mega 11.

### 2.3.3 Structural analysis and Homology Modelling

The domain mapping for Hep1, mtHsp70 and JDP orthologues was undertaken using the Simple Modular Architecture Research Tool (SMART7)(Letunic et al., 2021) and Prosite with Jpred and the consolidated programs of Quick2D being used for the prediction of secondary structures (Cuff & Barton, 2000; Sigrist et al., 2009; Drozdetskiy et al., 2015; Gabler et al., 2020). The programs involved in Quick2D include PSIPred (Jones, 1999), Spider3 (Heffernan et al., 2017), PSSPred4 (Yan et al., 2013), DeepCNF (Wang et al., 2016), NetSurfP2 (Klausen et al., 2019) and SpotD

(Hanson et al., 2017). Initial homology modelling for Hep1 was carried out using a MAFFT MSA followed by modelling of the zinc-finger binding domain using Swissmodel (Katoh et al., 2002; Waterhouse et al., 2018). The structure of the yeast derived Tim15c (PDB: 2E2Z) was used as a template with the lowest E-value being the determining value for the selection. Modelling was then carried out again using the AI driven online program Alphafold (Jumper et al., 2021) with pairwise sequence analysis being conducted using T-COFFEE (Dric Notredame et al., 2000). The resultant models were then aligned and rendered using ChimeraX (Pettersen et al., 2021) .

### 2.3.4 Mitochondrial interaction data

The interactions of mtHsp70, Hep1 and *T. brucei* derived JDPs were assessed using the online program STRING (Szklarczyk et al., 2021) for currently documented interactions. Interaction data pertaining to interactions not yet confirmed *in vitro* for *T. brucei* Hep1 and JDPs was collected from genomic and proteomic studies previously undertaken, (Ashburner et al., 2000; Acestor et al., 2009; Niemann et al., 2013; Güther et al., 2014; Bentley et al., 2019), and any visual representation of the data provided by the STRING program.

## 2.4 Results and discussion

### 2.4.1 Bioinformatic analysis of *T. brucei* mitochondrial Hsp70

Multiple sequence alignment was undertaken to assess the sequence similarity between the TbmtHsp70 and the orthologues in which the Hep1-mtHsp70 interaction has been documented. These include orthologues from *Arabidopsis thaliana* (*A. thaliana)* and *Chlamydomonas reinhardtii* (*C. reinhardtii*). With the *S. cerevisiae* paralogue Ssc1 included, one of three mtHsp70s found in

yeast, the other paralogues are Ssq1 and ECM1, Ssc1 was chosen because it is known to aggregate and the interaction with Hep1 has been confirmed (Blamowska et al., 2010). The sequences of *H. sapiens* and *L. braziliensus* mtHsp70 were included as the *H. sapiens* orthologue is relevant to this study and *L. braziliensus* represents a close relation of *T. brucei* from the kinetoplast family. All orthologues were chosen as previous studies have confirmed the self-aggregating tendencies and the solubilizing interaction with Hep1, therefore an analysis of conserved residues may indicate if these properties are maintained in TbmtHsp70. The sequence of *E. coli* DnaK was included to allow comparisons with an orthologue that is related to mtHsp70 but has no aggregating tendencies.

The alignment indicates that *T. brucei* maintains the domain layout common among mtHsp70s with the NBD maintaining a high degree of conservation (Figure 2.1). Within the NBD the GVFEV motif has been shown to play a role in the aggregation of mtHsp70 via interactions with the linker region, the mutation of this motif to the KTFEV motif of DnaK results in the abrogation of mtHsp70 aggregation (Blamowska et al., 2010). The GVFEV motif is present within the *T. brucei* orthologue, suggesting that the aggregation property may be maintained in this orthologue. The amino acids at positions 157 and 159 of the *T. brucei* sequence are of note due to evidence suggesting that these residues are involved in the interaction between mtHsp70 and Hep1, with the residues glycine (G) and threonine (T) frequently observed in these positions respectively (Figure 2.1) (Pareek et al., 2011). The glycine residue G157 is maintained across all aligned species; however, the threonine residue has been altered in the *T. brucei*, *S. cerevisiae*, *A. thaliana* and *C. reinhardtii* sequences. This residue is replaced by serine in *A. thaliana* (S184), this should be functionally similar as the residues are similar in size and polarity (Stephenson & Freeland, 2013) and the residue is replaced by proline (P) in the *S. cerevisiae* (P162) and *C. reinhardtii* (P172) orthologues and the interaction with Hep1 was not affected (Blamowska et al., 2010). The alteration of this amino acid to the large and positively charged lysine (K160) may have an effect within the *T. brucei* orthologue and is not maintained in the other aligned trypanosome *L. braziliensis* (Figure 2.1). However, K is present within this position in PfHsp70-3 from *P. falciparum* (data not shown) which did interact with PfHep1 (Nyakundi et al., 2016), implying that the interaction with Hep1 is maintained in *T. brucei*.

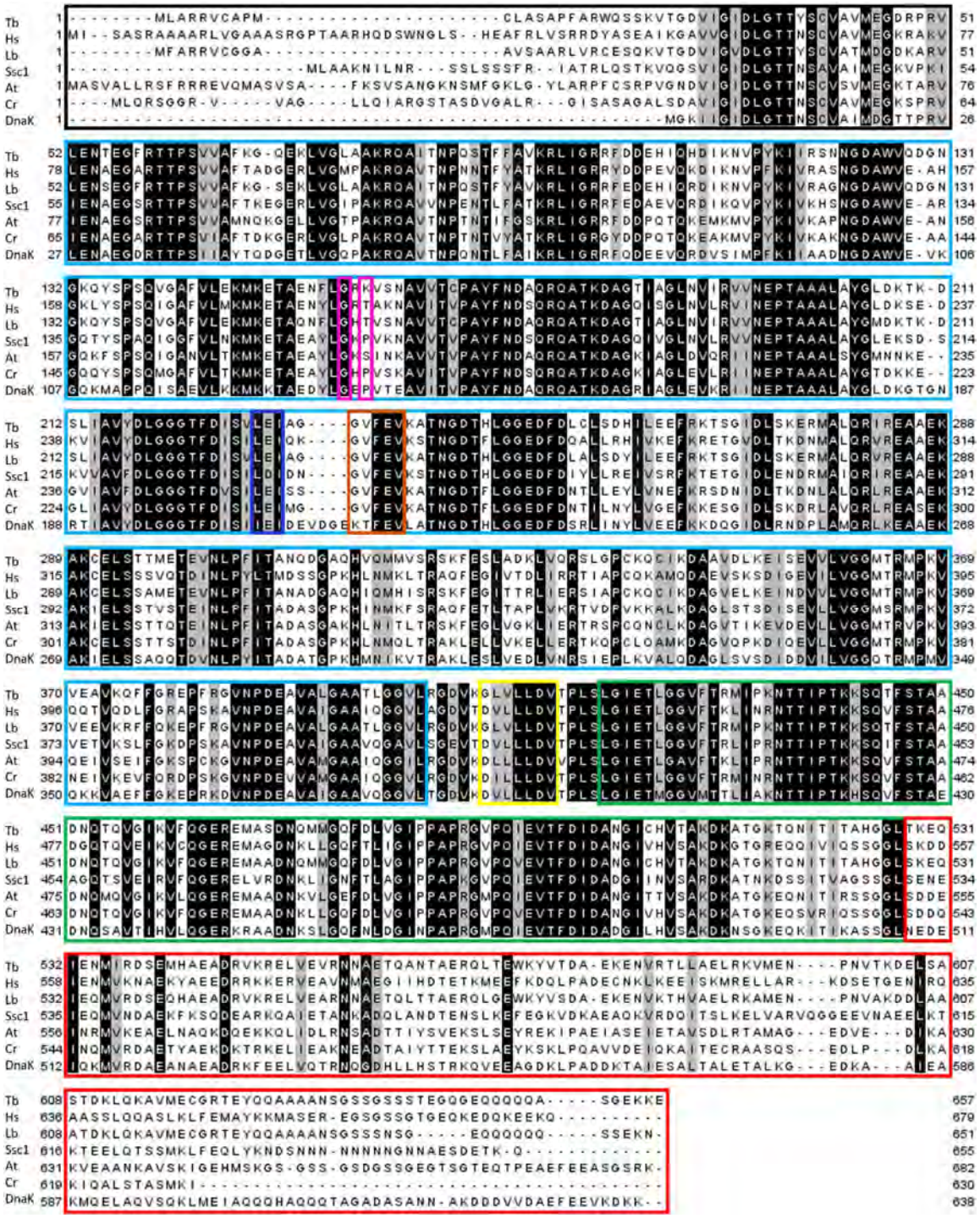


Figure 2.1: Multiple sequence alignment of TbmtHsp70 with previously described orthologues: The accession numbers used were Hs (*Homo sapien*) (NP_004125.3), Tb (*Trypanosoma brucei*) (XP_845493.1), Lb (*Leishmania braziliensis*) (XP_001566868.1), Ssc1 (NP_010884.1), AT (*Arabidopsis thaliana*) (NP_196521.1) and Cr (*Chlamydomonas reinhardtii*) (CAA65356.1), DnaK from *E. coli* (BAA01595.1) was included to allow comparison with a non-aggregating orthologue. The boxes indicate the different segments of the protein as follows: black represents the mitochondrial targeting sequence (MTS), light blue: the NBD, green: the SBDβ, red: the Lid or SBDα. The orange box indicates the GVFEV motif, and the yellow box indicates the conserved linker region, these are involved in interdomain communication and co-chaperone interactions. The pink boxes represent two residues involved in the interaction with Hep1. The dark blue box indicates a motif of interest identified in this study. Shaded residues represent > 70 % conservation with black boxes indicating 100 % conservation.

The highly conserved linker region is crucial for allosteric communication between domains and plays a significant role in mtHsp70 co-chaperone interactions, particularly with those involving JDP stimulation of the NBD (Kityk et al., 2018). The region is known to be involved in the aggregation properties of mtHsp70 with studies suggesting the interaction occurs between the GVFEV motif and the linker as the chaperone cycle proceeds (Blamowska et al., 2010). Evidence indicates that this occurs more often in the presence of ADP and when a nucleotide is absent from the NBD (Buchberger et al., 1995; Blamowska et al., 2010).

The linker motif, DVLLLDV, which is present in other mtHsp70 orthologues (Mayer & Bukau, 2005), has been altered to GLVLLDV in both *L. braziliensis* and *T. brucei* (Figure 2.1). Phylogenetic studies indicate a close evolutionary relationship between the *L. braziliensis* and *T. brucei* orthologues, this suggests that this may be common within the Trypanosomatida order (Figure 2.2). Glycine (G) and aspartic acid (D) display significant physiochemical differences; however, previous studies on *L. braziliensis* mtHsp70 suggest that this alteration has no effect on the aggregation properties of these orthologues (Stephenson & Freeland, 2013; Dores-Silva et al., 2017).

The overall structure of the SBD of mtHsp70 showed that the SBDβ maintained a high degree of conservation across all aligned orthologues and the SBDα was highly variable (Figure 2.1). Secondary structure analysis carried out using Jpred and the consolidated prediction program Quick2D indicated that the structure of the *T. brucei* orthologue maintained the α-helices-rich property (Appendix A1).

A

| | Tb | Hs | Lb | SSC1 | At | Cr |
|---|---|---|---|---|---|---|
| Tb | 100.00 | 59.38 | 86.33 | 58.63 | 58.46 | 63.70 |
| Hs | 59.38 | 100.00 | 60.47 | 63.65 | 61.49 | 66.83 |
| Lb | 86.33 | 60.47 | 100.00 | 57.67 | 59.84 | 65.02 |
| SSC1 | 58.63 | 63.65 | 57.67 | 100.00 | 58.70 | 63.53 |
| At | 58.46 | 61.49 | 59.84 | 58.70 | 100.00 | 70.95 |
| Cr | 63.70 | 66.83 | 65.02 | 63.53 | 70.95 | 100.00 |

B

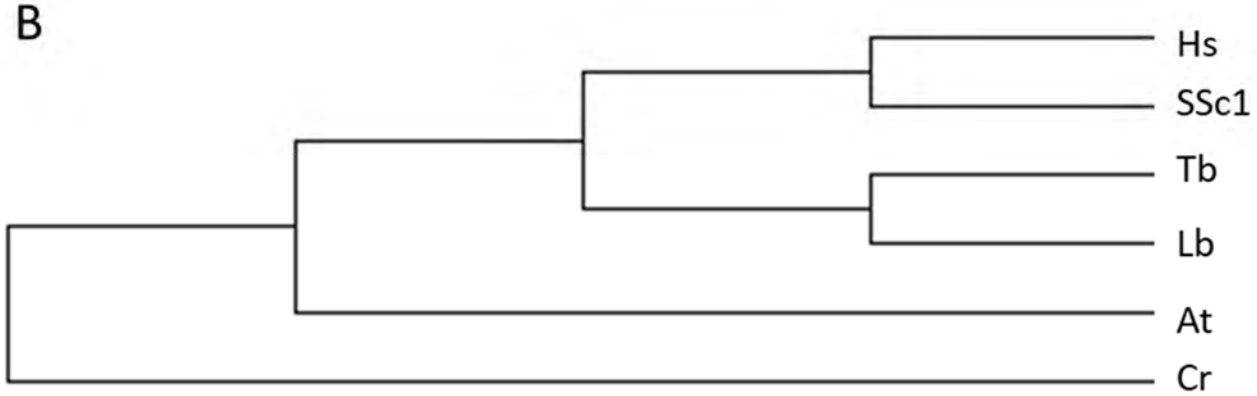


Figure 2.2: Phylogenetic analysis and sequence identity of TbmtHsp70 and orthologues: The accession numbers used were Hs (*Homo sapien*) (NP_004125.3), Tb (*Trypanosoma brucei*) (XP_845493.1), Lb (*Leishmania braziliensis*) (XP_001566868.1), Ssc1 (NP_010884.1), AT (*Arabidopsis thaliana*) (NP_196521.1) and Cr (*Chlamydomonas reinhardtii*) (CAA65356.1). Sequence ID was generated using MAFFT alignments and phylogenetic trees are the result of consensus amongst 1000 bootstrap iterations using a maximum likelihood statistical method following a poission distribution carried out on MEGA11.

The phylogenetic analysis of the aligned sequences indicated that no mtHsp70 orthologue had a sequence identity lower than 50 % (Figure 2.2A), this is likely due to the high conservation of mtHsp70 across all species suspected to be the result of convergence between mitochondrial chaperones involved in iron-sulfur cluster biogenesis (Schilke et al., 2006; Kleczewska et al., 2020). The orthologue from *L. braziliensis* showed the highest sequence similarity to *T. brucei* at 86 %, reflecting their shared evolutionary relationship as part of the Trypanosomatida order (Figure 2.2A). The lowest evolutionary relationship was observed with the orthologues from *A. thaliana* and *C. reinhardtii*, reflecting the evolutionary origin of these orthologues within the plant kingdom. The lowest sequence similarities were observed in *A. thaliana* (58 %) and Ssc1 (59 %) which is indicative of the uniquely structured *S. cerevisiae* mtHsp70 machinery in which multiple unique mtHsp70 paralogues are present as a result of expansion via gene duplication (Figure 2.2) (Schilke et al., 2006).

Structural modelling of mtHsp70 is lacking and no full-length models have been generated via X-ray crystallography or NMR. The generation of models for DnaK and cytosolic eukaryotic Hsp70s have been impeded by the dynamic movement of the domains. However, recent studies have achieved the generation of full-length models of DnaK, these were produced via X-ray diffraction through the combination of peptide-fusion in the SBDβ, nucleotide saturation and the use of various point-mutations to cysteines which allowed the arresting of domain movement through the formation of disulfide bonds, the combination of these approaches allowed the generation of DnaK models in multiple states (Grindle et al., 2021; Wang et al., 2021).

With the recent release of the AI-driven modelling software Alphafold an opportunity was provided to examine the orthologues of DnaK which exhibit a tendency to aggregate using a new method which has been shown to produce highly accurate protein predictions but has not yet been extensively used in the examination of mtHsp70 (Jumper et al., 2021). The model generated provides insights into the structural arrangement of mtHsp70 which may indicate how the previously described conserved motifs influence mtHsp70 properties (Figure 2.3).

The model does correlate with the biochemically produced model of DnaK (Wang et al., 2021) and the structural layout of the individual domains of mtHsp70 within the Alphafold-generated model (Figure 2.3) correlated strongly with previously generated structures of the individual domains of other orthologues (data not shown). Through the examination of the domain arrangements, it can be deduced that the model generated does closely resemble the closed state of DnaK previously produced by Wang et al. (2021). In this state ATP is bound within the NBD but no peptide-substrate is present within the SBDβ, this observation is further validated as the structure does correlate with previous studies undertaken by (Kityk et al., 2018) which describe the docking of the SBD to the NBD in the closed state.

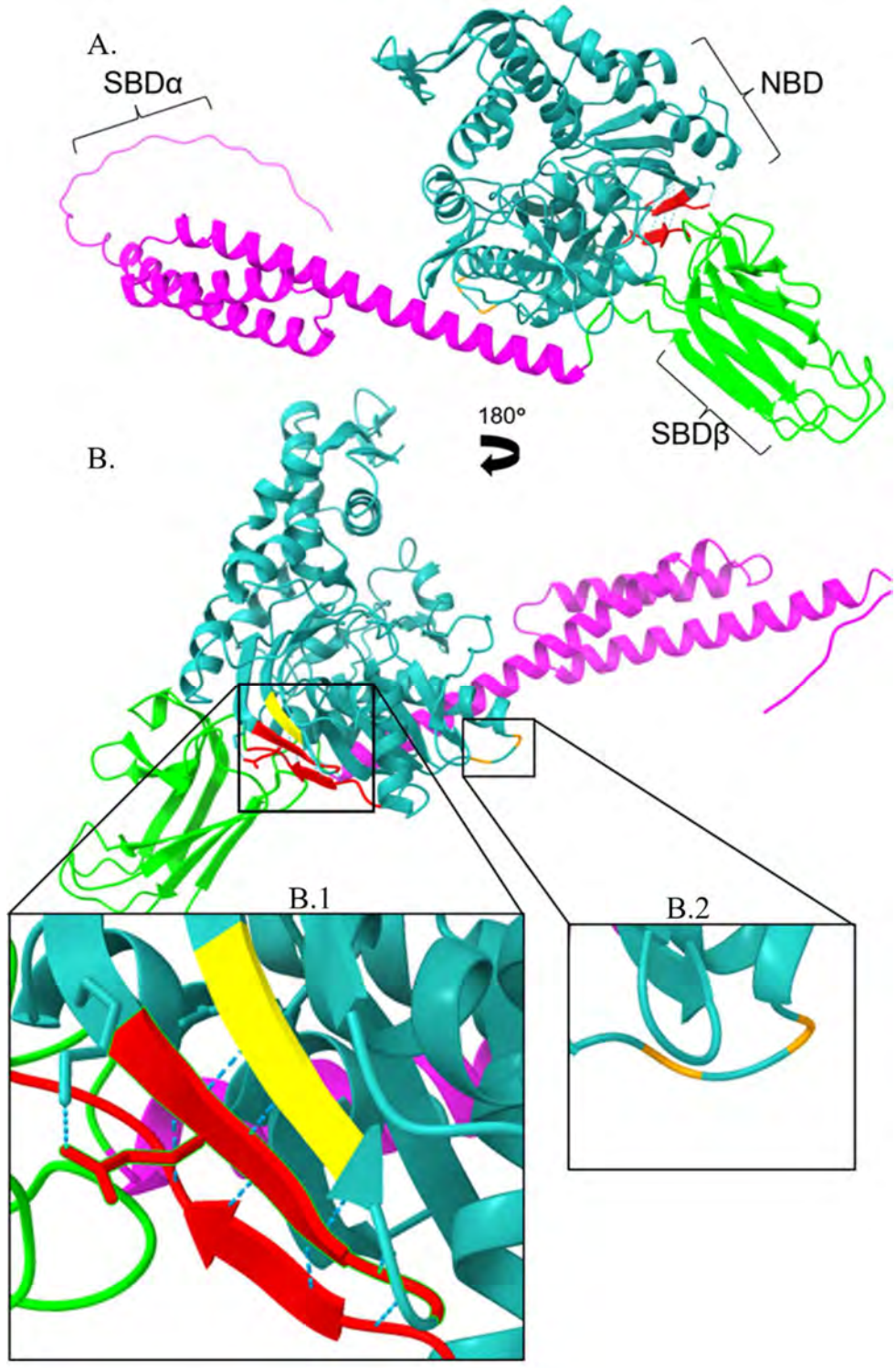


Figure 2.3: Structural prediction of *T. brucei* mtHsp70: The model was generated using Alphafold using the TbmtHsp70 UniProt code: Q585X3 as the input data, (A): The full model with domains and SBD subdomains indicated. (B) The model rotated approximately 180 degrees to indicate the highly conserved motifs of interest. (B.1) Highlight of the linker and GVFEV motif regions associated with aggregation properties displayed in red with the GVFEV motif outlined in green and a possible contributing LEI motif in yellow with hydrogen bonds in the region displayed in blue. (B.2) The G157 and K159 residues are theorized to play a role in the solubilizing interaction with Hep1 (shown in orange).

The Alphafold-driven generation of this model is therefore advantageous to this research as the release of the peptide product and transition to the closed state has previously been implicated as the point within the catalytic cycle of mtHsp70 in which the allosteric interaction between domains results in the aggregation of mtHsp70, in the absence of Hep1, which is exacerbated by the absence of ATP. The models produced of DnaK are less applicable as the orthologue does not aggregate and has no *E. coli* Hep1 orthologue; however, the structural arrangement does provide some validity to the model produced using Alphafold as the structural layout correlates closely with the DnaK model from Wang et al. (2021). These recent models allow for a visualization of what may be occurring during the aggregation of mtHsp70 as they allow the linker region and SBD to be included when viewing the GVFEV motif located in the NBD (Figure 2.3) that has been implicated in the aggregation of mtHsp70 via interactions with the linker region (Blamowska et al., 2010). The model generated indicates that in this state the GVFEV (234-238) motif is arranged parallel and within close proximity to the GLVLLDV (408-414) linker region, forming four hydrogen bonds located between G234-V410, F236-V410, F236-L412 and V238-L412 (Figure 2.3).

Previous investigations have replaced the GVFEV motif of Ssc1 with KTFEV from DnaK and have brought about the abrogation of Ssc1 aggregation (Blamowska et al., 2010). Examination of this area in DnaK using Alphafold indicates that there is little difference between the bonds which form between the linker region and the KTFEV motif relative the linker-GVFEV motif bond arrangements within TbmtHsp70. However, the presence of lysine (K) in DnaK results in multiple bonds forming between the nitrogen located at the sidechain terminal of lysine and a region buried within the NBD located between the IIa and Ia subdomains (Appendix A2 and A3). The presence of the lysine (K)-NBD bonds may result in an increase in the proximity between the linker and KTFEV residues, thereby introducing enough stress within this region to disrupt or avoid the formation of these bonds as the protein alternates between states. This may be a contributing factor to the prevention of aggregation between the domains of DnaK which would occur in a manner that is abrogated by the short glycine residue in the GVFEV motif of aggregating mtHsp70s. It must be stressed that cytosolic Hsp70s such as HSPA1A from *H. sapiens* do not have this lysine residue, however, cytosolic Hsp70s have remarkably dissimilar sequence and structural layouts in comparison to their mitochondrial counterparts (Moro et al., 2005).

Another region that should be investigated is a stretch of 3 amino acids: LEI, displayed in yellow (Figure 2.3) and indicated by a dark blue box (Figure 2.1). These residues may represent a motif of interest in this region as the glutamic acids (E) of both LEI and the GVFEV motif form multiple strong bonds (Figure 2.3). This may be important as this motif was maintained in all aligned mtHsp70 orthologues except for Ssc1 (Figure 2.1), in which glutamic acid is replaced by aspartic acid which exhibits similar chemical properties and has been shown to be capable of functionally and structurally replacing glutamic acid (Stephenson & Freeland, 2013). This motif is not maintained in DnaK or cytosolic Hsp70s and may represent a contributing factor in the aggregation of mtHsp70. This warrants future mutation studies to observe if mtHsp70 aggregation is influenced by the alteration of one or both glutamic acids to uncharged amino acids.

### 2.4.2 Sequence alignment and analysis of TbHep1

Multiple sequence alignment was undertaken to assess the sequence similarity between the Hep1 orthologue found within *T. brucei* and those found in *A. thaliana*, *C. reinhardtii*, *S. cerevisiae*, *H. sapiens* and *L. braziliensis.* Previously, the classification of Hep1 within a cell was based on sequence identity and localization to the mitochondria with those found in plant cells being an exception as multiple paralogues in plants have been identified as part of the zinc-ribbon (ZR) proteins with Heps being identified as both mitochondrial (Hep1) and plastidic (Hep2) (Kluth et al., 2012). Recent investigations have altered this view as human Hep1 has been identified as localizing to the nucleus of human cells (Dores-Silva et al., 2021).

Hep1 localized within the mitochondria of *T. brucei* was identified and denoted as TbHep1 (Bentley et al., 2019). Currently, several Hep1 orthologues have been identified as being capable of suppressing the thermally induced aggregation of their respective mtHsp70s, these include orthologues from *L. braziliensis* (LbHep1, XP_001565573.1), *S. cerevisiae* (ScHep1, AAS56692.1), *A. thaliana* (AtHep1 (ZR3), NP_974434) and *C. reinhardtii* (CrHep2, XP_042922817.1).

In this study, these orthologues and their interacting mtHsp70s have been the focus of comparative sequence and structural analyses. This property is not exclusive to the identified Hep1 orthologues as the Hep1 found within *P. falciparum* (PfHep1) has also been identified and the ability of the orthologue to suppress PfHsp70-3 aggregation has been confirmed (Nyakundi et al., 2016). *P. falciparum* orthologues were not included in this study as these show a strong divergence from other orthologues which is suspected to be a result of the unique evolution of *P. falciparum* with PfHep1 exhibiting the addition of large asparagine stretches, as is common within the *P. falciparum* genome (Caro et al., 2014). Multiple sequence alignments were initially carried out to identify if *T. brucei* retained the conserved sequences and motifs previously identified as important to the Hep1 – mtHsp70 interaction (Figure 2.4).

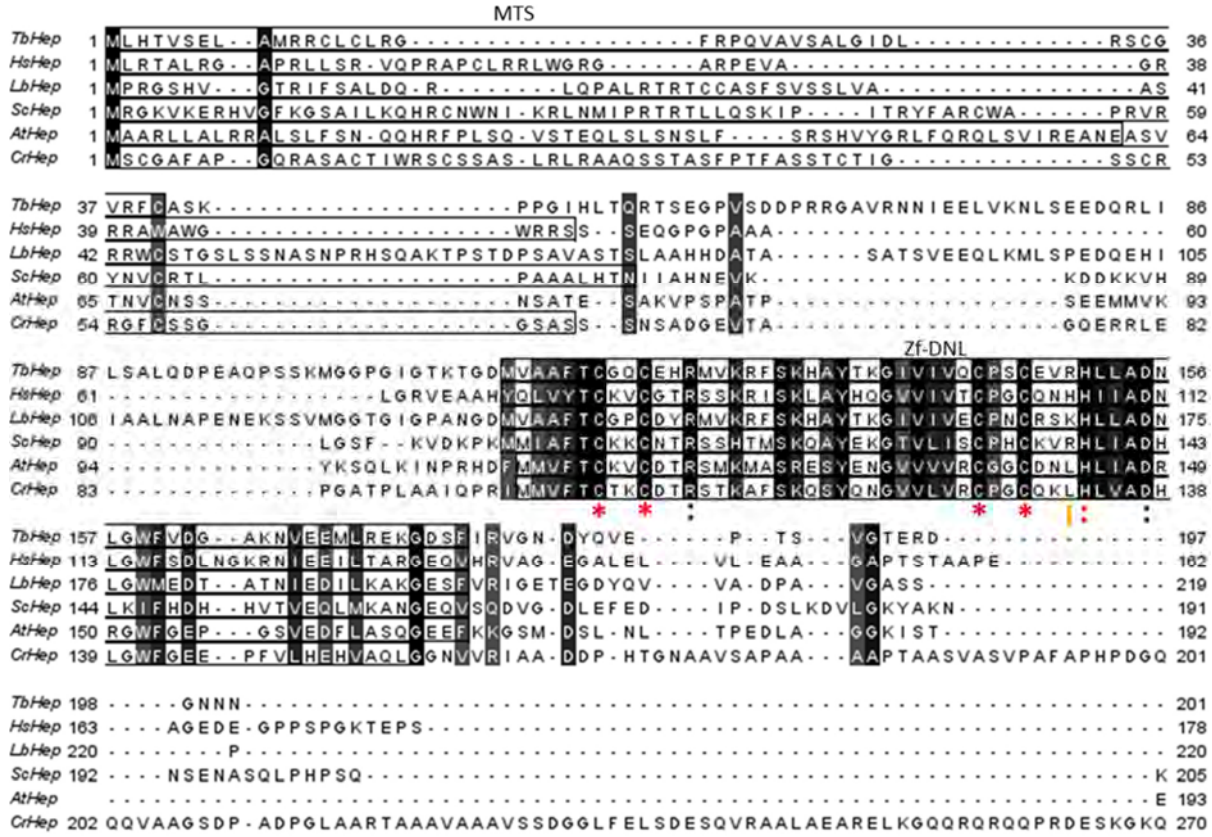


Figure 2.4: Multiple sequence analysis of TbHep1: Multiple sequence alignment of TbHep (XP_843824.1) and HsHep (NP_001074318.1) with previously studied orthologues from: *L. braziliensis* (LbHep, XP_001565573.1), *S. cerevisiae* (ScHep, AAS56692.1), *A. thaliana* (AtHep (ZR3), NP_974434), *C. reinhardtii* (CrHep, XP_042922817.1). The approximate mitochondrial/chloroplast targeting sequences and zinc-finger domains (zf-DNL) are displayed in labelled boxes with conserved residues (≤ 70%) indicated by dark boxes and black boxes indicating 100% conservation. The tetra-cysteine motif (CXXC) necessary for the interaction with mtHsp70 is indicated by red stars and those residues involved in the interaction with mtHsp70 are indicated by a colon with the histidine residue necessary for the ATPase stimulation indicated by a red colon. The unconserved residue involved in the interaction with Ssc1 from *S. cerevisiae* is indicated by a yellow line.

The tetracysteine-motif common to zf-DNL domains consisting of two CXXC motifs separated by 21 amino acids localizing the zinc-ion within the binding pocket of Hep1 was maintained in the *T. brucei* orthologue (Figure 2.4). Mutational studies conducted on these cysteines in which one from each motif was altered to serine have been shown to abrogate the ability of Hep1 to solubilize mtHsp70 in yeast cells (Yamamoto et al., 2005). The presence of this motif indicates that TbHep1 may maintain the solubilizing interaction exhibited by other orthologues.

The residues R81 and D111 have been shown to reduce the binding affinity of HsHep1 with mortalin when altered to tryptophan (Zhai et al., 2011). The H107 residue is crucial to the ATPase stimulating effect identified in HsHep1 as the mutation of this residue to tryptophan removed the ability to stimulate the NBD of mortalin (Zhai et al., 2011), this residue is maintained across all aligned orthologues although currently the ATPase stimulating property has only been confirmed in HsHep1 and LbHep1 (Dores-Silva et al., 2017). The D111, H107 and R106 residues have also been identified as important in the regular growth of yeast cells with their alteration resulting in mtHsp70 aggregation and reducing mitochondrial protein import (Momose et al., 2007). The R106 residue is not maintained within other orthologues although it is found in *T. brucei* (Figure 2.4) and the residue within the non-plant/algae-derived orthologues has been altered to H or K which have comparable physiochemical properties to arginine (Stephenson & Freeland, 2013).

The N-terminal region of the zf-DNL is significantly longer in the parasitically derived orthologues TbHep1 and LbHep1, a property not shared by the other aligned orthologues which suggests there may be more substantial structural arrangements here which are unique to the kinetoplast family. The region on the C-terminal side of the zf-DNL is very short in these two orthologues, a trait shared by all aligned orthologues apart from *C. reinhardtii* which displays an extended C-terminal region. This difference between *C. reinhardtii* and other orthologues could also be observed in the phylogenetic analysis (Figure 2.5).

A

| | TbHep1 | HsHep1 | LbHep1 | ScHep1 | CrHep1 | AtHep1 |
|---|---|---|---|---|---|---|
| TbHep1 | 100.00 | 33.33 | 45.70 | 27.95 | 28.05 | 23.23 |
| HsHep1 | 33.33 | 100.00 | 34.93 | 24.24 | 32.76 | 32.89 |
| LbHep1 | 45.70 | 34.93 | 100.00 | 30.30 | 30.18 | 27.78 |
| ScHep1 | 27.95 | 24.24 | 30.30 | 100.00 | 25.00 | 25.14 |
| CrHep1 | 28.05 | 32.76 | 30.18 | 25.00 | 100.00 | 28.81 |
| AtHep1 | 23.23 | 32.89 | 27.78 | 25.14 | 28.81 | 100.00 |

B

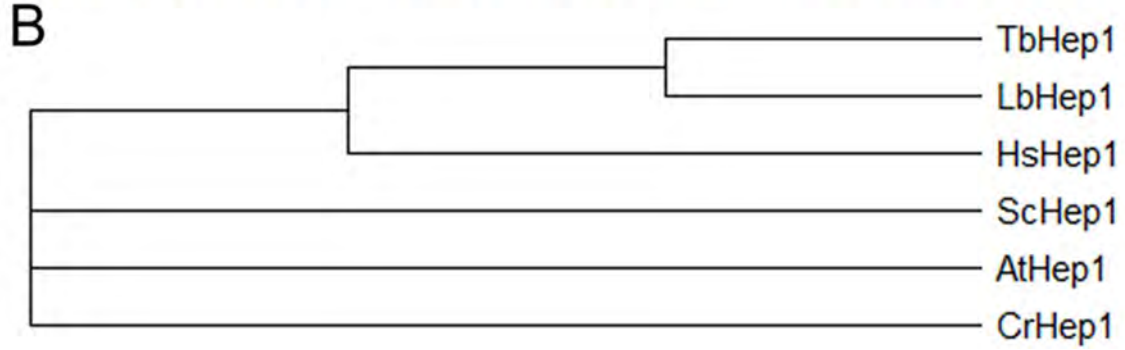


Figure 2.5: Sequence Identity and phylogenetic analysis of TbHep1 and orthologues: *H. sapiens* (HsHep1, NP_001074318), *L. braziliensis* (LbHep1. XP_001565573), *S. cerevisiae* (ScHep1, AAS56692.1), *A. thaliana* (AtHep1 (ZR3), NP_974434, UniProt: F4JE34), *C. reinhardtii* (CrHep1, XP_042922817.1). (A) Displays the percentage of sequence identity between TbHep1 and other orthologues generated by a tCOFFEE analysis. (B) A phylogenetic tree of TbHep1 was generated using a tCOFFEE alignment followed by the result of consensus amongst 1000 bootstrap iterations using a maximum likelihood statistical method following a poission distribution carried out on MEGA11.

The average sequence identity of the Hep1 orthologue was low with no orthologues being above 50 % identity, this correlates with previous studies in which Hep1 has been shown to have strong divergences between orthologues with the only areas of conservation found within the zf-DNL domain. The highest sequence identity was observed between TbHep1 and LbHep1 at 45 % and the proteins show the closest phylogenetic relationship, with both represented within the same sub-group (Figure 2.5). This is not surprising as both emanate from parasitic members of the kinetoplast family, TbHep1 also displayed a 33 % sequence identity with HsHep1. These results correlate with the phylogenetic analysis conducted on the Hep1 orthologues in which TbHep1, LbHep1 and HsHep1 were grouped within the same tree and the remaining orthologues were observed as divergent from TbHep1 and one another with *A. thaliana* representing the lowest similarity at 23 % (Figure 2.5). The results of the phylogenetic analysis indicate that TbHep1 is most closely related to LbHep1 followed by HsHep1 (Figure 2.5), which may suggest that the property of NBD stimulation may be shared by this orthologue.

### 2.4.3 A comparison of Hsp70 escort protein models produced using Swissmodel and Alphafold

Initially the structural analysis of TbHep1 was undertaken using the Swissmodel program, this approach was not ideal as models of Hep1 are limited to the NMR resolved zf-DNL domain structure of the yeast orthologue Tim15c, with short stretches of amino acids on either side (Figure 2.6). The Swissmodel program is a useful tool in bioinformatic analysis, however, the results depend on the models available. The sequence identity between the two orthologues is approximately 28 % (Figure 2.5A) overall, with this increasing to 38 % within the modelled zf-DNL domain. The model of TbHep1 produced resembles the template structure (Figure 2.6 A) and was initially validated by analysis with the secondary structure prediction software Jpred which estimated that only disordered regions were located outside the zf-DNL (Drozdetskiy et al., 2015).

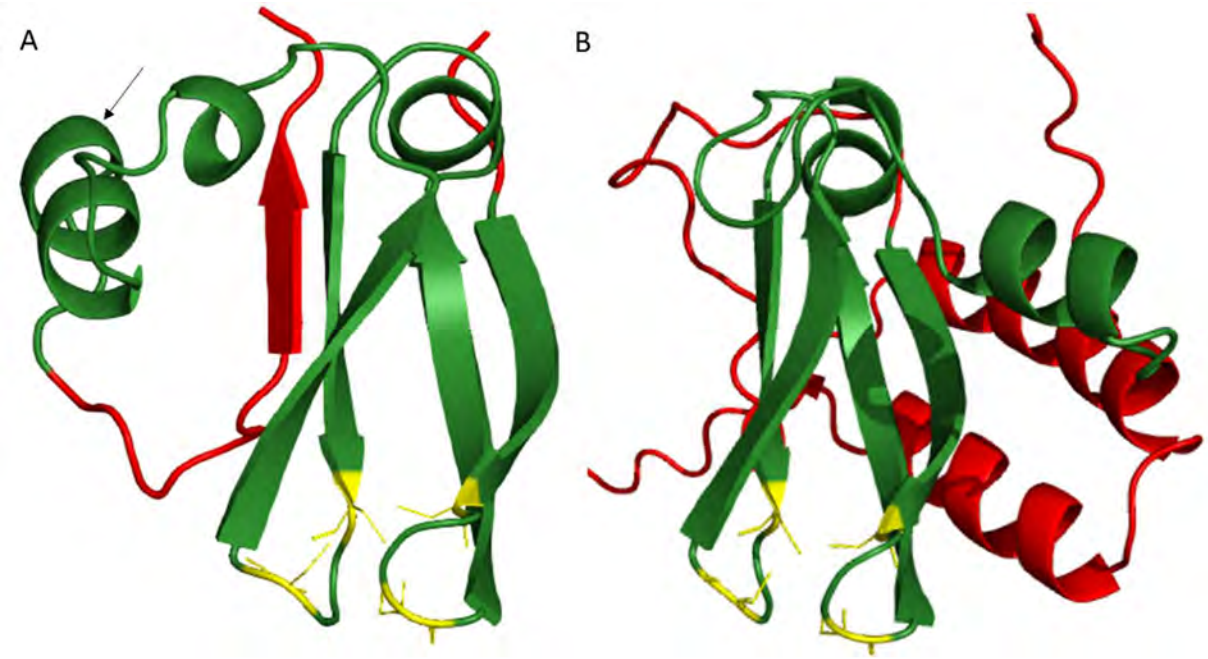


Figure 2.6: Comparison of TbHep1 models: TbHep1 (UniProt: Q582U3) was used as the input for both Alphafold and Swissmodel, the template sequence used in Swissmodel was Tim15c (UniProt: P42844), and images were visualized using Pymol. (A) TbHep1 model generated using Swissmodel displaying the zf-DNL (Green), tetra-cysteine motif (Yellow) and flanking regions (Red) with an arrow indicating the zf-DNL α-helices structure of interest. (B) TbHep1 model generated using Alphafold and coloured using the same scheme as A.

Previously the zf-DNL structure has been described as L-shaped (Momose et al., 2007), referring to the β-sheet sandwich making up the binding pocket which is perpendicular to the coil structures

indicated by the arrow (Figure 2.6A). The model of TbHep1 produced using Alphafold differs to the previous description, the structure of Tim15 (Appendix A4) was then examined to verify if this was unique to TbHep1. The Alphafold structures produced consistently arrange the previously perpendicular coiled structure to a position directly above the zf-DNL binding pocket (Figure 2.6B), resulting in a more globular structure than that produced via Swissmodel and eliminating the distinctive L-shape previously described with only a loop structure of approximately 10 amino acids located perpendicular to the binding pocket. The other structural difference evident is the presence of a β-sheet proceeding the zf-DNL within the Swissmodel derived structures, arranged parallel to the binding pocket (Figure 2.6A). This structure is not present within the Alphafold-derived model where this region is regarded as disordered in the TbHep1 model, while in yeast models this region extends into short, coiled structures, although these are regions of low to very low confidence and secondary structure predicting programs have little consensus in the area.

The area of most significance to this study is the long N-terminal region of the TbHep1 orthologue (Figure 2.6B), this region was not present in models created using the NMR-derived structure. Within the TbHep1 Alphafold model, this region of approximately 30 amino acids forms two α-helical structures arranged alongside the binding pocket of the zf-DNL (Figure 2.6B) with the first coil structure regarded as low confidence but the second described as confident by Alphafold (Appendix A5). Investigating this region using JPred indicates only disorder within this region, however, after identification of these structures using Alphafold further analysis was carried out using Quick2D, a consolidated secondary structure prediction program which incorporates several different predictive programs and presents the results of each (Zimmermann et al., 2018; Gabler et al., 2020) (https://toolkit.tuebingen.mpg.de). Using this predictive analysis there was consensus with the secondary structure prediction software programs PSIPred, Spider3, PSSPred4, DeepCNF and NetSurfP2 which indicated the presence of at least one of the coil structures with PSSPred4 and DeepCNF predicting both (Appendix A6) (Jones, 1999; Yan et al., 2013; Wang et al., 2016; Heffernan et al., 2017; Klausen et al., 2019;) with only the SpotD disorder predicting program indicating disorder across the whole region (Hanson et al., 2017).

The same extended N-terminal region in the other kinetoplast orthologue, LbHep1 could not be examined using Alphafold as this structure has not yet been determined using the software. This is

unfortunate as LbHep1 has been characterized using biochemical studies; however, relative to TbHep1 there was less consensus regarding this region amongst the secondary structure predicting software of Quick2D and more consensus amongst those programs predicting disorder (Appendix A7). However, HsHep1 showed a relatively close relationship to the two orthologues and could be generated using Alphafold. Comparisons of HsHep1 and TbHep1 models were therefore produced and superimposed using the ChimeraX model viewing software (Pettersen et al., 2021) (Figure 2.7).

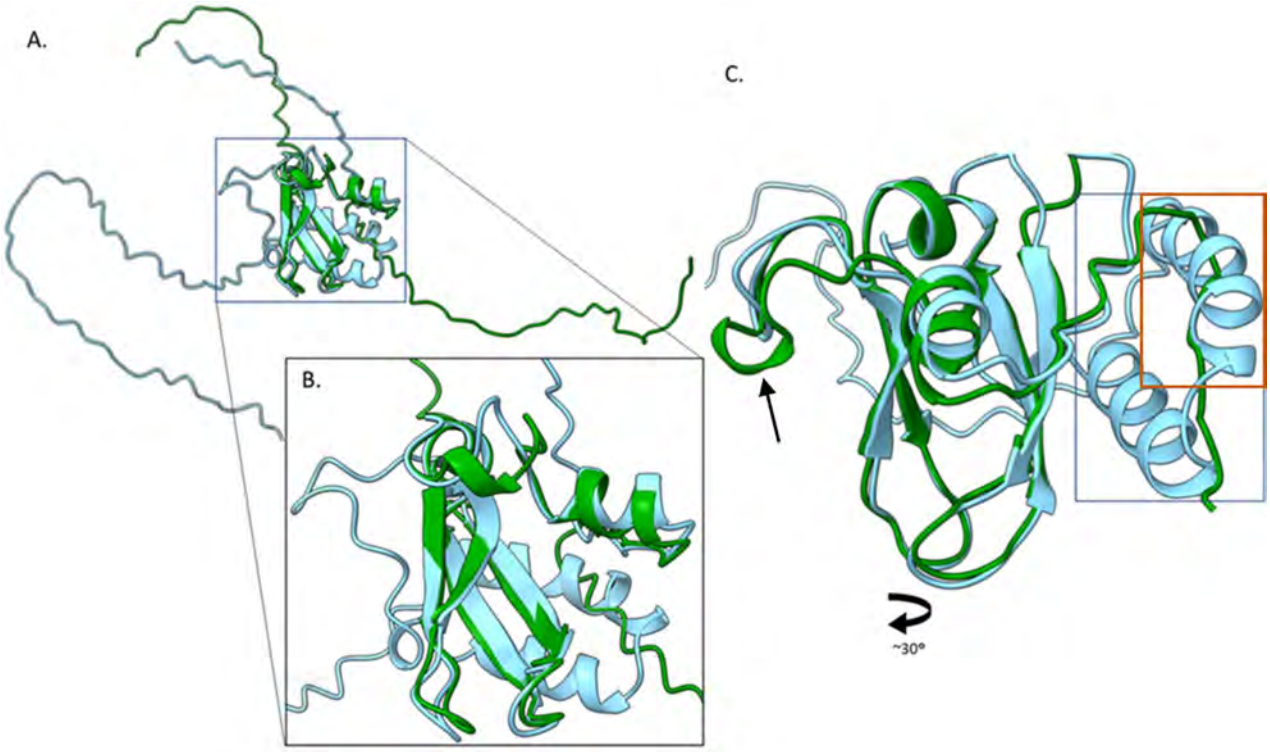


Figure 2.7: Structural comparison TbHep1 and HsHep1: TbHep1 (Cyan, PDB: Q582U3 ) and Human Hep1 (Green, PDB: Q5SXM8 ) were used as input sequences in Alphafold, the resultant models were matched and imaged in ChimeraX. (**A**) The full representation of the superimposed models, (**B**) Areas of confidence ( >70 % ) consisting primarily of the zf-DNL with the binding pocket located between the β-sheet sandwich in the center, (**C**) The zf-DNL rotated left by ~ 30° with a box indicating two α-helices unique to *Tb*Hep1 that may act as a dimerization point and an orange box indicating the first α-helices which has lower confidence (50 – 70 %). An arrow indicates a difference between the Hep1 models within the zf-DNL.

A significant portion of the HsHep1 structure is superimposable over TbHep1 within the zf-DNL, apart from a loop structure arranged perpendicular to the binding pocket in which HsHep1 has a small fragment of an α-helices structure which is absent in TbHep1 (Figure 2.7C). The models have significant differences outside of the zf-DNL, particularly in the N-terminal region. The N-terminal region of HsHep1 consists of only a short, disordered region (Figure 2.7B, Green); however, TbHep1 has the previously described α-helical structure that may influence the biochemical properties of the

orthologue. These structures are often indicative of a dimerization point in other proteins and may impart the property on this orthologue. HsHep1 has been shown to dimerize; however, this has only been observed in adverse conditions such as thermal stress and at high protein concentrations (2 mg/mL) (Dores-Silva et al., 2021). HsHep1 dimerization has also been observed as a hindrance as the protein functions as a monomer (Dores-Silva et al., 2021). The presence of the α-helical structures in TbHep1 may indicate that this orthologue operates in a different manner to the *H. sapien* orthologue. The need for new NMR-derived Hep1 models, using the advancements made in NMR techniques over the last decade, is required to confirm these results and allow comparisons to be made with the Alphafold-derived model, particularly with regard to the placement of the α-helix that determined the L-shape described in Momose et al. (2007).

### 2.4.4 An analysis of *T. brucei* mtHsp70 JDP machinery and the relationship to TbHep1

The Hsp70 superfamily is highly conserved across all organisms; however, the evolutionary progression of the chaperone and that of the co-chaperones and co-factors which interact with it has been shown to be dynamic. Studies indicate that heat shock machinery can be highly adapted to the species in which it is found, this process is especially prevalent within the Trypanosomatida order (Drini et al., 2016). It has been shown that phylogenetic analysis of Hsp70 is a viable approach when classifying the members of this order into species and clades as analysis of small subunit ribosomal RNA (SSU-rRNA) has a strong correlation with that of Hsp70 divergence between trypanosomes (Fraga et al., 2016). The proliferation of Hsp70 machinery within trypanosomes is substantial and several orthologues unique to *T. brucei* have been identified which bare mutations theorized to play specialized roles in the survival, transmission and proliferation of the parasite (Bentley et al., 2019).

MtHsp70 has less divergence between species than cytosolic Hsp70 and often exhibits more similarity to prokaryotic DnaK than cytosolic Hsp70s (Moro et al., 2005). These genes are often duplicated, *T. brucei* has three identical gene copies of *mtHsp70* and a considerable collection of interacting JDPs, this extensive proliferation is unique to the Trypanosomatida order and is

suspected to be a product of the differing roles in the lifecycle of the parasite (Drini et al., 2016; Bentley et al., 2019). Proteomic data indicates that mtHsp70 and the accompanying mitochondrial J-proteins are found in less abundance in the bloodstream form (BSF) of the parasite, which is initially unexpected as this is the point of highest stress in the lifecycle of the parasite; however, most mitochondrial proteins are reduced in this form due to the abundance of glucose substrate within the blood which results in a reduction of mitochondrial metabolic processes as this is shifted to direct glycosomal-based glycolysis (Lopes et al., 2010).

The mitochondrial Hsp70 machinery is vital to the survival, proliferation, and disease progression of the parasite, this is evident from the duplication of *mtHsp70* genes and the number of JDPs theorized to be within the genome of the species. Of the 67 identified JDPs, a significant portion (~ 17) are predicted to be located within the mitochondria (Bentley et al., 2019). Many of these JDPs have no currently identified human orthologue and their specific functions are unknown as few have been studied. However, studies carried out using RNAi knockdown methods on TbJ2 have shown this type-I JDP is vital to the normal growth of the parasite (Ludewig et al., 2015).

The proliferation of Hsp70 machinery within Trypanosoma, as well as several identified repair pathways utilizing a diverse range of kinases, has made it a candidate to become a model organism in the study of heat shock protein functionality (Folgueira et al., 2007). The Hsp70 machinery and how JDPs contribute to the diverse range of Hsp70 interactions may be a focus of interest, particularly within the mitochondria due to the extensive development of this organelle within the kinetoplast class as a whole (Folgueira et al., 2007). The proliferation of this machinery is best exemplified by the abundance of type-III JDPs as seen in Table 1 and is reflected in the non-mitochondrial J-proteins with an overall 56 of the 67 J-proteins identified within these species classified as type-III (Bentley et al., 2019).

Table 1: Comparison of *T. brucei* and *H. sapien* mitochondrial machinery. Collated from previous proteomic studies with JDPs suspected to be involved in mtHsp70 operations within *T. brucei* based on function and localization with Mt and Glyc indicating the mitochondria and glycosome respectively.

| A) Proteins involved in the operations of MtHsp70 and Hep1 found within *H.sapiens* and *T.brucei* | | | | | | |
|---|---|---|---|---|---|---|
| *H.sapien* Name: | *H.s* Gene ID | *T.brucei* Name: | Localisation: | TriTrypDB ID (*T.b*) | Reference: | Function |
| MtHsp70 | HSPA9 | MtHsp70 (A/B/C) | Mt , Cell surface | A) Tb927.6.3740<br>B)Tb927.6.3750<br>C)Tb927.6.3800 | Panigrahi et al. 2009<br>Niemann et al. 2013<br>Shimogawa et al. 2015 | |
| Hep1 | DNLZ | Hep1 | Mt | Tb927.3.2300 | Bentley et al. 2018 | mtHsp70 Solubilization |
| GrpE1 | GrpEL1 | GrpE1 | Mt, NUC | Tb927.6.2170 | Berriman et al. 2005 | Protein import-MITO<br>Protein folding |
| Tid-1 | DNAJA3 | J50 | Mt | Tb927.9.12730 | Týč et al. 2015<br>Acestor et al. 2009<br>Niemann et al. 2013 | Protein aggregation and folding<br>mtDNA maintenance |
| MCJ | DNAJC15 | J27 / J8 | Mt, Glyc | Tb927.9.8410 | Hatle et al. 2013<br>Guther et al. 2014<br>Niemann et al. 2013<br>Acestor et al. 2009 | Protein aggregation and folding<br>mt DNA Maintenance<br>Mt Import * |
| JAC1 | DnaJC20 | J36 | Mt | Tb927.3.1760 | Mokranjac et al. 2003<br>Uhrigshardt et al. 2010<br>Acestor et al. 2009 | FeS cluster Biosynthesis |
| Pam18 | DnaJC19 | J68 | Mt | Tb927.8.6310 | Ashburner et al. 2000 | Protein import-Mt |
| B) *T.brucei* J-proteins involved in mitochondrial protein quality control operations: | | | | | | |
| Type: | *T.brucei* Name: | Localisation: | TriTrypDB ID (*T.b*) | Reference: | Function | |
| III | J1 / J5 | Mt | Tb927.11.16980 | Ashburner et al. 2000<br>Niemann et al. 2013<br>Panigrahi et al. 2009 | Protein folding<br>Protein import- Mt | |
| | J18 | Mt | Tb927.11.1010 | Ashburner et al. 2000<br>Acestor et al. 2009<br>Peikert et al. 2017 | Protein import - Mt | |
| | J21 | Mt, Glyco | Tb927.7.540 | Panigrahi et al. 2009<br>Guther et al. 2014<br>Peikert et al. 2017 | Protein import | |
| | J23 | Mt | Tb927.10.13830 | Ashburner et al. 2000<br>Acestor et al. 2009<br>Niemann et al. 2013 | Protein import - Mt | |
| | J26 | Mt, Glyco | Tb927.7.6200 | Ashburner et al. 2000<br>Acestor et al. 2009<br>Niemann et al. 2013<br>Guther et al. 2014 | Protein import - Mt | |
| | J28 | Mt | Tb927.7.740 | Ashburner et al. 2000<br>Panigrahi et al. 2009<br>Peikert et al. 2017 | Protein import - Mt | |
| | J38 | Mt | Tb927.6.3730 | Ashburner et al. 2000<br>Panigrahi et al. 2009<br>Peikert et al. 2017 | Protein import - Mt | |
| | J44 | Mt | Tb927.8.7010 | Ashburner et al. 2000<br>Panigrahi et al. 2009<br>Peikert et al. 2017 | Protein import - Mt | |
| | J48 | Mt | Tb927.8.1030 | Ashburner et al. 2000<br>Panigrahi et al. 2009<br>Peikert et al. 2017 | Protein import - Mt | |
| | J49 | Mt | Tb927.6.2480 | Ashburner et al. 2000<br>Panigrahi et al. 2009<br>Peikert et al. 2017 | Protein import - Mt | |
| | J65 | Mt | Tb927.4.880 | Ashburner et al. 2000 | Protein folding | |
| | J67 | Mt | Tb927.10.5180 | Ashburner et al. 2000 | Protein folding | |
| IV | J47 | Mt | Tb927.1.1230 | Panigrahi et al. 2009 | Protein Folding | |

Due to this multiplication of JDP machinery, *T. brucei* provides an opportunity to investigate the hypothesis put forward by Burri et al. (2004), that Hep1 may operate as the zinc-finger for type-III JDPs, particularly those recruited to the translocase of the inner membrane (TIM) complex. To further this investigation a phylogenetic analysis was carried out using the mitochondrial JDPs of *T. brucei* to identify any significant evolutionary relationship that may be present between these JDPs and TbHep1 (Figure 2.8). A similar analysis was also carried out on HsHep1 using a large collection of identified JDPs within the human genome to identify any similarities between these Hep1 orthologues and their respective cohorts of JDPs, the results for this *H. sapien* analysis can be found in Appendix A8.

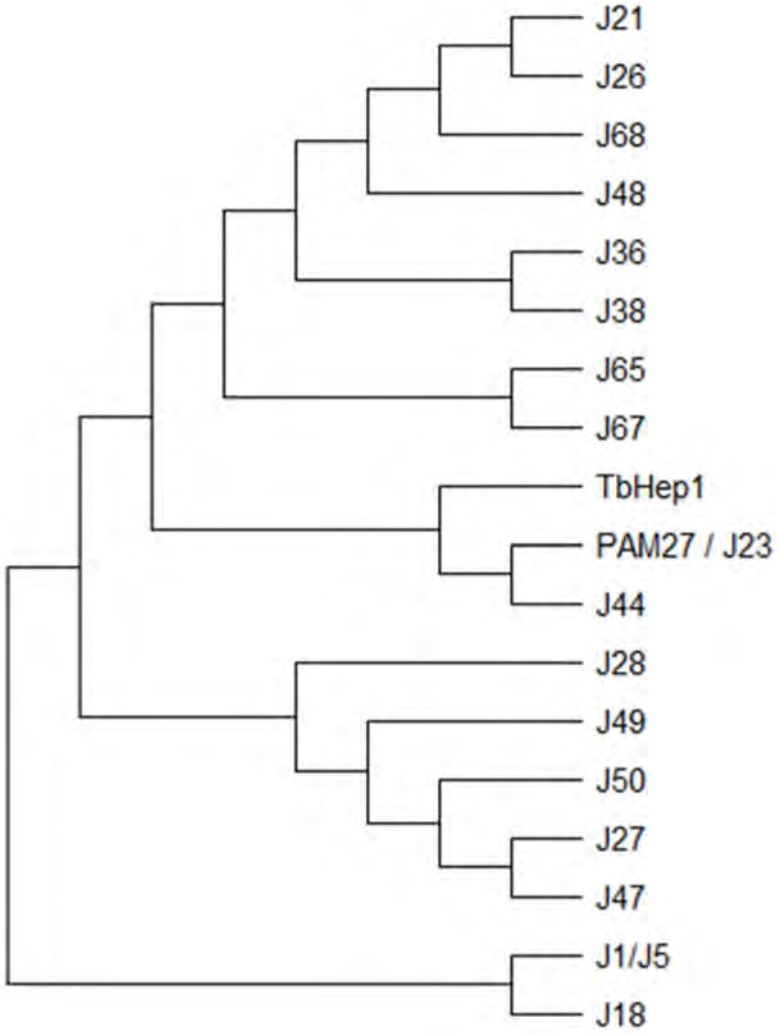


Figure 2.8: Phylogenetic analysis of TbHep1 and the mitochondrial J-proteins of *T. brucei*:
Sequences were obtained from TritrypDB using the accession numbers in Table 1, phylogenetic trees are the result of consensus amongst 1000 bootstrap iterations using a maximum likelihood statistical method following a poission distribution carried out on MEGA11.

The closest phylogenetic relationship to TbHep1 was identified as being two type-III JDPs, J44 and J23. The function of J44 is unknown as no experimental data is available; however, the STRING database suggests it is involved in protein folding and interacts with TbmtHsp70 (Szklarczyk et al., 2021). J23 is a JDP involved in the presequence translocase-associated motor (PAM) otherwise referred to as PAM27, this is a trypanosome-specific co-chaperone which replaces PAM18 functions in the import of mitochondrial preproteins (D'Silva et al., 2008; von Känel et al., 2020). This result correlates with the idea proposed by Burri et al. (2004) as it indicates that the evolution of TbHep1 may be closely tied to J23. This type-III JDP has only a J-domain and TbHep1 may operate in tandem with the JDP to allow preprotein import through the stimulation of mtHsp70 recruited by the TIM complex. This data is contradicted by STRING analysis which indicates that TbHep1 interacts with PAM18 (Appendix A9) (Szklarczyk et al., 2021) as PAM18 is maintained in the *T. brucei* genome although the function of the protein is unknown. As described in Känel et al. (2020), this is likely a byproduct of misidentification using bioinformatic procedures as the interaction is not experimentally determined and there is insufficient data regarding J23 to allow analysis of the interactions the unique JDP is involved in.

The phylogenetic analysis of HsHep1 indicated that the closest relationship to the orthologue was DNAJC20, otherwise known as HscB, a type-III JDP baring a region which is a homologue of a zinc-finger binding domain but has a less defined structure (Bitto et al., 2008). HscB is located within the cytoplasm and mitochondria, it is involved in iron-sulfur cluster biogenesis and protein translocation, it is not a part of the TIM complex like J23. This result correlates with previous studies which describe the convergence of mitochondrial Hsp70 machinery involved in iron-sulfur cluster biogenesis (Kleczewska et al., 2020). This result indicates that *T. brucei* may provide a valuable study in how Hep1 operates in tandem with JDPs involved in the TIM complex-based protein translocation due to the uniqueness of the J23 homologue and the close relationship it shows to TbHep1.

### 2.4.5 Conclusion

The results of this bioinformatic study have allowed insight into the mtHsp70 and Hep1 orthologues within *T. brucei*. TbmtHsp70 maintains the motifs and residues implicated in the property of aggregation and the residues shown to be involved in the interaction with Hep1 resemble those of the orthologue from *L. braziliensis*. This indicates that TbmHsp70 may aggregate and have the solubilizing interaction with Hep1 observed in other orthologues. The use of Alphafold has allowed observations on how the implicated residues may bring about the self-aggregation of mtHsp70 through the prevention of bonds with the NBD which are observed in non-aggregating DnaK and provided a possible new target for examination, the LEI motif. TbHep1 was also shown to share the tetra-cysteine motif which is required for the localization of the zinc-ion crucial to the structure and function of Hep1 which indicates that this orthologue may share the solubilizing activity of other orthologues. The *T. brucei* orthologue has additional α-helical structures, in comparison to HsHep1. These may cause oligomerization, which may imply that TbHep1 acts in a manner different to other orthologues such as HsHep1.

The analysis of JDPs against TbHep1 showed that the closest evolutionary relationship to the orthologue was J23 (PAM27), a JDP unique to kinetoplasts which has functionally replaced PAM18 within the PAM complex. This result provides evidence which reinforces the ideas put forward by Burri et al (2004) and Kleczewska et al. (2020) which postulate that Hep1 may act in tandem with type-III JDPs and that the machinery involved in iron-cluster biogenesis is subject to convergent evolution respectively. Due to J23 being a unique JDP within kinetoplasts this co-chaperone and TbHep1 may be a good model to allow further investigations into how Hep1 may influence the operations of type-III JDPs. Studies into the interactions of J23 may also provide insight into the operations of the co-chaperone as currently the extent of knowledge regarding the orthologues of J23 within the kinetoplast family is limited.

# Chapter 3: Biochemical characterization of TbHep1 and TbmtHsp70

## 3.1 Introduction

The genomic sequence of *T. brucei* and other trypanosomes have been available for approximately 10 years and a number of proteomic studies have been undertaken to identify a large number of putative proteins as well as their expression during different life cycle stages of the *T. brucei* parasite (Acestor et al., 2009; Panigrahi et al., 2009; Niemann et al., 2013). Relatively few of these proteins have been produced in a cell-based expression system and studied *in vitro* although some have been produced successfully, indicating that prokaryotic expression vectors are capable of producing proteins from this organism (Ludewig et al., 2015; Bentley & Boshoff, 2019). There is a need for this to be undertaken as it will allow an easier approach in the identification of new drug targets and the screening of new therapeutic compounds. This may provide methods of treating HAT which are less reliant of the formation of amines which are known to cause severe discomfort for patients. The targeting of the mtHsp70 of *T. brucei* could also provide a new strategy in HAT treatment against cases of remission as the quiescent form of the parasite is known to shift metabolism towards reliance on the mitochondrion for energy production and prevention of mtHsp70 activity may be an ideal method of preventing this activity (Vickerman, 1965; Soares & de Souza, 1988; Guler et al., 2008).

Protozoan proteins have been challenging to express in prokaryotes, particularly those of *P. falciparum* origin in which a high AT of the genome content contributes significantly to the formation of non-functional, insoluble aggregates (Mudeppa & Rathod, 2013). This characteristic is not exhibited in Trypanosomes; however, the prevalence of post-translational modifications within kinetoplast protein production can be a hinderance in prokaryotic-based expression systems which are unable to carry these out these functions (Francis & Page, 2010). Methods of protein production must therefore be analyzed and optimized on a protein-to-protein basis to ensure the protein of

interest can be expressed in a soluble and functional native form (Rosano & Ceccarelli, 2014). Particularly the identification of the correct combination of plasmid vector and host to express the protein in a soluble state that can be purified (Hartley, 2006; Bernaudat et al., 2011).

The trypanosome proteins TbJ2 and two cytosolic Hsp70 orthologues have previously been expressed and purified using *E. coli*-based expression systems (Burger, 2014; Ludewig et al., 2015) . This is a positive development as *E. coli* has been extensively used for the over-expression of recombinant proteins, its characteristics are well-known (Baneyx, 1999; Rosano & Ceccarelli, 2014), most strains are fast growing and can be cultured using inexpensive media thereby easing protein production (Baneyx, 1999; Shiloach & Fass, 2005). If successful production can be replicated to produce mtHsp70 and Hep1 from *T. brucei* this will be advantageous and allow for relatively inexpensive production of the orthologues. Levels of expression and solubility can also be easily altered by decreasing expression temperatures and Isopropyl-β-D-thiogalactopyranoside (IPTG) concentration to allow for increased solubility during protein production (Studier, 2005; Vera et al., 2007).

The feasibility of producing *T. brucei* mtHsp70 and Hep1 from prokaryotic cells requires confirmation, particularly for mtHsp70 expression as this is known to be bound within insoluble aggregates upon production (Szklarz et al., 2005). Aggregates can be solubilized using a few methods including treatments with chaotropic agents, organic solvents and detergents. Chaotropic agents are effective; however, they are known to produce dysfunctional proteins that require extensive treatment to return them to an active form if it is reversible at all (Singh & Panda, 2005). Some of these agents like guanidine hydrochloride can even worsen aggregation and destroy secondary structures (Emadi & Behzadi, 2014). Organic solvents and detergents like N-lauroyl sarcosine have been shown to produce more effective results despite only providing mild solubilization due to the retention of secondary structures (Singh et al., 2012).

Another effective method of producing soluble and functional protein within a prokaryotic-based cell system is the co-expression of the protein with a molecular chaperone that may facilitate proper folding (de Marco et al., 2007). Hep1 is documented as being necessary to fold and produce soluble, functional mtHsp70 in other orthologues (Szklarz et al., 2005; Sichting et al., 2005; Shonhai et al., 2008; Ludewig et al., 2015; Bentley and Boshoff, 2019). This method is effective in other

orthologues and an analysis of this property in *T. brucei* orthologues is necessary to allow future examination into the activity of *T. brucei* mtHsp70 and Hep1.

The suppression of mtHsp70 aggregation and maintenance of the chaperone is the primary action of Hep1 and it must be examined if this is maintained in the *T. brucei* orthologue. It would also be important to note the ability of TbHep1 to suppress the aggregation of other model proteins such as malate dehydrogenase. The zinc ion located within the zinc-finger binding domain also plays a critical role in Hep1 activities and structure within other orthologues (Fraga et al., 2012; Dores-Silva et al., 2013😉. This property must be investigated to confirm if the zinc ion plays a similarly important role within *T. brucei*. Investigations into the suppression of thermally induced mtHsp70 and MDH aggregation could be undertaken by making comparisons with the activities of the previously described *H. sapien* orthologue. Therefore, an initial investigation could be made into the fundamental properties of this orthologue.

## 3.2 Objectives

- The heterologous expression of TbmtHsp70 and TbHep1 from *T. brucei* and the *H. sapien* orthologues mortalin and HsHep1 in an *E. coli*-based expression system.

  Solubility studies of TbmtHsp70 expression to observe if the orthologue aggregates upon expression and confirm if detergents such as N-lauroyl sarcosine or co-expression with Hep1 is necessary for soluble protein purification
- .

  Investigations into the ability of TbHep1 to suppress the thermally induced aggregation of TbmtHsp70 and MDH via comparative analysis with the *H. sapien* orthologues HsHep1 and mortalin
- .

  Observations regard the importance of the zinc ion to TbHep1 structural stability
- .

## 3.3 Materials and Methods

### 3.3.1 Materials

The genomic and amino acid sequences of TbmtHsp70, TbHep1, mortalin (HSPA9) and HsHep1 can be found in Appendix A. The expression vectors pET28a (Novagen, USA), pQE2 (Qiagen, Germany), pQE30 (Qiagen, Germany) and pACYCDuet-1™ (Novagen, USA) were used (Table 2). The restriction enzymes used in plasmid conformation were *Bam*HI, *Xho*I, *Hind*III, *Nde*I and *Kpn*I (Thermo Scientific, USA), and a 1 Kb DNA ladder (Biolabs, New England) was also used. Expression was carried out using *E. coli* BL21 (DE3) and *E. coli* M15(pPRP4) cells (Stratagene, USA). The antibiotics ampicillin (Sigma-Aldrich, Germany), chloramphenicol (Calbiochem, Germany) and kanamycin (Sigma-Aldrich, Germany) were used. Ultracentrifuge (Beckman Coulter Life Sciences, USA), microcentrifuge (Eppendorf, Germany), 7315 UV-Vis spectrophotometer (Jenway, UK), Chemidoc chemiluminescence imaging system (Bio-Rad, USA), a quartz cuvette (Sigma-Aldrich, USA), 96 well-microplate (Greiner Bio-One, Germany), UV 96-well microplate (Corning Inc., USA), Microtiter plate reader (Epoch2, Biotek Instruments Inc, USA) and water bath (Memmert, Germany) were used in this study. Single-use filters (GVS, USA), Snakeskin dialysis tubing: 10,000 MWCO (Thermos Scientific, USA), and Precision plus protein marker (Biorad, USA) were also used. PEG 30,000 (Sigma-Aldrich, USA), The Better Bradford Assay reagent (Promega, USA), bovine serum albumin (BSA, Roche Diagnostics), lysozyme (Sigma-Aldrich, USA), malate dehydrogenase (MDH, Roche Diagnostic, Germany) and IPTG (Thermo Fischer Scientific, USA) were used in this study. An Anti-His-Tag antibody (Santa Cruz, USA), HRP-conjugated goat anti-mouse IgG secondary antibody (Santa Cruz, USA), ECL™ Western blotting substrate kit (GE Healthcare, UK) and 0.2 uM nitrocellulose membrane (Bio-Rad, USA) were used. Gel analysis was done using Jalview (Waterhouse et al., 2009). The collection of statistical data was undertaken using Microsoft Excel (Microsoft Corporation, USA), and the consolidation of data, the

generation of standard deviations and graphic representations were carried out using GraphPad (Dotmatics, USA).

Table 2: The plasmid constructs used in this study

| Plasmid Construct | Description | Source or Reference | Restriction Endonuclease | Competent cells |
|---|---|---|---|---|
| pQE30-TbHep1 | pQE30 encoding TbHep1, $Amp^R$ | Mr Maduma Mahlalela | *Nde*I, *Kpn*I | *E. coli* M15 (pPRP4) |
| pQE30-TbmtHsp70 | pQE30 encoding TbmtHsp70, $Amp^R$ | Mr Maduma Mahlalela | *Nde*I, *Kpn*I | *E. coli* BL21 (DE3) |
| pACYCDuet-1-TbHep1 | pACYC-Duet-1 encoding TbHep1, $Cm^R$ | Mr Maduma Mahlalela | *Nde*I, *Kpn*I | *E. coli* BL21 (DE3) |
| pQE2-HsHep1 | pQE2 encoding HsHep1, $Amp^R$ | Prof. J.C Borges, (Dores-Silva et al., 2013) | *Nde*I, *Kpn*I | *E. coli* BL21 (DE3) |
| pET28a-Mortalin | pET28a encoding Mortalin, $Kan^R$ | Prof. J.C Borges, (Dores-Silva et al., 2013) | *Bam*HI, *Hind*III | *E. coli* BL21 (DE3) |

### 3.3.2 The preparation of plasmid DNA

Plasmid preparation was carried out using the Pureyield™ Miniprep System (Promega, USA) via the transformation of *E. coli* JM109 cells. The overnight cultures were harvested by centrifugation using a microcentrifuge (Eppendorf, Germany) (13,500*g*, 15 seconds), and the pellet was resuspended in TE buffer (10 mM Tris-HCl, 1 mM EDTA, pH 8). The resuspension was then treated using 100 uL Blue Cell Lysis Buffer, followed by 350 uL of Neutralization Solution (4 °C) with repeated inversions proceeding the addition of each; this was followed by centrifugation using a

microcentrifuge (Eppendorf, Germany) (13,500*g*, 3 minutes). The lysate was then transferred to a PureyieldTM Miniprep column, placed into a collection tube and centrifuged using a microcentrifuge (Eppendorf, Germany) (13,500*g*, 3mins); the flowthrough was discarded. The column was then washed by adding 200 uL Endotoxin Removal Wash and centrifuged using a microcentrifuge (Eppendorf, Germany) (13,500*g*, 15 seconds). This was followed by adding 400 uL Column Wash Solution and centrifugation using a microcentrifuge (Eppendorf, Germany) (13,500*g*, 30 seconds); the minicolumn was then transferred to a 1,5 mL microcentrifuge tube. Elution was performed by adding 30 uL TE Buffer and incubating at room temperature (RT) for 1 minute, followed by centrifugation using a microcentrifuge (Eppendorf, Germany) (13,500*g*, 15 seconds). The DNA solution was then stored at -20°C.

### 3.3.3 Plasmid confirmation via restriction endonuclease digest and agarose gel electrophoresis

The plasmids were verified with a restriction enzyme digest followed by an agarose gel analysis, the plasmid constructs with the respective restriction endonucleases are shown in Table 2. The reactions were carried out using 2 uL of plasmid and 2 uL restriction endonuclease with the appropriate 10x restriction buffer (2 uL); the final reaction volume was brought up to 20 uL using nuclease-free ddH2O, and the reactions were carried out at 37°C for 3 hours. The agarose gels (1 %) were prepared using TAE Buffer (40 mM Tris-HCl, 20 mM acetic acid, 0,5 mM EDTA) with 20 ug/mL ethidium bromide added immediately before casting. The digested DNA samples were prepared for loading with the addition of 6x loading dye (Biolabs, USA). The gel electrophoresis was carried out in TAE Buffer running buffer for one hour at 85 volts. The gels were imaged under UV light using a Chemidoc chemiluminescence imaging system (Bio-Rad, USA). The plasmid constructs were later digested using their respective restriction enzymes and analyzed via agarose gel electrophoresis to confirm the size of the sequence inserts, apart from pQE2-TbmtHsp70 and pET28a-Mortalin which were digested using *Xho*I and *Hind*III.

### 3.3.4 The preparation of competent cells

An isolated colony of *E. coli* cells was used to inoculate 5 mL of 2x Yeast Tryptone (YT) broth and incubated shaking overnight at 37℃. The overnight culture was used to inoculate 225 mL of 2x YT broth (1:50 dilution). The culture was left to incubate, shaking at 37℃ until an optical density (OD) of A600 = 0,5 was reached. The culture was then centrifuged using a JA-14 rotor (Beckman, USA) (5000g, 5 mins, 4℃), resuspended in chilled, sterile 0.1 M $MgCl_2$ and kept on ice for 20 mins. The $MgCl_2$ cell solution was then centrifuged using a JA-14 rotor (Beckman, USA) (5,000*g*, 5 mins, 4℃), resuspended in chilled, sterile 0.1 M $CaCl_2$ and kept on ice for 45 mins. The $CaCl_2$ cell solution was centrifuged using a JA-14 rotor (Beckman, USA) (5000*g*, 5 mins, 4℃) and resuspended in chilled, sterile 0.1 M $CaCl_2$ with 30 % glycerol. The $CaCl_2$ cell solution was then aliquoted and stored at -80℃.

### 3.3.5 The transformation of competent cells

Plasmid DNA (2 uL) was added to 50 uL of thawed competent cells and left on ice for 20 mins. The cells were then heat shocked at 42℃ for 1 minute using a water bath and left on ice for 5 mins. 2x YT broth (950 uL) was then added, and the cell suspension was incubated at 37℃ for 1 hour before harvesting via centrifugation using a microcentrifuge (Eppendorf, Germany) (10,000*g*, 1 min, RT). The pellet was resuspended in 200 uL of supernatant and plated on 2x YT agar plates with the appropriate antibiotics using the concentration found in Table 2, co-expressions were carried out using *E. coli* BL21(DE3) cells with a pACYCDuet-1-TbHep1 construct used for Hep1 expression in the co-expression of the *T. brucei* orthologues. The plates were incubated overnight at 37℃ to allow colony formation.

### 3.3.6 Protein induction studies

A seed culture was prepared via the inoculation of 25 mL 2x YT broth using an isolated colony of transformed *E. coli* cells in the presence of the appropriate antibiotics and left shaking overnight at 37°C, the *E. coli* strain and antibiotic used are listed in table 2. The seed culture was inoculated into 225 mL of 2x YT broth with the appropriate antibiotics and grown to an OD of A600 = 0,7. Protein expression was initiated by adding IPTG to a final concentration of 1 mM. Protein production was then monitored via hourly sampling taken over 5 hours, followed by one sample taken after overnight expression. Samples were centrifuged using a JA-10 rotor (Beckman, USA) (5 000*g*, 5 mins, 4°C) and resuspended in Phosphate-buffered saline (PBS) (137 mM NaCl, 2.7 mM KCl, 10 mM $Na_2HPO_4$, 1.8 mM $KH_2PO_4$, pH 7.4); the volume of PBS used was determined using the following formula in which OD600 represents the absorbance reading taken at the time of sampling:

$$\text{PBS Volume (uL)} = \text{OD600}/0{,}5 \times 150 \times \text{Dilution Factor}$$

An aliquot of 100 uL of each sample was then analyzed on a 10 % SDS-PAGE gel to identify the ideal expression times.

### 3.3.7 Sodium dodecyl polyacrylamide gel electrophoresis (SDS-PAGE)

The SDS-PAGE procedure was adapted from the method described in Laemmli (1970). The samples to be analyzed were treated by adding 5 % SDS-PAGE sample buffer (10 % glycerol, 2 % SDS, 5 % β-mercaptoethanol, 0.05 % bromophenol blue, 0.0625 M Tris, pH 6.8) followed by heating at 95°C for 8 mins. A 10 % resolving gel (1.5 M Tris-HCl, 10 % SDS, 40 % Bis-acrylamide, pH 8.8) was used with the polymerization reaction initiated by the addition of 10 % ammonium persulphate (APS) and N,N,N,N-tetramethylene diamine (TEMED). Once the resolving gel had polymerized, a

4 % stacking gel (1.0 M Tris-HCl, 10 % SDS, 40 % Bis-acrylamide, pH 6.8) was applied. Electrophoresis of the gels was undertaken in SDS Running Buffer (25 mM Tris-HCl, 192 mM Glycine, 1 % SDS) at 120 volts for 95 mins. The gels were then stained using Coomassie staining solution (50 % methanol, 7.5 % glacial acetic acid, 0.24 % Coomassie brilliant blue), followed by destaining with SDS-PAGE destaining solution (20 % methanol, 7.5 % glacial acetic acid), the gels were then imaged using a Chemidoc chemiluminescence imaging system (Bio-Rad, USA).

### 3.3.8 Solubility studies

An overnight culture of transformed *E. coli* cells was diluted at 1:20 using 2x YT broth and incubated, shaking at 37°C, the strains and appropriate antibiotic used are listed in Table 2. Protein production was induced by the addition of IPTG to a final concentration of 1 mM once an OD of A600 = 0.6 was reached. The cells were harvested after 3 hours of protein production via centrifugation using a JA-14 rotor (Beckman, USA) (10,000*g*, 4 mins, 4°C). The pellet was resuspended in lysis buffer (10 mM Tris-HCl, 300 mM NaCl, pH 7.5) with the addition of lysozyme and phenylmethylsulfonyl fluoride (PMSF) to a final concentration of 1 mg/mL and 1 mM, respectively. Separate samples were taken and treated using 3 % N-lauroyl sarcosine, 2 M Urea and 2 M guanidinium chloride. Mixing was undertaken via multiple inversions followed by leaving the samples for 10 mins at RT. The treated samples were sonicated (4 times, 20 seconds, 60 Hz), and a whole cell sample was taken; the remainder was centrifuged using a JA-14 rotor (Beckman, USA) (13,500*g*, 40 mins, 4°C). A sample was taken of the supernatant and the pellet following resuspension using PBS. The samples were then treated and analyzed on a 10 % SDS-PAGE gel as described in section 3.2.7.

### 3.3.9 The purification of His-tagged recombinant proteins using a nickel-affinity bead resin

An overnight culture of transformed cells was used to inoculate 2x YT broth at a 1:10 dilution; this was incubated, shaking at 37℃ until an OD of A600 = 0.7 was reached. Protein expression was induced by adding IPTG to a final concentration of 1 mM, this procedure was carried out with all transformed cells. Protein production was carried out for 3 hours before cell harvesting by centrifugation using a JA-10 rotor (Beckman, USA) (10,000*g*, 10 mins, 4℃), and the pellet was resuspended in lysis buffer and frozen at -80℃. The frozen cell suspensions were thawed on ice in the presence of lysozyme and PMSF to a final concentration of 1 mg/mL and 1 mM, respectively, with inversions every 5 minutes until no ice crystals remained. Cell suspensions containing mitochondrial Hsp70 with no Hep1 were further treated with the addition of N-lauroyl sarcosine to a final concentration of 3 %. All cell suspensions were sonicated (4 times, 20 seconds, 60 Hz), and the cell debris was removed via centrifugation using a JA-14 rotor (Beckman, USA) (13,500*g*, 40 mins, 4℃). The supernatant was added to 2 mL Complete$^{TM}$ His-Tag Sepharose Beads suspended in lysis buffer and left shaking at 4℃ overnight. The suspension was centrifuged using a JA-14 rotor (Beckman, USA) (7,500*g*, 5 mins, 4℃), and the non-bound flowthrough was sampled and discarded. Four washes were performed with 20 mins shaking at 4℃ in 5 mL wash buffer (100 mM Tris-HCl, 300 mM NaCl, 5 mM imidazole, pH 7.5) followed by centrifugation using a JA-14 rotor (Beckman, USA) (7,500*g*, 4 mins, 4℃) with sampling of the initial and final wash iterations. Protein elution was initiated by adding 3 mL elution buffer (100 mM Tris-HCl, 300 mM NaCl, 250 mM imidazole, pH 7.5) followed by 20 mins shaking at 4℃ and centrifugation using a JA-14 rotor (Beckman, USA) (7,500*g*, 4 mins, 4℃). Three further iterations of protein elution were then carried out with samples taken of each and a sample of the beads taken proceeding the final elution. All samples were treated and analyzed on a 10 % SDS-PAGE as described in section 3.2.7. The protein elutions were stored at 4℃ until sample analysis was complete.

### 3.3.10 Protein dialysis and concentration

Collected protein samples were added to 10,000 MW SnakeSkin Dialysis Tubing, placed in 1 L of dialysis buffer (100 mM Tris-HCl, 150 mM NaCl, 0.5 mM DTT, 10 % glycerol, 50 mM KCl, 2 mM $MgCl^2$, pH 7.5) and left at 4°C overnight with gentle stirring. Protein samples treated with EDTA used an EDTA dialysis buffer (2 mM EDTA) for the overnight dialysis. The dialysis buffer was then replaced with a new liter of dialysis buffer and returned to 4°C with gentle stirring for 4 hours. Concentration was undertaken by placing the dialyzed samples on a bed of PEG 20,000 and left at 4°C to concentrate until a volume of approximately 1,5 mL was reached. The concentrated protein samples were then placed into 1,5 mL microcentrifuge tubes and stored at -20°C.

### 3.3.11 Determination of protein concentration

Determining protein concentration was undertaken using icrotiterre plate-based Bradford's assay adapted from Bradford, (1976). A linear standard curve was made using 245 uL of The Better Bradfords Assay™ added to 5 uL of BSA standards ranging from 100-1000 ug/mL, this mixture was also made using 5 uL of protein sample. The plate was incubated at RT for 10 minutes before absorbance reading at 595 nm. The protein concentrations were then determined by comparing the sample readings to that of the generated standard linear curve. The standards and samples were conducted in triplicate.

### 3.3.12 Dot blot assay

Confirmation of the presence of a His-tagged protein within each protein sample was carried out via a dot blot assay, the protocol was adapted from the methods described in Frazer & Wisdom, (1985)

and Stott, (1989), and was carried out on all proteins produced by the constructs described in Table 2. Two sections of nitrocellulose membrane (A and B) were divided into a grid, and 2 uL of each protein sample was dotted onto designated locations, 2 uL of lysozyme and 2 uL of cytosolic TbHsp70 previously documented in (Bentley & Boshoff, 2019) was also dotted to act as a negative and positive control respectively. These were blocked for one hour at room temperature using 3 % (w/v) BSA in Tris-buffered saline-tween solution (TBST) (50 mM Tris-HCl, 150 mM NaCl, 0.1 % (v/v) Tween-20, pH 7.5). Membrane A was then incubated shaking in 3 % (w/v) BSA TBST with 1:2500 anti-his primary antibodies (Santa-Cruz, USA) for 1 hour at room temperature; membrane B was used as a negative control and was only incubated in TBS for this step. The membranes were then washed three times using TBST in 20-minute intervals followed by incubation in 3 % (w/v) BSA TBST with 1:3000 HRP-conjugated goat anti-mouse IgG secondary antibody (Santa Cruz, USA) for one hour at room temperature; the membranes were then washed three times using TBST in 10-minute intervals followed by one 5-minute wash in TBS (50 mM Tris-HCl, 150 mM NaCl, pH 7.5). The detection of chemiluminescent signals was then achieved using a ECL™ Western blotting substrate kit (GE Healthcare, UK) following the manufacturers provided protocol and imaging was carried out using a Chemidoc chemiluminescence imaging system (BioRad, USA).

### 3.3.13 The suppression of thermally induced mtHsp70 aggregation by Hep1

A comparison of the abilities of HsHep1 and TbHep1 to suppress the thermally induced aggregation of their respective mtHsp70s was carried out according to a protocol adapted from Dores-Silva et al. (2021). The temperature at which both mtHsp70s would aggregate was initially determined using a peltier-integrated UV spectrophotometer and a quartz cuvette (Sigma-Aldrich, USA). The assay was then carried out on an Epoch 2 96-well plate reader (Biotek Instruments Inc, USA), which has an integrated peltier, using UV-compatible 96-well plates (Greiner Bio-One, Germany). The suppression of mtHsp70 aggregation via the addition of Hep1 was monitored by light scattering at 340 nm for 1.5 hours at 45°C in assay buffer (100 mM Tris-HCl, 150 mM NaCl, pH 7.5). The

concentration of mtHsp70 orthologues was maintained at 1 uM, and the concentrations of Hep1orthologues used were 0.5 uM, 1 uM, 2 uM and 4 uM; parallel assays of Hep1 alone using the same concentrations were run to observe and establish a baseline for their aggregation. Separate assays were carried out using 1 uM mtHsp70 and 1 uM EDTA-treated Hep1 in combination and separately to observe the effect of zinc-ion removal on Hep1 aggregation and the ability to suppress mtHsp70 aggregation. Each assay was conducted in triplicate, and three separate experiments were undertaken using independently produced batches of purified protein; endpoint data was plotted as a percentage relative to the aggregation of mtHsp70 alone, and kinetic data had the initial reading removed from subsequent data to observe the change in aggregation over time.

### 3.3.14 Suppression of malate dehydrogenase aggregation by TbHep1 and HsHep1

A comparison of the ability of HsHep1 and TbHep1 to suppress the thermally induced aggregation of the model substrate malate dehydrogenase (MDH) from porcine heart (Sigma-Aldrich, USA); the method for this assay was adapted from (Bentley & Boshoff, 2019). The concentration of MDH was maintained at 0.72 uM, and the concentrations of Hep1 used were 0.36 uM, 0.72 uM and 1.44 uM in combination and individually; parallel assays were conducted as negative controls using BSA in place of MDH and another using 0.72 uM EDTA-treated Hep1 in place of Hep1, all reactions were carried out in assay buffer (100 mM Tris-HCl, 150 mM NaCl, pH 7.5).

The assay was conducted at 48°C in a water bath (Memmert, Germany) for 1 hour, followed by centrifugation using a microcentrifuge (Eppendorf, Germany) (13,500*g*, 10 mins, 4°C) to separate the insoluble and soluble fractions; these were treated and analyzed on a 10 % SDS-PAGE as previously described in section 3.1.3. Densitometric analyses of the gels were carried out on ImageJ (NIH, USA) and MDH run individually was used as a comparison to quantify the degree of solubilization achieved through the addition of Hep1. Each assay was conducted in triplicate, and three separate experiments were undertaken using independently produced batches of purified protein.

### 3.3.15 The suppression of TbmtHsp70 aggregation by TbHep1 using densitometric analysis

An analysis of TbHep1s ability to suppress the thermally induced aggregation of TbmtHsp70 was conducted, the method for this assay was adapted from Zininga et al. (2017). The concentration of TbmtHsp70 was maintained at 1 uM, and the concentrations of Hep1 used were 0.5 uM, 1 uM, 2 uM and 4 uM, and 1 uM EDTA-treated Hep1 was also used; these were run individually and in combination. The assay was conducted in assay buffer (100 mM Tris-HCl, 150 mM NaCl, pH 7.5) at 48°C in a water bath (Memmert, Germany) for 1.5 hours, followed by centrifugation using a microcentrifuge (Eppendorf, Germany) (13,500*g*, 10 mins, 4°C) to separate the insoluble and soluble fractions, these were treated and analysed on a 10 % SDS-PAGE as previously described in section 3.1.3. Densitometric analyses of the gels were carried out on ImageJ (NIH, USA), and TbmtHsp70 run individually was used as a comparison to quantify the degree of solubilization achieved

## 3.4 Results and discussion

### 3.4.1 Plasmid confirmation via restriction digest

The plasmids used to produce the mtHsp70 orthologues were pET28a(+) and pQE2, which was used to produce mortalin and TbmtHsp70 respectively. These plasmids were also used for the co-expression of these orthologues in the presence of their respective Hep1 orthologues. The plasmids selected for the production of the Hep1 orthologues were pQE2 and pQE30, which were used for the production of HsHep1 and TbHep1 respectively. The same plasmid was used for the co-

expression of HsHep1 in the presence of mortalin although the use of pACYC-Duet-1 was implemented for the production of TbHep1 when co-expressed with TbmtHsp70 to avoid an overlap of antibiotic resistance between the plasmids used. The use of these plasmids allowed the purification of these proteins using nickel affinity chromatography due to the presence of His-tags and allowed confirmation of the recombinant protein using a His-probe-based dot blot analysis following protein production. The plasmid maps were constructed from the sequences obtained from the National Centre for Biotechnology Information (NCBI) and the plasmid manufacturers with the maps constructed manually on Microsoft office as seen in Figure 3.1.

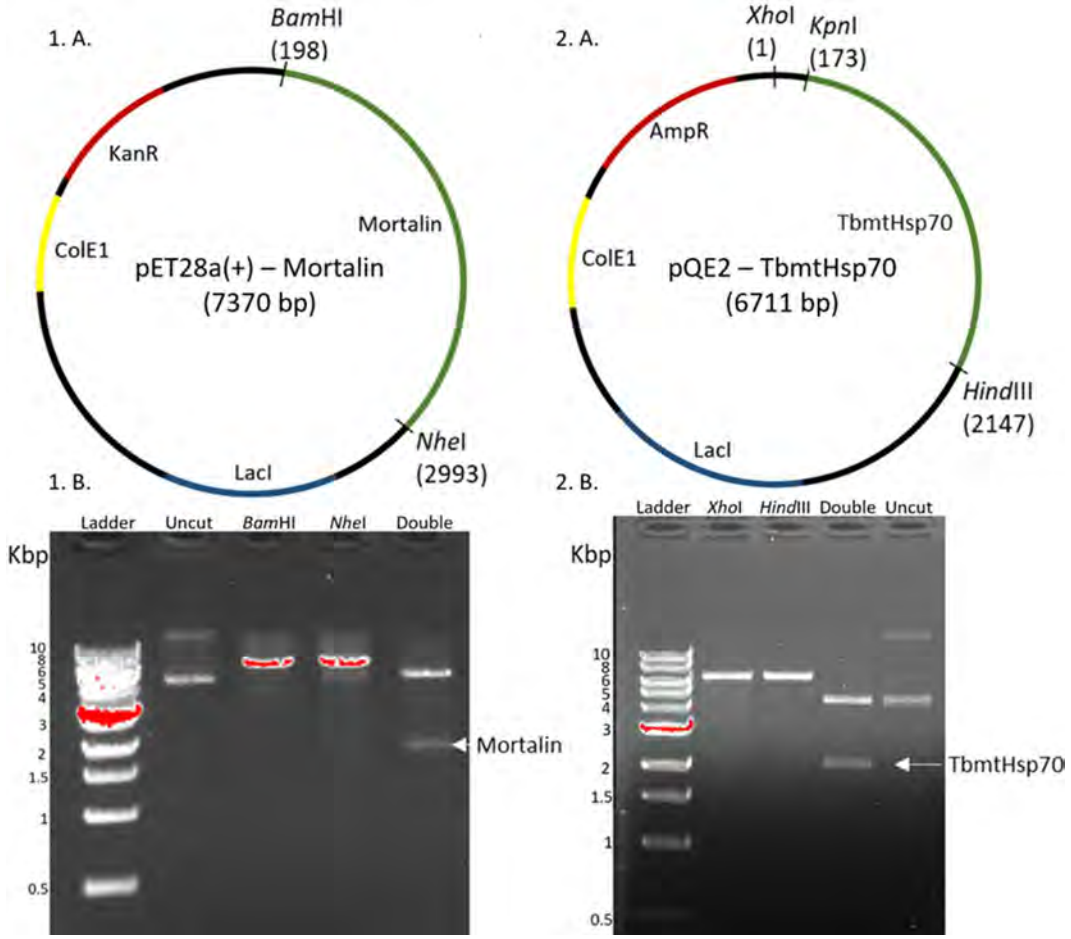


Figure 3.1: Plasmid maps and restriction digest analysis of mtHsp70 plasmid constructs: (A) The plasmid maps of (1) pET28a(+)-Mortalin and (2) pQE2-TbmtHsp70 with the protein coding regions indicated in green, the antibiotic resistance genes in red, the LacI genes in blue and the ColE1 ori sequence in yellow with the sites for the restriction enzymes used for insertion indicated (1) *Bam*HI (198) and *Nhe*I (2993); (2) *Kpn*I (173) and *Hind*III (2147). (B) RE analysis of (1) pET28a(+)-Mortalin and (2) pQE2-TbmtHsp70 undertaken using insertion restriction enzymes with the single digest lanes labelled accordingly and the inserts removed via double-digest indicated by white arrows, *Xho*I was used in place of *Kpn*I for (B) due to a shortage of *Kpn*I, Lane: Ladder represents the 1 Kb DNA marker and Lane: Uncut indicates the undigested plasmid.

After digestion using restriction endonucleases, an agarose gel electrophoresis was undertaken. The agarose gel electrophoresis indicated that the plasmid constructs were successfully linearized with the single digests appearing at 7370 bp for pET28a(+)-Mortalin (Figure 3.1.1B) and 6711 bp for pQE2-TbmtHsp70 (Figure 3.1.2B). The double digestions were carried out successfully as the inserts of mortalin and TbmtHsp70 appeared as bands at 2795 bp and 2146 bp respectively. The remainder of the plasmid constructed following double digestion were located at 4575 bp and 4565 bp for pET28a(+) and pQE2 respectively (Figure 3.1.B). The appearance of the TbmtHsp70 insert at a high bp number was due to the use of *Xho*I in place of *Kpn*I in the confirmation digest due to a lack of *Kpn*I. The agarose gel electrophoresis indicated that the linearization of the TbHep1 constructs was carried out successfully with pQE30-TbHep1 at 3927 bp (Figure 3.2.1.B) and pACYC-Deut-1-TbHep1 at 4580 bp (Figure 3.2.2.B).

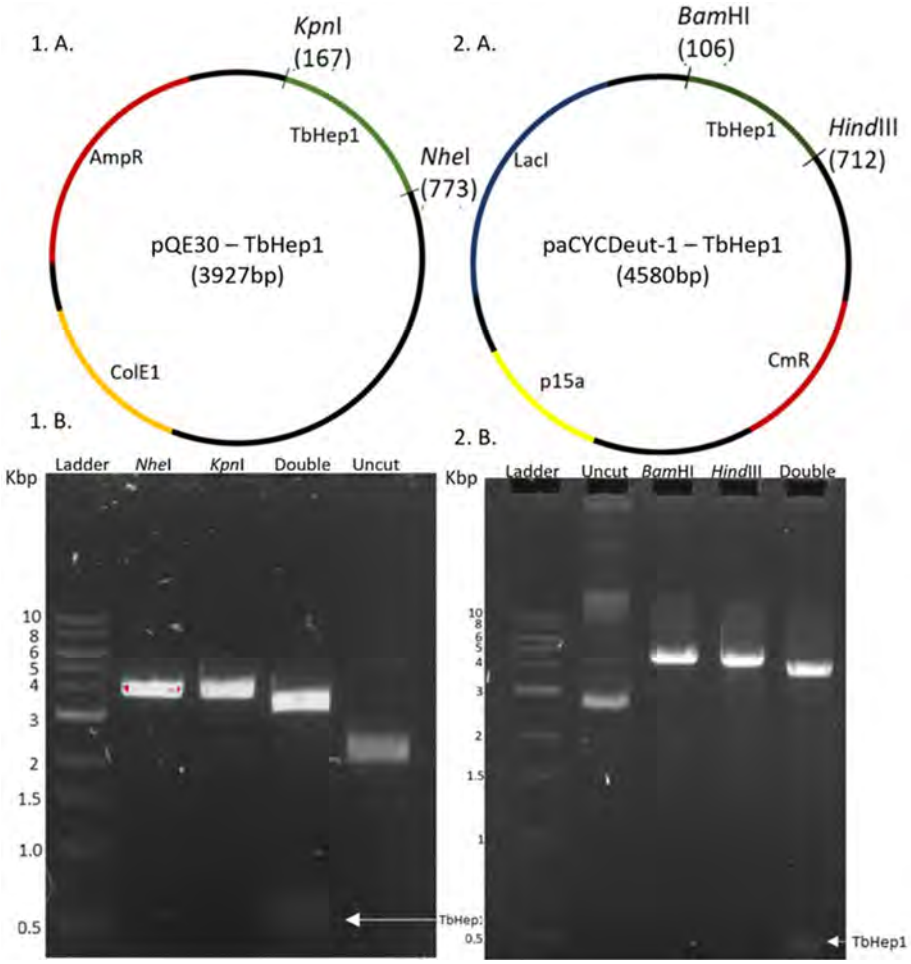


Figure 3.2: Plasmid maps and restriction digest analysis of TbHep1 plasmid constructs: (A) The plasmid maps of (1) pQE30-TbHep1 and (2) pACYCDEUT-1-TbHep1 with the protein coding regions indicated in green, the antibiotic resistance genes in red, the LacI genes in blue and the ori sequences in yellow with the sites for the restriction enzymes used for insertion indicated (1) *Kpn*I (167) and *Nhe*I (773); (2) *Bam*HI (106) and *Hind*III (712). (B) RE analysis of (1) pQE30-

TbHep1, (2) pACYCDEUT-1-TbHep1 undertaken using insertion restriction enzymes with the single digest lanes labelled accordingly and the inserts removed via double-digest indicated by white arrows. Lane: Ladder represents the 1 Kb DNA marker and Lane: Uncut indicates the undigested plasmid.

The insert fragments were observed at the correct sizes for the TbHep1 inserts which appeared at 606 bp (Figure 3.2). The remainder of the double-digested, linearized constructs were observed at 3321 bp and 3971 bp for pQE30-TbHep1 and pACYC-Deut-1-TbHep1 respectively. These successful results were also observed when producing the HsHep1 co-expression construct (Figure 3.3).

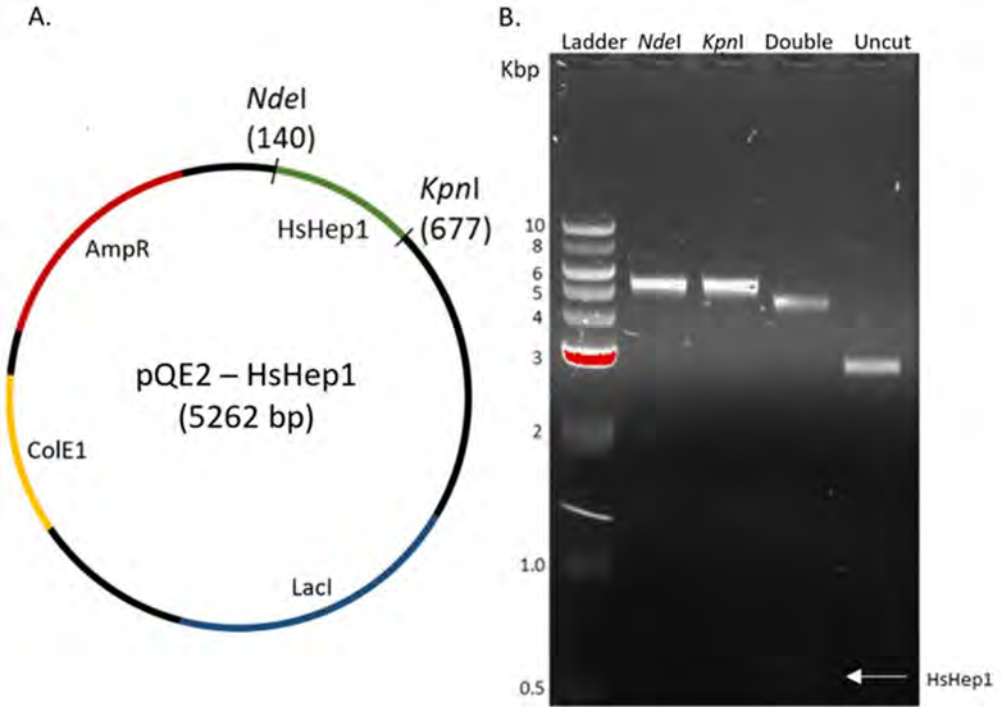


Figure 3.3: Plasmid map and restriction digest analysis of HsHep1 plasmid construct: (A) Plasmid map of pQE2-HsHep1 with the protein coding regions indicated in green, the antibiotic resistance genes in red, the LacI genes in blue and the ori sequence in yellow with the sites of the restriction enzymes used for insertion (*Nde*I (140) and *Kpn*I (677)) indicated. (B) RE analysis of pQE2-HsHep1 undertaken using insertion restriction enzymes with the single digest lanes labelled accordingly and the insert removed via double-digest indicated by a white arrow. Lane: Ladder represents the 1 Kb DNA marker and Lane: Uncut indicates the undigested plasmid.

The agarose gel electrophoresis of pQE2-HsHep1 indicated that the linearization was successful with the construct located at 5262 bp (Figure 3.3.B). The double digest of HsHep1 was also successful with the insert fragment appearing at 537 bp and the remainder of the construct located at 4725 bp.

### 3.4.2 The analysis of recombinant protein production

Protein induction studies were initially carried out to ascertain the optimal protein expression times for each protein with the aim of producing the most amount of protein that could be purified without a degradation in quality and to observe the effects that co-expression had on protein production. SDS-PAGE analysis of the whole cell lysate showed that the overexpression of the proteins was successfully carried out. With bands appearing at approximately 74 kDa, due to the size and overexpression of the band this is presumed to be TbmtHsp70 as well as overexpression of a protein of approximately 75 kDa, which may be mortalin (Figure 3.4 A and B), however, this cannot be confirmed without western blots using an anti-His probe, these were attempted but the results were inconclusive and a dot blot was later undertaken to provide a degree of confirmation.

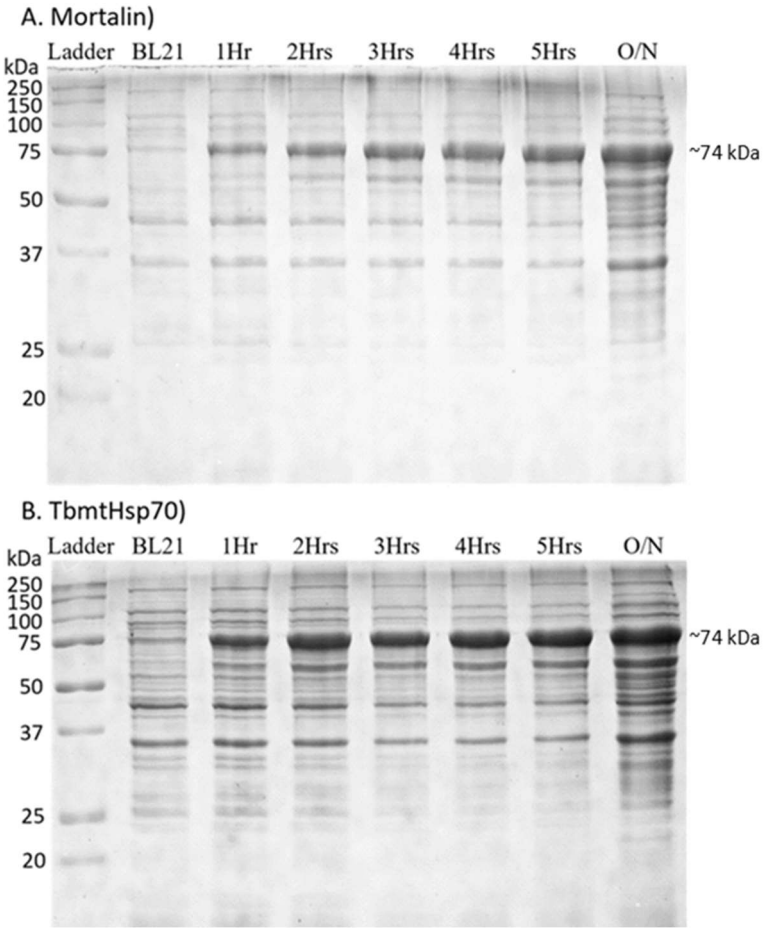


Figure 3.4: Protein induction studies of recombinantly produced mtHsp70 orthologues: SDS-PAGE (10 %) analysis of recombinant protein expression displaying (A) Mortalin expression and (B) TbmtHsp70 expression. Lane: Ladder indicates the Precision plus protein marker, Lane: BL21 indicates the uninduced cells (*E. coli* BL21(DE3)), Lanes: 1Hr –

5Hrs indicate the cell samples taken hourly for 5 hours after the addition of IPTG and Lane: O/N indicates samples taken after overnight expression with labels denoting the location of the recombinant protein being produced at ~ 74 kDa.

The concentrations of both mortalin (Figure 3.4.A) and TbmtHsp70 (Figure 3.4.B) appeared to increase 1 hour after induction and the concentration increased in each subsequent hour, with the highest concentration observed in the overnight cultures. It was previously observed that increased aggregation was encountered when attempting to purify the overnight cultures (data not shown). The optimal expression time for the mtHsp70 orthologues was therefore determined to be three hours. The expression of the Hep1 orthologues was then carried out (Figure 3.5)

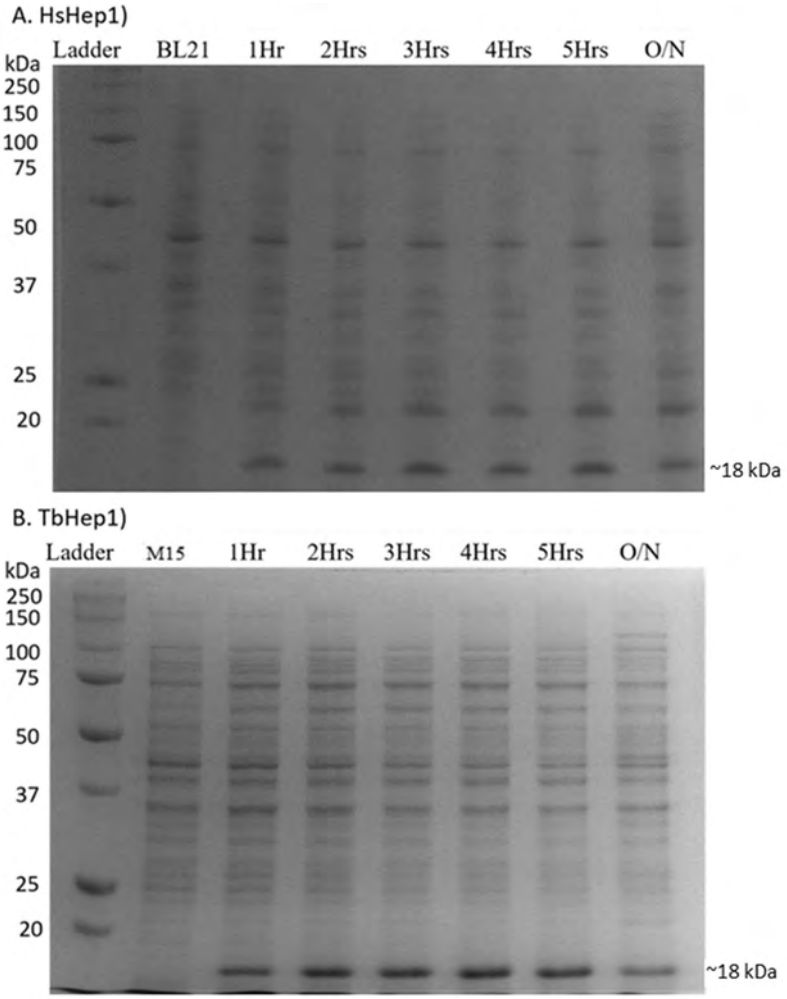


Figure 3.5: Protein induction studies of recombinantly produced Hep1 orthologues: SDS-PAGE (10 %) analysis of recombinant protein expression displaying (A) HsHep1 expression and (B) TbHep1 expression. Lane: Ladder indicates the protein marker, Lane: BL21/M15 indicates the uninduced cells (*E. coli* BL21(DE3) and *E. coli* M15[pPRP4] cells respectively), Lanes: 1Hr – 5Hrs indicate the cell samples taken hourly for 5 hours after the addition of IPTG and Lane: O/N indicates samples taken after overnight expression with labels denoting the location of the recombinant protein being produced at ~ 18 kDa.

The expression of HsHep1 was successfully carried out in *E. coli* BL21(DE3) cells (17 kDa) (Figure 3.5.A). Expression was observed an hour after induction using IPTG; the concentration increased

until the third hour; the overnight culture had a reduced concentration (Figure 3.5.A). These results determined the optimal expression time for the *H. sapien* Hep1 orthologue to be 3 hours which was similar to that of HsHep1 in previous studies (Dores-Silva et al., 2013). The expression of TbHep1 was successfully carried out in *E. coli* M15[pPRP4] cells (16 kDa) (Figure 3.5.B) and was observed from the first-hour post-induction using IPTG. The concentration of TbHep1 increased until the 3rd hour of expression. Similar to the production of HsHep1 the overnight culture had a reduced concentration and the third hour after induction was determined to be the optimal expression time (Figure 3.5.B). The co-expression of mortalin and HsHep1 was carried out in *E. coli* BL21(DE3) cells (~ 74 kDa) (Figure 3.6.A).

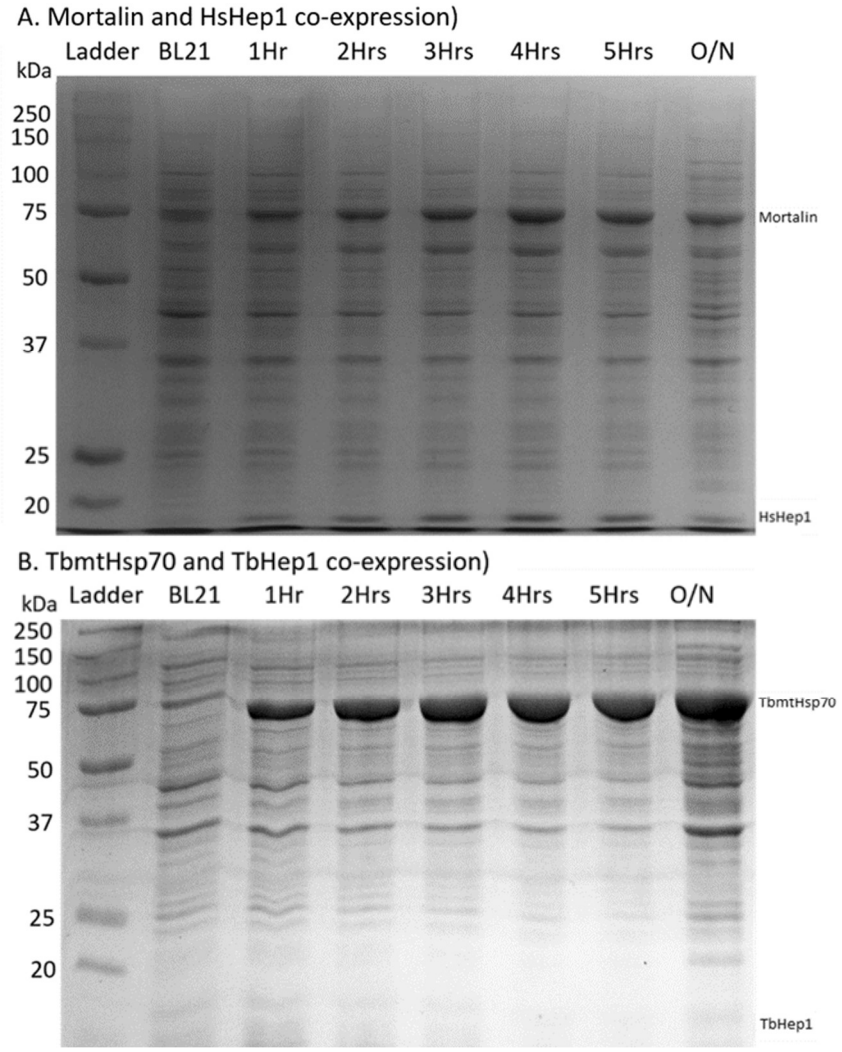


Figure 3.6: Protein induction study of mtHsp70 co-expressed with Hep1: SDS-PAGE (10 %) analysis of recombinant protein expression displaying (A) Mortalin co-expressed with HsHep1 and (B) TbmtHsp70 co-expressed with TbHep1. Lane: Ladder indicates the protein marker, Lane: BL21 indicates the uninduced *E. coli* BL21(DE3) cells, Lanes: 1Hr – 5Hrs indicate the cell samples taken hourly for 5 hours after the addition of IPTG and Lane: O/N indicates samples taken after overnight expression with stars denoting the location of the recombinant protein being produced.

Expression of mortalin was observed prior to induction and the presence of HsHep1 was observed from the first-hour post-induction with IPTG (~ 18 kDa). The concentration of both proteins increased in concentration until the fourth hour (Figure 3.6.A) and decreased in the 5 hour and overnight cultures. The optimum expression time was determined to be 4 hours due to this being the peak concentration of mortalin. The co-expression of TbmtHsp70 was successfully carried out in *E. coli* BL21(DE3) cells (~ 74 kDa) (Figure 3.6.B). A protein of ~ 16 kDa could be observed one-hour post-induction with IPTG; however, the concentration remained remarkably low with the highest concentration observed in the overnight culture, this was due to the use of the pACYCDeut-1 plasmid, which has a low copy number. The concentration of TbmtHsp70 appeared to remain constant after 3 hours post-induction using IPTG, however, the overnight culture had the highest concentration. The optimal expression time for the TbmtHsp70 co-expression was determined to be 3 hours post-induction due to the high concentration of TbmtHsp70 present.

### 3.4.3 Solubility studies of the mtHsp70 orthologues

The self-aggregating property of mtHsp70 orthologues results in the purification of the protein requiring the presence of Hep1 or treatment using detergents. Treatments using N-lauryl sarcosine and urea have previously been shown to disrupt aggregate formation and allow the solubilization of insoluble proteins and aggregates; however, their inclusion disrupts tertiary protein structures, retaining only secondary structures and rendering most proteins non-functional (Khabiri et al., 2013; Pandey & Singh, 2012). To produce and purify soluble mtHsp70, various experiments were conducted using varying concentrations of urea, N-lauryl sarcosine and guanidine chloride to identify what concentrations could be used to solubilize TbmtHsp70 and mortalin (data not shown). A concentration of 3 % N-lauryl sarcosine was determined to be the most effective solubilization agent (Figure 3.7), with urea and guanidine chloride displaying little effect unless present in high concentrations of 5 M and 3 M, respectively.

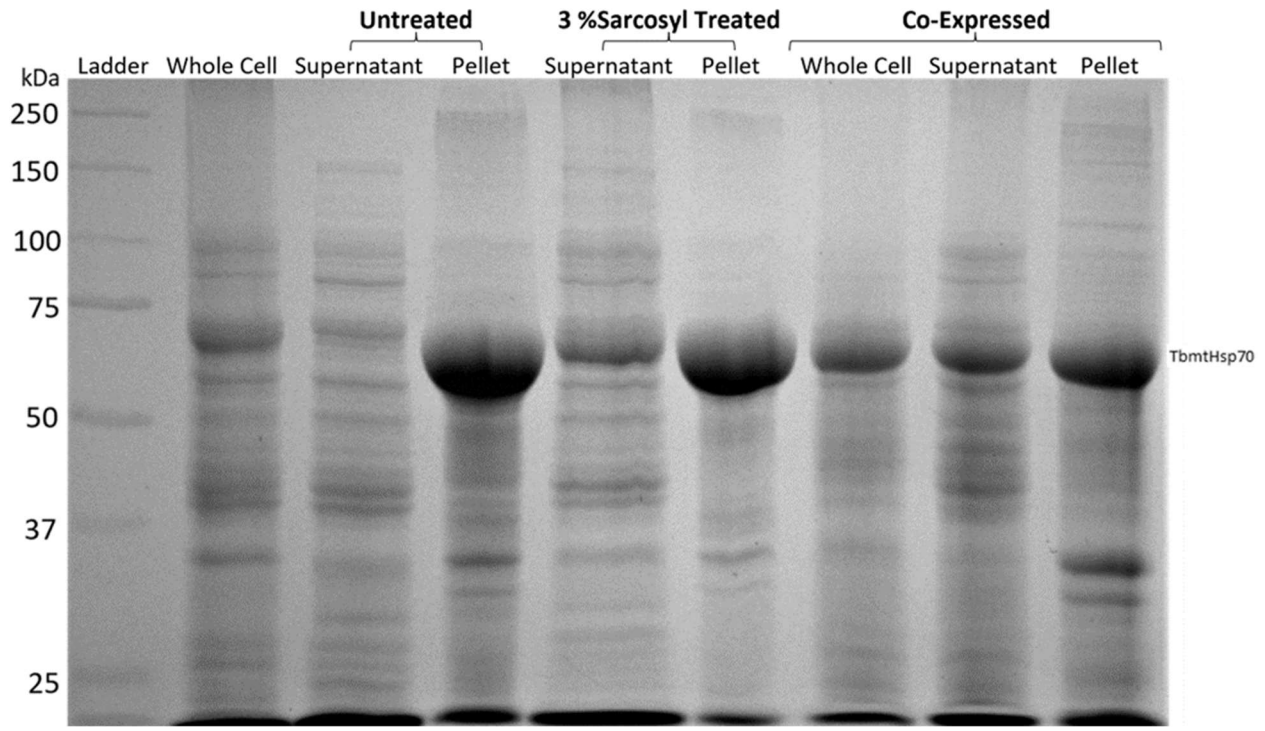


Figure 3.7: The effect of N-lauroyl sarcosine treatment and co-expression with TbHep1 on the solubility of TbmtHsp70: SDS-PAGE (10 %) analysis of TbmtHsp70 solubility studies. Lane: Ladder indicates the protein marker, Lane: WC indicates the whole cell before treatment and centrifugation, Lane: Supernatant is the supernatant or soluble fraction after centrifugation and Lane: Pellet represents the insoluble fraction. Untreated lanes indicate mtHsp70 expressed with no Hep1 or detergent present. 3 % sarcosyl treated lanes indicate mtHsp70 treated with 3 % N-lauroyl sarcosine and Co-Expressed lanes indicate cultures in which mtHsp70 was co-expressed with Hep1.

The *E. coli* BL21(DE3) cell cultures were harvested 3 hours after induction using IPTG. The first culture was untreated while the second was treated using N-lauroyl sarcosine to a final concentration of 3 %. These cells were treated with lysozyme and ruptured via freeze-thawing followed by sonication and centrifugation to remove the cell debris and separate the soluble fraction of protein content. TbmtHsp70 was found to be insoluble with a significant amount of the protein located in the insoluble pellet fraction (~ 74 kDa) (Figure 3.7 Lane Untreated Pellet), this resembled the results observed in the solubility study conducted on mortalin (~ 74 kDa) (Figure 3.8 Lane Untreated Pellet). Treatment using 3 % lauroyl sarcosine solubilized a portion of TbmtHsp70 (Figure 3.7 Lanes 3 % Sarcosyl Treated). The proportion of TbmtHsp70 solubilized was lower than that observed after similar treatments conducted on the cultures used to express mortalin (Figure 3.8 Lanes 3 % Sarcosyl Treated). Following this, comparisons were made by carrying out the same procedure using *H. sapien* orthologues (Figure 3.8).

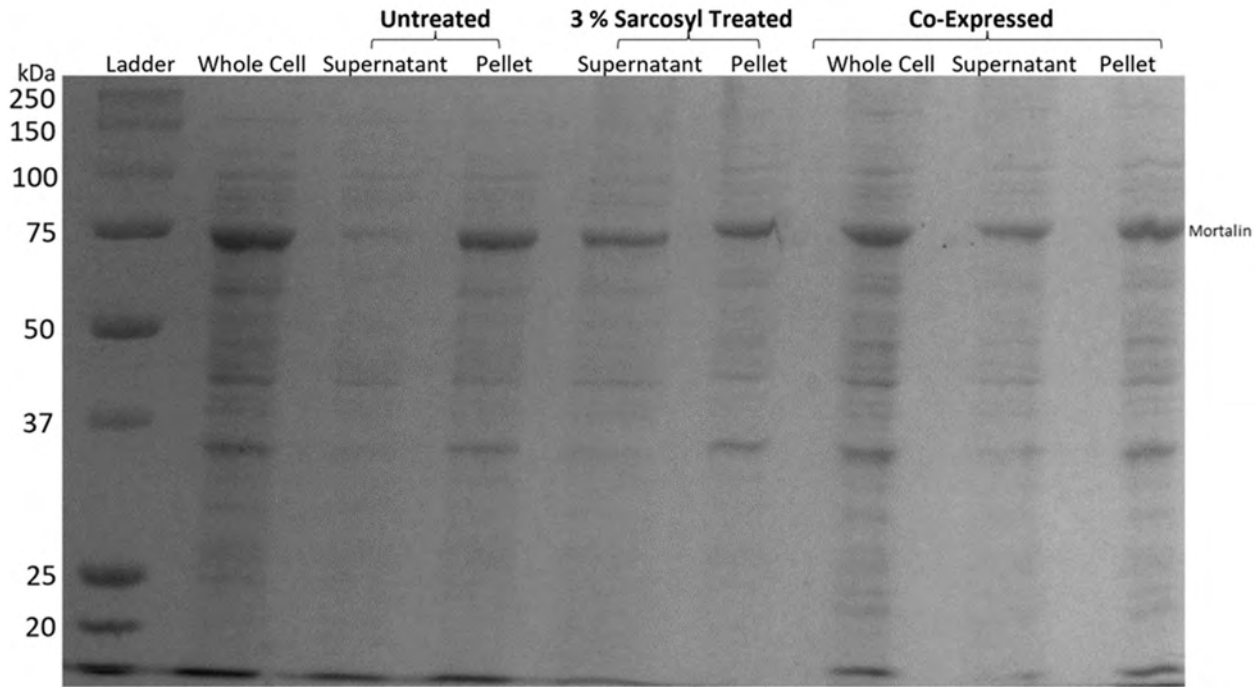


Figure 3.8: The effect of N-lauroyl sarcosine treatment and co-expression with HsHep1 on the solubility of mortalin: SDS-PAGE (10 %) analysis of TbmtHsp70 solubility studies. Lane: Ladder indicates the protein marker, Lane: WC indicates the whole cell before treatment and centrifugation, Lane: Super is the supernatant or soluble fraction after centrifugation and Lane: Pellet represents the insoluble fraction. Untreated lanes indicate mtHsp70 expressed with no Hep1 or detergent present. 3 % sarcosyl treated lanes indicate mtHsp70 treated with 3 % N-lauroyl sarcosine and co-Expressed lanes indicate cultures in which mtHsp70 was co-expressed with Hep1.

The co-expression of TbmtHsp70 with TbHep1 increased the solubility of TbmtHsp70 compared with the supernatant of TbmtHsp70 expressed alone (Figure 3.7 Lane Untreated Supernatant and Co-Expressed Supernatant) with a large portion of TbmtHsp70 present in the soluble fraction. The effect on solubility was similar to that of 3 % N-lauryl sarcosine despite the low concentration of expressed TbHep1; however, a large portion of TbmtHsp70 was still observed within the pellet (Figure 3.7 Lanes 3 % Sarcosyl Treated and Co-Expressed). Similar results were observed in the solubilization of mortalin with the co-expression solubilizing to the same degree as 3 % N-lauryl sarcosine treatment as indicated by the presence of mortalin in the supernatant fraction (Figure 3.8 Lanes 3 % Sarcosyl Treated Supernatant and Co-Expression Supernatant). These results suggest that TbmtHsp70 may be insoluble upon expression in the absence of Hep1 and produced in a more soluble form when co-expressed in the presence of Hep1.

### 3.4.4 The purification of His-tagged mtHsp70 and Hep1 orthologues

The purification of the Hep1 and mtHsp70 orthologues was undertaken using nickel-affinity chromatography which uses the affinity the amino acid histidine has for nickel ions to purify proteins with a C-terminal His-tag via the chelating of the protein and binding to agarose beads (Petty, 2001). The solubility studies undertaken indicated that themtHsp70 orthologues were insoluble upon expression, the purification of the mtHsp70 was therefore undertaken with the inclusion of 3 % N-lauroyl sarcosine to solubilize the protein (Figure 3.9).

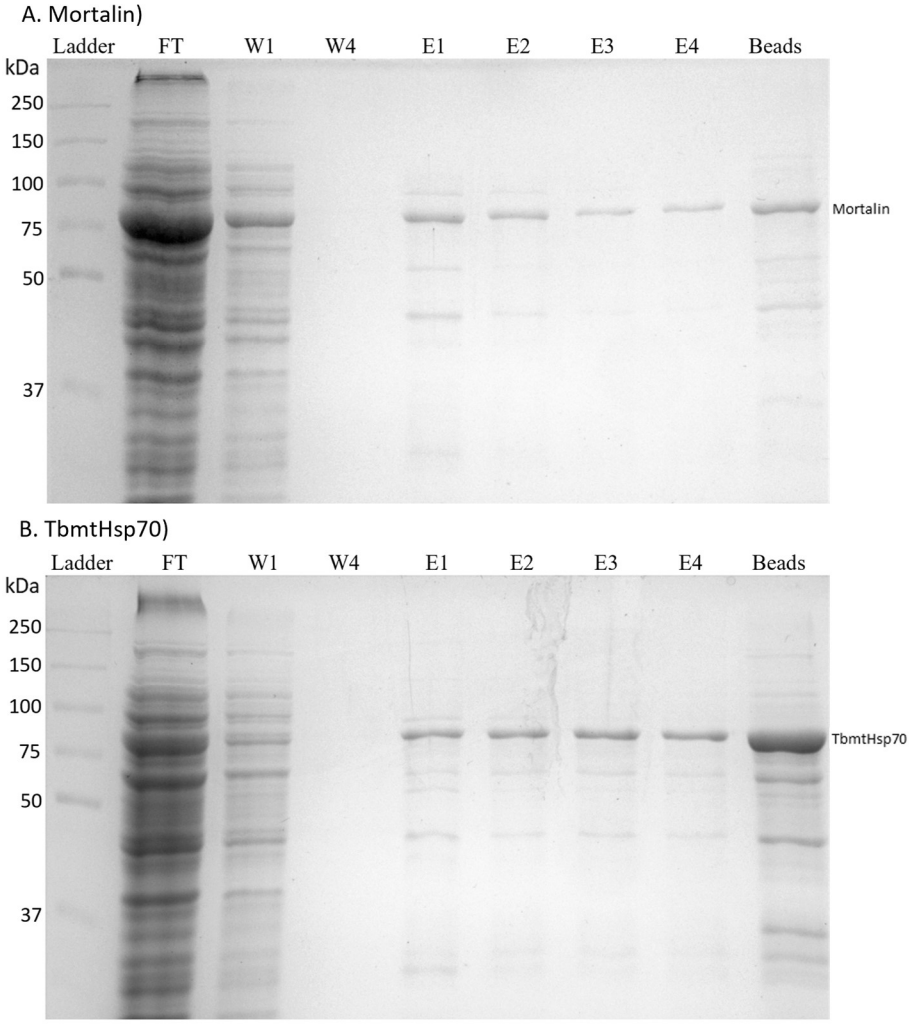


Figure 3.9: The purification of His-tagged mtHsp70 orthologues: SDS-PAGE (10 %) analysis of samples collected during His-Tag bead-based purification with (A) displaying the purification of mortalin and (B) TbmtHsp70. Lane: Ladder indicates the protein marker, Lane: FT indicates the flowthrough, Lanes: W1, W4 indicate the initial and final (fourth) wash, Lanes: E1 – E4 indicate the four elution steps and Lane: Beads indicates a sample of the beads taken after the 4th elution.

Factors previously shown to prevent or reverse aggregate formation include the presence of ATP or co-chaperones, a reduction in temperature and substrate binding (Benaroudj et al., 1996). ATP (2 uM) was therefore used in the first two wash steps of the mtHsp70 purifications to reduce the presence of aggregates and maintain the chaperone in a closed state to reduce contaminating proteins which can be bound by Hsp70 and co-purified.

Four washes were carried out, followed by four elution steps using a 250 mM imidazole concentration in the elution procedures of the mtHsp70 orthologues. Both mtHsp70 orthologues had small amounts of protein in the initial wash step but appeared to be absent from the final wash step of TbmtHsp70 (Figure 3.9B Lanes: W1 and W4) and mortalin (Figure 3.9A Lanes: W1 and W4). A low concentration of contaminating protein was observed in all elution steps for both mortalin and TbmtHsp70 (Figure 3.9, lanes E1 – E4). These amounts were reduced relative to previous experiments in which ATP was not included (data not shown).

MtHsp70 was observed bound to the beads for the purification of both orthologues (~ 74 kDa) although these were less prevalent within the beads used to purify TbmtHsp70 (Figure 3.7.B Lane: Beads) than that of mortalin (Figure 3.7A Lane: Beads). The use of increasing imidazole concentrations was ineffective; however, the use of 3 % N-lauroyl sarcosine successfully facilitated the purification of both mtHsp70 orthologues, despite the bead-bound proteins an adequate amount of protein was routinely obtained (> 5 uM).

A similar procedure was carried out for the Hep1 orthologues (Figure 3.10), four washes were carried out, these were followed by four elution steps undertaken using a 250 mM imidazole concentration in the elution procedure of the Hep1 orthologues. Solubility studies which were previously undertaken indicated that TbHep1 resembled HsHep1 and was soluble upon expression (data not shown), this allowed a native purification to be undertaken without the need for N-lauroyl sarcosine.

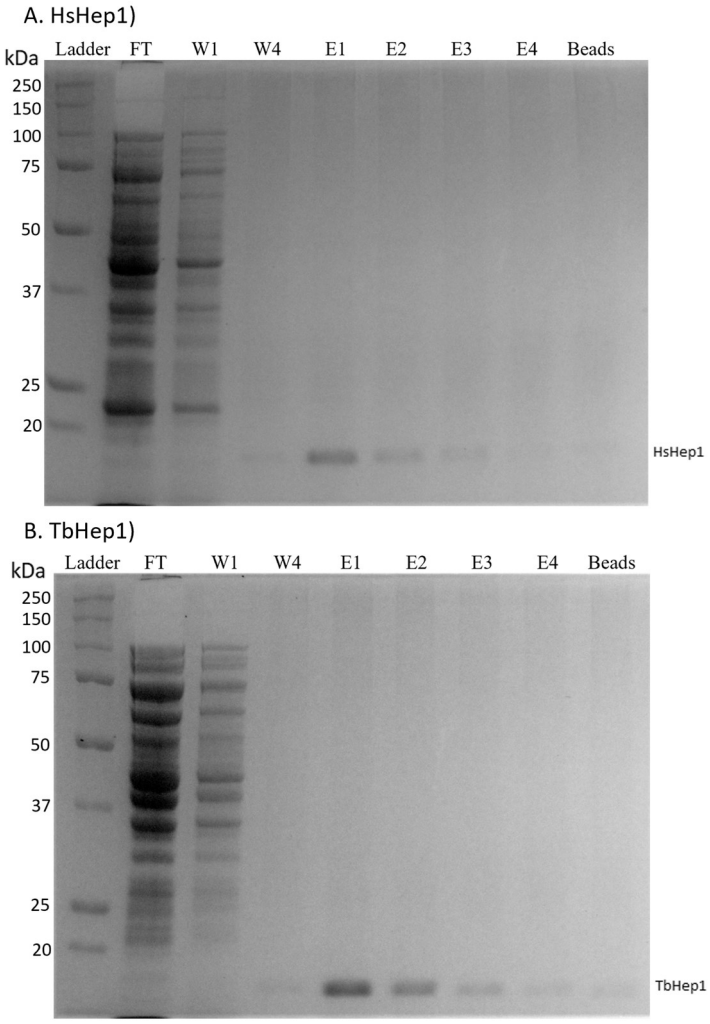


Figure 3.10:The purification of His-tagged Hep1 orthologues: SDS-PAGE (10 %) analysis of samples collected during His-Tag bead-based purification with (A) displaying the purification of HsHep1 and (B) TbHep1. Lane: Ladder indicates the protein marker, Lane: FT indicates the flowthrough, Lanes: W1, W4 indicate the initial and final (fourth) wash, Lanes: E1 – E4 indicate the four elution steps and Lane: Beads indicates a sample of the beads taken after the 4th elution.

Low concentrations of protein, which is most likely TbHep1 (Figure 3.10B Lanes W1 and W4) and HsHep1 (Figure 3.10A Lanes W1 and W4), were observed in the final wash step. TbHep1 was eluted with the largest amount observed in the first elution step, followed by decreasing amounts in the subsequent elutions with small amounts of TbHep1 evident in the final elution (Figure 3.10B Lanes E1 – E4) and beads post-elution (Figure 3.10B Lane Beads). HsHep1 was observed in all elutions (Figure 3.10A Lanes E1 – E4), with the majority present in the first two elution steps and a low concentration observed in the beads post-elution (Figure 3.10A Lane Beads). No additional proteins co-purified with Hep1 and a high degree of purity was achieved.

### 3.4.5 The purification of mtHsp70 orthologues co-expressed with Hsp70 escort protein 1

The purification of mtHsp70 after co-expression with Hep1 was undertaken using nickel-affinity chromatography to purify the His-tagged recombinant proteins. The solubility studies conducted on the mtHsp70 orthologues indicated that both mortalin and TbmtHsp70 were soluble when co-expressed with HsHep1 and TbHep1 respectively (Section 3.3.3), allowing purification under native conditions. ATP (2 uM) was added to the first two wash steps to reduce protein contamination by maintaining the mtHsp70 chaperones in a closed state and reducing the concentration of co-eluted Hep1 in the elution steps (Figure 3.11).

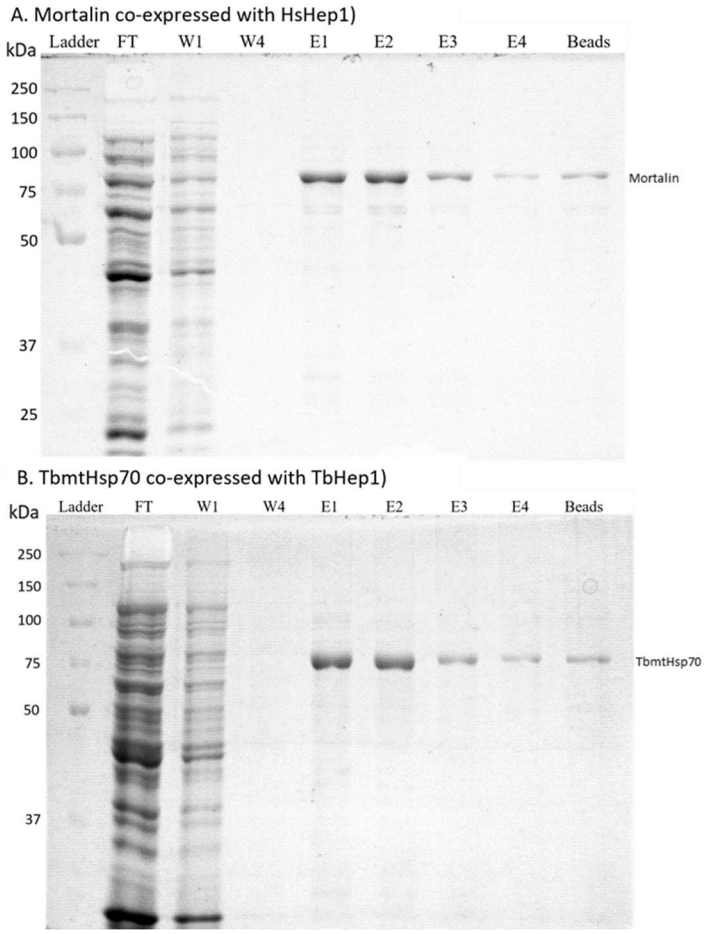


Figure 3.11: The purification of His-tagged mtHsp70 co-expressed with Hep1: SDS-PAGE (10 %) analysis of samples collected during His-Tag bead-based purification with (A) displaying the purification of mortalin co-purified with HsHep1 and (B) displaying the purification of TbmtHsp70 co-purified with TbHep1. Lane: Ladder indicates the protein marker, Lane: FT indicates the flowthrough, Lanes: W1, W4 indicate the initial and final (fourth) wash, Lanes: E1 – E4 indicate the four elution steps and Lane: Beads indicates a sample of the beads taken after the 4th elution.

Four wash steps were undertaken, followed by four elutions conducted using 250 mM imidazole. Low concentrations of mortalin (Figure 3.11A Lanes W1 and W4) and TbmtHsp70 (Figure 3.11B Lanes W1 and W4) were observed in the initial wash step and neither orthologue was observed in the final wash step. Low concentrations of contamination were observed in the initial two mortalin elutions (Figure 3.11A Lanes E1 and E2) with no contamination evident in the TbmtHsp70 elutions (Figure 3.11B Lanes E1 and E2). The amount of bead-bound protein post-elution was reduced in the co-expressions with a larger proportion observed within the beads used to purify mortalin (Figure 3.11A Lane Beads) than that of the beads used to purify TbmtHsp70 (Figure 3.11B Lane Beads). Despite the presence of bead-bound protein, large amounts of TbmtHsp70 (> 30 uM) and mortalin (> 20 uM) were routinely obtained. Western analysis was attempted to confirm the presence of recombinant protein and ensure that Hep1 did not bind to Hsp70 after elution, but the western blot procedures were unsuccessful

The co-expression of TbmtHsp70 with TbHep1 has allowed the production and elution of soluble TbmtHsp70 in a manner similar to the *H. sapien* orthologue. This resembles previous observations made with other Hep1 orthologues such as those from *S. cerevisiae* (Sichting et al., 2005), *H. sapiens* (Zhai et al., 2008), *L. braziliensus* (Dores-Silva et al., 2017), *C. reinhardtii* (Willmund et al., 2008) and *A. thaliana* (Kluth et al., 2012). TbmtHsp70 has therefore resembled other orthologues which require the presence of Hep1 to remain soluble. As with previous observations, this is likely due to Hep1 acting as a co-factor, ensuring the correct folding upon expression and forming temporary complexes to reduce the instances of hydrophobic regions causing self-aggregation. These results provide initial evidence that TbmtHsp70 requires TbHep1 to function as documented in previous orthologues.

### 3.4.6 Dot blot analysis of purified proteins

Dot-blot analysis of purified protein was undertaken to confirm the presence of His-tagged recombinant proteins. The presence of His-tagged recombinant proteins was detected using an anti-mouse Ig, HRP conjugated antibody (Figure 3.12).

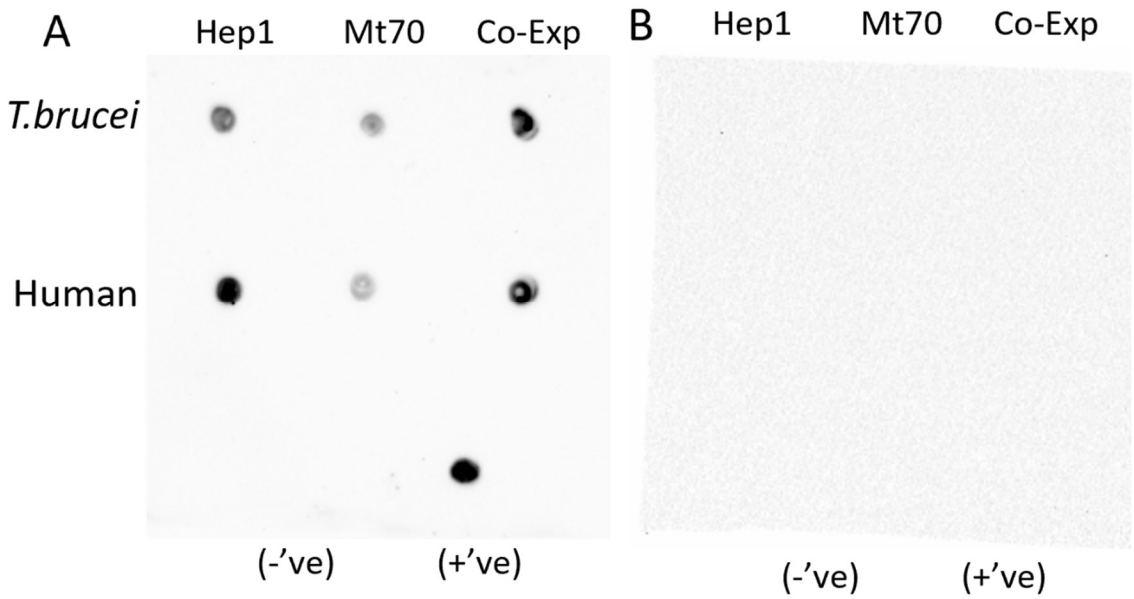


Figure 3.12: Dot-blot analysis of His-tagged proteins: (A) Dot blot of purified proteins immunostained with a mouse-Ig based His-probe and a HRP-conjugated anti-mouse goat secondary antibody using a $H_2O_2$/luminol based substrate kit with each protein labelled accordingly, Mt70 represents mtHsp70, samples (-'ve) and (+'ve) represents lysozyme (1 mg/mL) and cytosolic TbHsp70 respectively. (B) Negative control was carried out using the same protein samples as (A) and immunostained using only the HRP-conjugated secondary antibody.

The positive control (+' ve) used was a cytosolic His-tagged Hsp70 from *T. brucei* previously documented in (Bentley & Boshoff, 2019). The negative control (-' ve) used was lysozyme and indicated that the protein did not have a His-tag. The same proteins were dotted onto a second membrane and treated using the same methodology but without the addition of a primary antibody. The lack of signal on this membrane indicated that the HRP-conjugated secondary antibody could not produce a signal when the primary antibody was absent (Figure 3.12B). The presence of the His-tag was confirmed for all recombinant proteins with each sample of the *T. brucei* and *H. sapien* orthologues producing a signal with no signal produced by the negative control (Figure 3.12A). This method was capable of detecting the presence of His-tagged proteins; however, it was not capable of determining if Hep1 co-purified with mtHsp70 and provides no reliable data regarding the concentration of the protein samples produced.

### 3.4.7 TbHep1 suppressed TbmtHsp70 aggregation

TbmtHsp70 aggregated at 45°C while TbHep1 appeared to remain soluble; similar results were observed for mortalin and HsHep1 (Dores-Silva et al., 2015). This allowed a comparison of the ability of TbHep1 to suppress the thermally induced aggregation of TbmtHsp70 in relation to the suppression of mortalin aggregation using HsHep1 placed under similar conditions (Figure 3.13). In previous studies, 340 nm readings of Hep1 thermal aggregation conducted in the absence of mtHsp70 were subtracted from the corresponding concentration of Hep1 in the presence of 1 uM mtHsp70 to allow comparisons of only mtHsp70 aggregation (Dores-Silva et al., 2017). This has previously been confirmed as a viable approach and has allowed basic characterization of Hep1 orthologues before further analytically based assays were conducted (Sichting et al., 2005; Zhai et al., 2008; Dores-Silva et al., 2017).

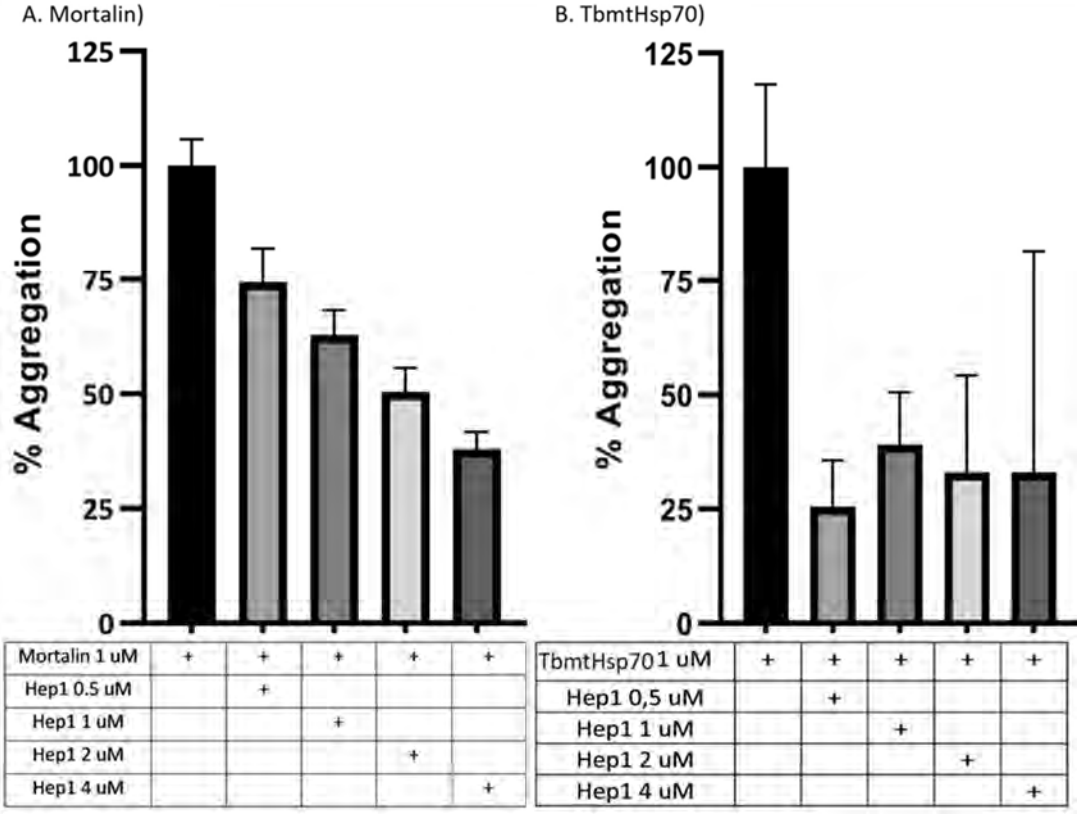


Figure 3.13: The suppression of thermally induced mtHsp70 aggregation: (A) Endpoint values of mortalin aggregation in the presence of increasing amounts of HsHep1. (B) Endpoint values of TbmtHsp70 aggregation in the presence of increasing amounts of TbHep1. Endpoint values indicate the change in 340 nm readings over the course of the assay with readings of Hep1 alone using the same concentrations subtracted to observe only mtHsp70 aggregation. These results were consolidated from 3 separate assays.

The presence of 0,5 uM HsHep1 decreased mortalin aggregation by ~ 25 % and aggregation was reduced in a dose-dependent manner with 4 uM of HsHep1 resulting in 65 % prevention of aggregation of mortalin (Figure 3.13A). These results correspond with observations made in

previous studies which describe HsHep1 showing increasing effectiveness in a dose dependent manner (Dores-Silva et al., 2013). The presence of 0,5 uM TbHep1 decreased TbmtHsp70 aggregation by ~ 75 %, indicating that it was more effective than other studied orthologues. However, the amounts of aggregation suppression varied in subsequent doses, indicating that the orthologue did not suppress aggregation in a dose dependent manner.

Inconsistencies were increasingly observed in the TbHep1 controls at concentrations beyond 0,5 uM. TbHep1 absorbance readings increased with concentration to a greater degree than the HsHep1 controls which indicated that TbHep1 may be self-aggregating in a dose-dependent manner. The possible self-aggregation of TbHep1 produces considerable variation and an inconsistent reduction in TbmtHsp70 aggregation values in a manner which did not resemble data seen in the *H. sapien* orthologues (Figure 3.13B). This variation may indicate that the spectrophotometric approach may not be applicable to the study of this orthologue. The bioinformatic analysis undertaken using Alphafold may provide further evidence, with the N-terminal α-helical structures described in Chapter 2 possibly being involved in the formation of oligomers.

To confirm if TbHep1 suppresses the thermally induced aggregation of mtHsp70, a second assay was generated using a method derived from MDH aggregation assays using heating at 45 ℃ followed by SDS-PAGE and densitometric analyses undertaken instead of absorbance readings Figure 3.14). Using this method, ratios between the soluble supernatant and insoluble pellet fractions of TbmtHsp70 were made over a range of Hep1 concentrations and compared with the values generated using TbmtHsp70 alone, which was used to represent 100 % aggregation.

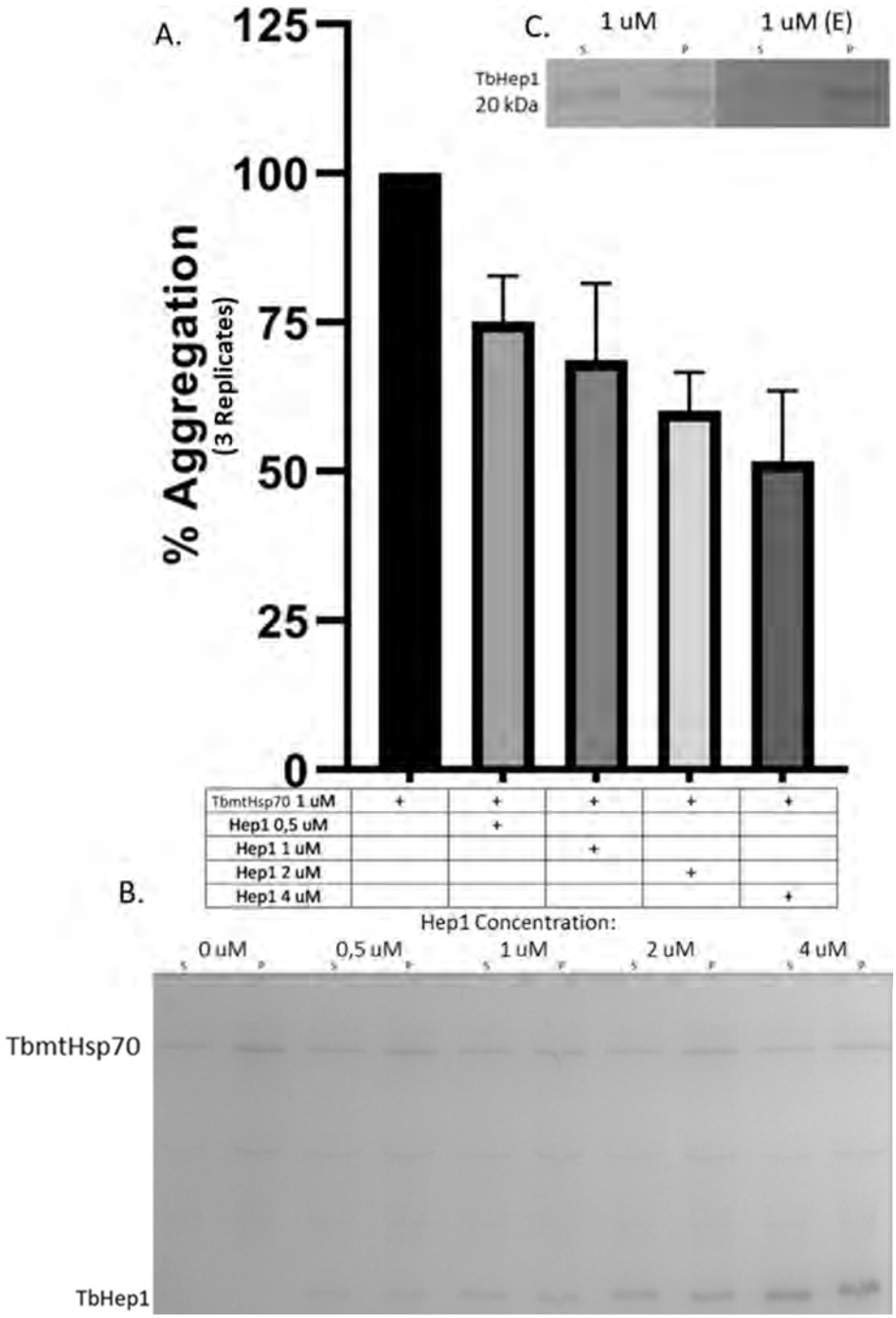


Figure 3.14: Densitometric analysis of TbmtHsp70 aggregation: (A) The aggregation of TbmtHsp70 displayed as a proportion of 100 % aggregation in the absence TbHep1. (B) An SDS-PAGE (12 %) displaying the solubilization of TbmtHsp70 from the insoluble pellet (P) into the soluble supernatant fraction (S) in the presence of increasing amounts of TbHep1. (C) A comparison of solubility between 1 uM of TbHep1 (1 uM) and 1 uM EDTA-treated TbHep1 (1 uM (E)) after thermal aggregation in the presence of 1 uM TbmtHsp70.

This method provided more reliable data which indicated that TbHep1 does suppress the thermally induced aggregation of TbmtHsp70 in a dose-dependent manner with the presence of 0,5 uM

TbHep1 decreasing the aggregation of TbmtHsp70 by approximately 25 % (Figure 3.14A). The lowest values were observed in the presence of 4 uM TbHep1 which reduced aggregation by approximately 50 %. The formation of a complex between TbHep1 and TbmtHsp70 may be occurring as the negative controls undertaken displayed a higher concentration of TbHep1 within the insoluble pellet fraction in the absence of TbmtHsp70, suggesting that the presence of TbmtHsp70 may reduce TbHep1 aggregation (Appendix A10).

Unfortunately, the use of this method and the inconsistency of the light scattering assay provided no standard data to allow comparisons with TbHep1 treated with EDTA and prevented analysis of the effects of EDTA treatment on the activity of TbHep1. However, the densitometric analysis of 1 uM EDTA-treated TbHep1 did exhibit a larger portion of insoluble TbHep1 within the pellet in comparison to 1 uM of untreated TbHep1 when in the presence of 1 uM TbmtHsp70 (Figure 3.14C). These results provide preliminary evidence that suggests the structure of this orthologue does rely on the zinc-ion localized within the zf-DNL as described in previous studies of Hep1 orthologues.

### 3.4.8 TbHep1 does not affect the thermally induced aggregation of malate dehydrogenase

The ability of TbHep1 to suppress the thermally induced aggregation of proteins other than TbmtHsp70 was analyzed using MDH as a model substrate. MDH is a ubiquitous protein within the plant and animal kingdoms and is often used to study the effectiveness of a chaperone when suppressing protein aggregation (Goloubinoff et al., 1999; Basha et al., 2004; Botha et al., 2007). In studies of co-chaperones such as Hep1, MDH is used to demonstrate the specificity of a co-chaperone to the client chaperone and whether it can suppress the aggregation of other proteins (Dores-Silva et al., 2013).

MDH was found to aggregate at 48°C, while TbHep1 at concentrations ranging between 0,30–1,44 uM produced minor aggregation. This allowed an assessment of the specificity of TbHep1 by comparing this activity to HsHep1, which has previously been observed to reduce MDH aggregation

(Dores-Silva et al., 2013). This method was carried out using densitometric analysis, using this method, ratios between the soluble supernatant and insoluble pellet fractions of MDH were observe. These were then compared to readings generated using the same concentration of MDH exposed to the same environment, but in the presence of Hep1 at a range of concentrations. The values generated using MDH alone, was used to represent 100 % aggregation as described in Dores-Silva et al. (2013) (Figure 3.15).

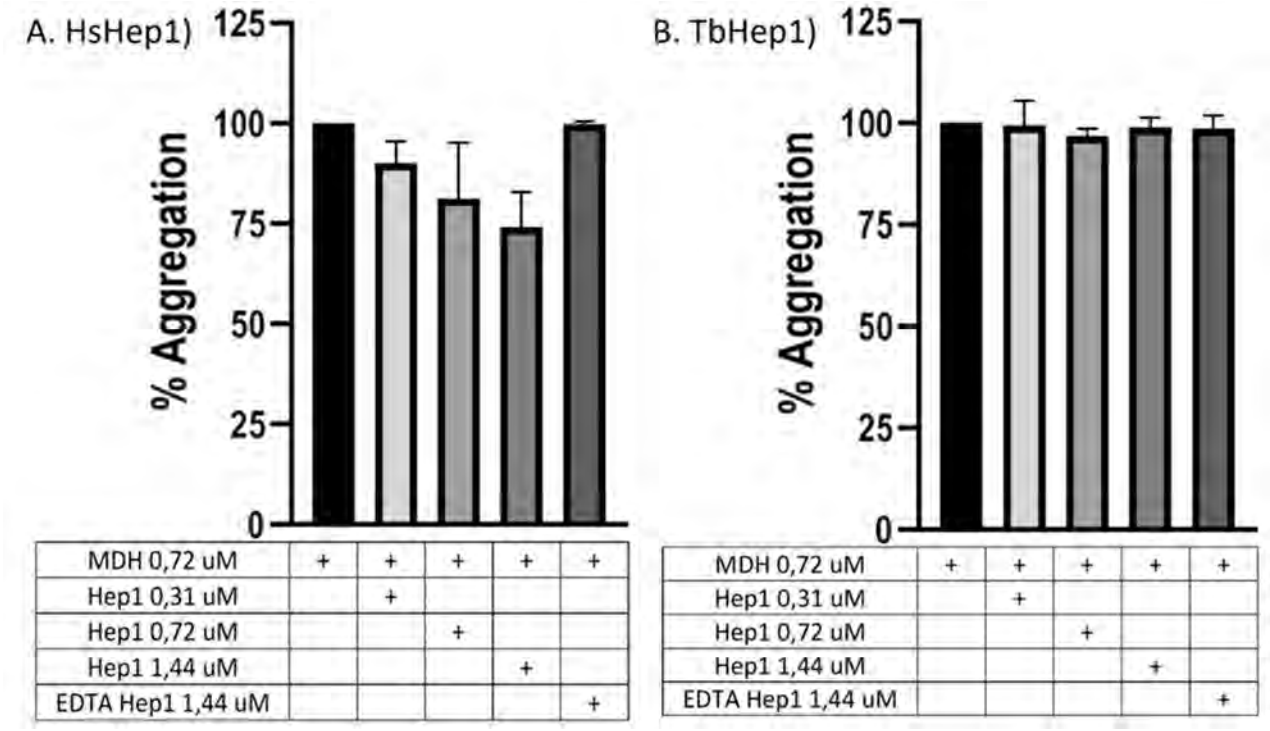


Figure 3.15: The suppression of thermally induced malate dehydrogenase aggregation by Hep1: The aggregation of MDH displayed as a proportion of 100 % aggregation in the absence of Hep1 with (A) indicating HsHep1 and (B) showing TbHep1. With the lower table indicating the concentrations used. These results are the product of 3 separate assays.

TbHep1 had no effect on the aggregation of MDH over the range of concentrations used (Figure 3.15B); this contrasted with HsHep1, which indicated that MDH was solubilized by approximately 25 % at a concentration of 1,44 uM (Figure 3.15A), resembling results previously generated in other HsHep1 studies (Dores-Silva et al., 2021). This resembles previous studies of orthologues derived from other protozoan parasites such as *P. falciparum* and *L. braziliensis* which could not suppress the aggregation of MDH (Nyakundi et al., 2016; Dores-Silva et al., 2017). The observations made regarding possible complex formation between TbmtHsp70 and TbHep1, in which the presence of TbmtHsp70 may have reduced TbHep1 aggregation, were not observed in these experiments as

TbHep1 aggregated in similar concentrations regardless of the presence of MDH. This observation may indicate that TbmtHsp70 and TbHep1 form a complex in a manner that does not occur between TbHep1 and MDH.

### 3.4.9 Conclusion

The *T. brucei* orthologue of mtHsp70 shares the property of self-aggregation described in other orthologues and requires the actions of TbHep1 to be produced in a soluble form. TbHep1 is also capable of suppressing the thermally induced aggregation of TbmtHsp70 although this orthologue is less effective than HsHep1 with a maximum of ~ 50 % reduction in TbmtHsp70 aggregation when 4 uM of TbHep1 was present with 1 uM of TbmtHsp70, while HsHep1 decreased mortalin aggregation by ~ 65 % at this ratio.

TbHep1 is unable to affect the aggregation of the model substrate MDH, no reduction in aggregation was observed whilst HsHep1 was capable of reducing MDH aggregation by ~ 25 % when 1,44 uM HsHep1 was present with 0,72 uM of MDH. The effect that the loss of the zinc-ion within the zf-DNL has on the functionality of TbHep1 could not be confirmed. However, densitometric observations could be made which suggested a loss of TbHep1 structural integrity when the zinc-ion was chelated using EDTA due to the increased concentration of insoluble TbHep1 following aggregation assays relative to untreated TbHep1.

TbHep1 aggregation may suggest that the orthologue oligomerizes, a characteristic which has only been observed in the orthologues derived from *P. falciparum* which has unique arginine repeats and HsHep1 at high concentrations greater than 2 mg/mL and these orthologues were observed functioning as monomers (Nyakundi et al., 2016; Dores-Silva et al., 2021). The oligomerization state at which TbHep1 operates therefore required further investigation.

# Chapter 4: Conclusions and future work

To ensure that the eradication of *T. brucei* is complete and lasting, an understanding of the organism's life cycle is required. Knowledge of the quiescent form that the parasite adopts is required to ease transmission between vectors, respond to medications and adapt to adverse conditions; this is particularly important in preventing remission cases and eradicating the parasite within reservoirs (Njiokou et al., 2006, 2010). The mitochondrion of kinetoplasts is essential for the viability of the organisms and is particularly crucial to the cell cycle pathways which govern the differentiation of parasitic species within the class (Fenn & Matthews, 2007; Quintana et al., 2021). MtHsp70 has been shown to play a central role in multiple cell cycle pathways within other organisms and may undertake similar processes within *T. brucei*. The chaperone also plays a critical role in other mitochondrial functions; these include acting as a motor to provide the driving force to the TIM complex during pre-protein translocation (Bohnert et al., 2007), maintenance and formation of the complexes involved in the electron transport chain (Herrmann et al., 1994; Böttinger et al., 2015) and maintenance of mtDNA (Herrmann et al., 1994). MtHsp70 is also crucial to properly folding and maintaining mitochondrial proteins (Pfanner & Geissler, 2001; Young et al., 2001). MtHsp70 often operates in tandem with the chaperonin pathways (Hsp60) (Kaul, et al., 2006). The central role of the mitochondria and mtHsp70 has made it a candidate for drug targeting in treating other parasitic protozoa, such as *P. falciparum* (Zininga et al., 2015).

*T. brucei* has three genes that code for mtHsp70 (A, B and C); these genes are identical and are the product of gene duplication within *T. brucei* (Louw et al., 2010). However, *T. brucei* mtHsp70 requires further biochemical characterization. This is required to confirm if the orthologue bares the same properties observed in other orthologues. Previous studies of mtHsp70 orthologues have been slowed by difficulties regarding the aggregation of mtHsp70 upon expression, which prevented purification without treatment using detergents or solvents, which resulted in the abrogation of activity. MtHsp70 within yeast was found to require the presence of Hep1 to be expressed in a soluble form while maintaining functionality and the absence of Hep1 abrogated cellular viability (Szklarz et al., 2005; Sichting et al., 2005). Hep1 was later found to be necessary to the folding of

mtHsp70 and the abrogation of mtHsp70 self-aggregation, which has made the protein essential to the functionality of the chaperone (Sichting et al., 2005; Blamowska et al., 2012).

This study investigated the biochemical properties of TbmtHsp70 to discern if the orthologue maintains the properties of aggregation and an examination of TbHep1 to observe if the orthologue could maintain TbmtHsp70 in a functional and soluble state as previously described in other orthologues. The recently described Alphafold modelling program was also implemented to allow an examination of conserved regions and residues implicated in the aggregation properties of TbmtHsp70. This would also allow the production of TbmtHsp70 and TbHep1 models, which have previously been elusive due to the aggregation of mtHsp70 orthologues and the availability of only the zf-DNL of Hep1 from the yeast orthologue (Tim15c) (Momose et al., 2007).

Sequence analysis indicated that TbmtHsp70 maintained the residues implicated in aggregation properties and was likely to possess this characteristic suggesting that it may require interaction with TbHep1 to maintain structural and functional integrity. TbHep1 shared little similarity outside the zinc finger domain with other orthologues and had a larger C-terminal than other aligned orthologues apart from the Hep1 orthologue from *L. braziliensis*. The tetracysteine motif found to be required for Hep1 functionality and structure was maintained in TbHep1 and indicated that it operates in a similar manner. These results suggest that the orthologues shared the characteristics previously identified in other orthologues, with TbmtHsp70 requiring TbHep1 for its expression and activity.

*In vitro* analysis confirmed that TbmtHsp70 aggregated when heterologously expressed in *E. coli* cells. Several treatments using detergents successfully solubilized TbmtHsp70 and allowed purification of the chaperone. Soluble TbmtHsp70 was produced when co-expressed with TbHep1, indicating that Hep1 is required for the correct folding and maintenance of TbmtHsp70. Preliminary aggregation assays did indicate that Hep1 was capable of reducing the aggregation of non-functional TbmtHsp70 solubilized through chemical treatments. These results indicate that the *T. brucei* orthologues may resemble the typical mtHsp70 properties previously described and requires the actions of TbHep1 to be produced in an active form. These findings in this study can confirm that TbHep1 acts as a co-factor which prevents the self-aggregating tendency of TbmtHsp70 and maintains it in a functional state. Further work should be undertaken using size exclusion chromatography and isothermal titration calorimetry (ITC) to identify the oligomeric state of

TbmtHsp70 in the presence of Hep1 and if it resembles the monomeric form observed in other orthologues (Palleros et al., 1993).

When studying the suppression of thermally induced TbmtHsp70 aggregation, TbHep1 was not seen to operate similarly to orthologues previously described in other studies. Initially, this was suspected to be a result of assay conditions. However, extensive alterations to the assay conditions and troubleshooting did not affect the results obtained, which indicated that TbHep1 aggregated in a dose-dependent manner. It appeared to be more susceptible to aggregation than HsHep1. Densitometric analysis was undertaken, which allowed the analysis of TbmtHsp70 aggregation separate from TbHep1 aggregation, which was not possible during spectrophotometric-based assays adapted from previous studies of this interaction. This allowed confirmation of the ability of TbHep1 to suppress thermally induced TbmtHsp70 aggregation, although it did not explain why TbHep1 aggregated at such low concentrations. Aggregation has also been observed in the *H. sapien* orthologue, although this was only at high concentrations (2 mg/mL) and the orthologue was shown to operate in a monomer form (Dores-Silva et al., 2021). Future work must be undertaken to investigate the folding characteristics of TbHep1 using ITC and circular dichroism (CD) analysis, as this would provide information on the structure of TbHep1 under varying conditions of stress. Investigations into what oligomeric state TbHep1 operates in using ITC, as described in Dores-Silva et al. (2021), would also allow investigations into how similar the operations of TbHep1 and HsHep1 are to one another.

TbHep1 was incapable of suppressing MDH thermal aggregation, suggesting that the TbHep1 interaction was more specific than that observed within orthologues such as HsHep1 (Dores-Silva et al., 2021). However, future work must be undertaken using other aggregation-prone model proteins, such as citrate synthase and rhodanese, to confirm this. If the specificity of TbHep1 for TbmtHsp70 can be confirmed, then the inhibition of this interaction may be a promising target for pharmaceuticals due to TbmtHsp70s reliance on TbHep1.

Due to the inconsistencies within the spectrophotometrically based data, the ability of EDTA to abrogate the functions of TbHep1 via removal of the zinc ion could not be confirmed as it has been in the study of other Hep1 orthologues. This was due to the addition of TbHep1 readings to TbmtHsp70 aggregation readings when using TbHep1 that wasn't treated with EDTA, thereby

preventing the generation of a standard to compare with EDTA-treated TbHep1. However, a collapse in the structure of the orthologue could be confirmed as EDTA-treated TbHep1 was observed aggregating to a greater degree relative to the native TbHep1 when exposed to temperatures of 48℃, with no portion remaining in the soluble fraction. Future work must be undertaken to confirm that the abrogation of TbHep1 functionality also occurs with the removal of the zinc-ion. The lack of western blot confirmation is the largest issue experienced in the biochemical analyses of the protein, while dot-blots have provided a degree of confirmation this is far less reliable and this issue needs to be addressed to examine if the results of this study are maintained in other studies which are capable of western confirmation.

The phylogenetic analyses indicate that the most closely related orthologues to TbHep1 are HsHep1 and LbHep1 and share a sequence identity of 43.7 and 33.3 %, respectively, and TbHep1-LbHep1 sequence identity is similar to that of HsHep1-LbHep1 which is 34.9 %. Previously the extended C-terminal of HsHep1 was theorized to play a role in the stimulation of mtHsp70 ATPase activity; however, LbHep1 lacks this region but maintains the co-chaperoning activity (Dores-Silva et al., 2017). Future work should also be undertaken to observe if co-chaperoning activities are present within TbHep1, such as the stimulation of TbmtHsp70 ATPase activity, which has been observed in the HsHep1 and LbHep1 orthologues (Zhai et al., 2008; Dores-Silva et al., 2017). If this ability is shared in TbHep1, an investigation into the influence of the extended N-terminal region of these orthologues may be warranted as they share this characteristic, and there is considerable sequence similarity between the two in this region. Cell-based microscopy studies should also be undertaken to investigate the possibility of TbHep1 being localized outside of the mitochondrion, as has been observed with HsHep1 (Dores-Silva et al., 2021).

Observations of the relationship of TbHep1 to the extensive JDP network of *T. brucei* indicate that the orthologue's closest phylogenetic relationship is J23, otherwise known as PAM23. This type-III JDP unique to kinetoplasts functionally replaces PAM18, found in other organisms and provides the ATPase stimulation to mtHsp70 bound to the TIM complex. This stimulation is required in the translocation of preproteins via the presequence pathway. The close evolutionary relationship may provide insight into the theory that Hep1 orthologues may operate as a 'fractured' JDP, providing the zinc finger domain to type-III JDPs that lack the domain (Burri et al., 2004). STRING analysis did not correlate with these results; however, as described by Känel et al. (2020), this is likely a

failure of bioinformatic characterization brought about by a lack of data on the J23 protein and the current role that PAM18 plays within kinetoplast organisms. This result must be investigated in future work, possibly via observations of TbmtHsp70 ATPase activity stimulation via J23 in the presence and absence of TbHep1 with the use of peptide substrates to observe if TbHep1 plays a role in substrate delivery as theorized by Burri et al., (2004). Studies should also be conducted on the PAM18 protein within *T. brucei* to ascertain the current function it plays that has resulted in kinetoplasts maintaining the protein despite the functional replacement of J23 within the PAM complex. These results provide compelling evidence that using *T. brucei* as a model organism in studying heat shock machinery may be beneficial as structures may be more specialised to particular activities, providing insight into specific interactions (Folgueira et al., 2007).

The release of the AI-driven Alphafold modelling program provided a means of examining the entire structure of TbHep1. Previously, only the NMR-derived structure of the zinc finger domain from *S. cerevisiae*, Tim15c, has been available to model Hep1 orthologues (Momose et al., 2007). This has hampered the bioinformatically based analysis of structures which may be of interest to Hep1 operations, such as the extended C-terminal of HsHep1, which is suspected to impart the ability to stimulate the ATPase domain of mortalin (Zhai et al., 2011). Using this new program, the extended N-terminal of TbHep1 could be analysed. The model indicated the presence of α-helical structures within this region, which are not present in HsHep1; these may act as an oligomerization point for the orthologue. The presence of these structures and inconsistent results of the biochemically based assays may suggest that TbHep1 operates in a unique manner when compared to HsHep1 and other orthologues. Future work must be undertaken to confirm this biochemically. If these results are maintained, it may provide an avenue by which the TbHep1-TbmtHsp70 interaction within *T. brucei* can be targeted without interfering with this interaction between host orthologues.

Following the use of Alphafold in identifying a possible structure impairing the biochemical characterization of TbHep1, an investigation of mtHsp70 was undertaken to observe if the program could shed light on how residues previously implicated in the self-aggregation of the chaperone may impart the property. Models of non-aggregating Hsp70, such as DnaK, have been produced via peptide-fusion studies and the implementation of cysteine mutations which lock the orthologue in a desired state to allow the production of a model (Grindle et al., 2021; Wang et al., 2021). This has provided insights into how Hsp70 operates; however, it has not permitted investigations into how

conserved residues, such as the GVFEV motif and the linker region, cause mtHsp70 orthologues to self-aggregate.

Alphafold allowed investigations into the GVFEV motif and linker regions. These indicated that the replacement of the lysine (K) of the KTFEV motif of DnaK with glycine (G) might prevent the formation of bonds to a region buried between the subdomains of lobe II within the NBD, thereby reducing bond stress in the linker region and possibly allowing aggregation to take place. This must be investigated in future work; studies have already indicated that replacing the GVFEV motif with the one found in DnaK abrogated the self-aggregating property of Ssc1 in yeast (Blamowska et al., 2010). However, if the replacement of the glycine residue with lysine is shown to abrogate the self-aggregation of mtHsp70, the range of implicated residues can be reduced from a motif to a single residue. This would also provide valuable observations regarding the validity of Alphafold-produced models when identifying critical residues in protein structures.

Another observation made using Alphafold was that all aggregating orthologues have a conserved LEI sequence located parallel to the GVFEV motif, which forms multiple bonds between the two (Appendix A11 and A12). However, in Ssc1, the glutamic acid (E) has been altered to aspartic acid (D), disrupting the sidechain bonds between the GVFEV motif and the LDI residues of Ssc1 (Appendix A13). Since mutation studies of the GVFEV motif have only been conducted using Ssc1, this may warrant a repeat of the experiment carried out in Blamowska et al. (2010) using an alternative mtHsp70 to confirm that the abrogation of aggregation is consistent across multiple orthologues. This may be necessary as the glutamic to the aspartic acid alteration within Ssc1 may have resulted in the removal of a bond contributing to the aggregation brought about by the GVFEV motif that has been missed due to the unique evolutionary progression of this *S. cerevisiae* orthologue.

When Alphafold is combined with several secondary structure prediction tools, such as the consolidated Quick2D program, this can amount to a powerful way of rapidly characterizing proteins that lack models derived from other methods, such as NMR and X-ray crystallography. An example is the structure of TbHep1; in previous studies, Hep1 orthologues, even that of LbHep1 from the Trypanosomatida order, have exhibited similar properties and structures. The difficulties experienced in characterizing TbHep1 as a result of unique structural additions which are not

available to previous modelling techniques indicate that this new technology may be a crucial addition, providing information which can significantly reduce laboratory costs in both time and expenses.

This new technology will need to be confirmed, the results can differ significantly from previously determined protein structures, and further experimentation is required to elucidate the causes between these differences. Initially it must be investigated whether Alphafold has provided a more accurate view of protein folding than the previous NMR-determined structures with particular emphasis on Tim15c. This will require comparative studies to be undertaken by those specialized in NMR procedures who are more versed in the positives and negatives of NMR protein structure analysis; preferably, any investigation can be conducted in conjunction with the programmers behind DeepMind technology to elucidate where these differences have originated and thereby contribute to the development of this new bioinformatic tool.

Alphafold is still in its infancy and is expected to be improved in subsequent iterations. Of particular interest would be the ability to include small molecules such as ATP and peptide substrates so that different states of proteins like Hsp70 could be examined. The ability to alter the virtual environment that the protein is theoretically folded in to observe what effects differing pH, salt concentrations and temperature alterations can bring about would also be fascinating. Future work must be devoted to confirming the results of this program; however, its development and release to the general public is appreciated, and developments in this technology will be monitored with great interest.

This study has provided initial confirmation regarding the idea that TbmtHsp70 shares the property of aggregation common to other mtHsp70 orthologues, it has also been shown that this property is abrogated in the presence of TbHep1, indicating that the solubilizing interaction with Hep1 is maintained. TbHep1 was seen to operate less effectively than HsHep1, however, it may act in a unique manner when compared to other orthologues. This requires further examination because if this mechanism is significantly different to that of the *H. sapien* orthologue, this may provide a new drug target for the treatment of HAT. Further work into this field will be closely followed as this may represent a new approach to targeting parasite-derived diseases and multiple forms of cancer.

# References


Acestor, N., Panigrahi, A. K., Ogata, Y., Anupama, A., & Stuart, K. D. (2009). Protein composition of *Trypanosoma brucei* mitochondrial membranes. *Proteomics*, *9*(24), 5497. https://doi.org/10.1002/PMIC.200900354

Alsford, S., Turner, D. J., Obado, S. O., Sanchez-Flores, A., Glover, L., Berriman, M., Hertz-Fowler, C., & Horn, D. (2011). High-throughput phenotyping using parallel sequencing of RNA interference targets in the African trypanosome. Genome Research, 21(6), 915–924. https://doi.org/10.1101/GR.115089.110

Amos, B., Aurrecoechea, C., Barba, M., Barreto, A., Basenko, E. Y., Bażant, W., Belnap, R., Blevins, A. S., Böhme, U., Brestelli, J., Brunk, B. P., Caddick, M., Callan, D., Campbell, L., Christensen, M. B., Christophides, G. K., Crouch, K., Davis, K., Debarry, J., … Zheng, J. (2022). VEuPathDB: The eukaryotic pathogen, vector and host bioinformatics resource center. *Nucleic Acids Research*, *50*(D1), D898–D911. https://doi.org/10.1093/NAR/GKAB929

Ashburner, M., Ball, C. A., Blake, J. A., Botstein, D., Butler, H., Cherry, J. M., Davis, A. P., Dolinski, K., Dwight, S. S., Eppig, J. T., Harris, M. A., Hill, D. P., Issel-Tarver, L., Kasarskis, A., Lewis, S., Matese, J. C., Richardson, J. E., Ringwald, M., Rubin, G. M., & Sherlock, G. (2000). Gene Ontology: tool for the unification of biology. *Nature Genetics 2000 25:1*, *25*(1), 25–29. https://doi.org/10.1038/75556

Aslett, M., Aurrecoechea, C., Berriman, M., Brestelli, J., Brunk, B. P., Carrington, M., Depledge, D. P., Fischer, S., Gajria, B., Gao, X., Gardner, M. J., Gingle, A., Grant, G., Harb, O. S., Heiges, M., Hertz-Fowler, C., Houston, R., Innamorato, F., Iodice, J., Wang, H. (2009). TriTrypDB: A functional genomic resource for the Trypanosomatidae. *Nucleic Acids Research*, *38*(SUPPL.1). https://doi.org/10.1093/NAR/GKP851

Autheman, D., Crosnier, C., Clare, S., Goulding, D. A., Brandt, C., Harcourt, K., Tolley, C., Galaway, F., Khushu, M., Ong, H., Romero-Ramirez, A., Duffy, C. W., Jackson, A. P., & Wright, G. J. (2021). An invariant *Trypanosoma vivax* vaccine antigen induces protective immunity. *Nature 2021 595:7865*, *595*(7865), 96–100. https://doi.org/10.1038/s41586-021-03597-x

Bahl, A., Brunk, B., Crabtree, J., Fraunholz, M. J., Gajria, B., Grant, G. R., Ginsburg, H., Gupta, D., Kissinger, J. C., Labo, P., Li, L., Mailman, M. D., Milgram, A. J., Pearson, D. S., Roos, D. S., Schug, J., Stoeckert, C. J., & Whetzel, P. (2003). PlasmoDB: the Plasmodium genome resource. A database integrating experimental and computational data. *Nucleic Acids Research*, *31*(1), 212. https://doi.org/10.1093/NAR/GKG081

Bahr, T., Katuri, J., Liang, T., & Bai, Y. (2022). Mitochondrial chaperones in human health and disease. *Free Radical Biology and Medicine*, *179*, 363–374. https://doi.org/10.1016/J.FREERADBIOMED.2021.11.015

Balch, W. E., Morimoto, R. I., Dillin, A., & Kelly, J. W. (2008). Adapting proteostasis for disease intervention. *Science*, *319*(5865), 916–919. https://doi.org/10.1126/SCIENCE.1141448

Baloyannis, S. J. (2006). Mitochondrial alterations in Alzheimer's disease. *Journal of Alzheimer's Disease : JAD*, *9*(2), 119–126. https://doi.org/10.3233/JAD-2006-9204

Baneyx, F. (1999). Recombinant protein expression in Escherichia coli. *Current Opinion in Biotechnology*, *10*(5), 411–421. https://doi.org/10.1016/S0958-1669(99)00003-8

Barouch, W., Prasad, K., Greene, L., & Eisenberg, E. (1997). Auxilin-induced interaction of the molecular chaperone Hsc70 with clathrin baskets. *Biochemistry*, *36*(14), 4303–4308. https://doi.org/10.1021/BI962727Z

Basha, E., Lee, G. J., Demeler, B., & Vierling, E. (2004). Chaperone activity of cytosolic small heat shock proteins from wheat. *European Journal of Biochemistry*, *271*(8), 1426–1436. https://doi.org/10.1111/J.1432-1033.2004.04033.X

Bateman, A., Martin, M. J., Orchard, S., Magrane, M., Agivetova, R., Ahmad, S., Alpi, E., Bowler-Barnett, E. H., Britto, R., Bursteinas, B., Bye-A-Jee, H., Coetzee, R., Cukura, A., da Silva, A., Denny, P., Dogan, T., Ebenezer, T. G., Fan, J., Castro, L. G., Teodoro, D. (2021). UniProt: the universal protein knowledgebase in 2021. *Nucleic Acids Research*, *49*(D1), D480–D489. https://doi.org/10.1093/NAR/GKAA1100

Benaroudj, N., Triniolles, F., & Ladjimi, M. M. (1996). Effect of nucleotides, peptides, and unfolded proteins on the self-association of the molecular chaperone HSC70. *The Journal of Biological Chemistry*, *271*(31), 18471–18476. https://doi.org/10.1074/JBC.271.31.18471

Bentley, S. J., & Boshoff, A. (2019). *Trypanosoma brucei* J-Protein 2 functionally co-operates with the cytosolic Hsp70 and Hsp70.4 Proteins. *International Journal of Molecular Sciences 2019, Vol. 20, Page 5843*, *20*(23), 5843. https://doi.org/10.3390/IJMS20235843

Bentley, S. J., Jamabo, M., & Boshoff, A. (2019). The Hsp70/J-protein machinery of the African trypanosome, *Trypanosoma brucei*. *Cell Stress & Chaperones*, *24*(1), 125–148. https://doi.org/10.1007/S12192-018-0950-X

Bernaudat, F., Frelet-Barrand, A., Pochon, N., Dementin, S., Hivin, P., Boutigny, S., Rioux, J. B., Salvi, D., Seigneurin-Berny, D., Richaud, P., Joyard, J., Pignol, D., Sabaty, M., Desnos, T., Pebay-Peyroula, E., Darrouzet, E., Vernet, T., & Rolland, N. (2011). Heterologous expression of membrane proteins: choosing the appropriate host. *PloS One*, *6*(12). https://doi.org/10.1371/JOURNAL.PONE.0029191

Bertelsen, E. B., Chang, L., Gestwicki, J. E., & Zuiderweg, E. R. P. (2009). Solution conformation of wild-type *E. coli* Hsp70 (DnaK) chaperone complexed with ADP and substrate. *Proceedings of the National Academy of Sciences of the United States of America*, *106*(21), 8471–8476. https://doi.org/10.1073/PNAS.0903503106

Bhat, S. S., Anand, D., & Khanday, F. A. (2015). p66Shc as a switch in bringing about contrasting responses in cell growth: implications on cell proliferation and apoptosis. *Molecular Cancer 2015 14:1*, *14*(1), 1–12. https://doi.org/10.1186/S12943-015-0354-9

Bitto, E., Bingman, C. A., Bittova, L., Kondrashov, D. A., Bannen, R. M., Fox, B. G., Markley, J. L., & Phillips, G. N. (2008). Structure of human J-type co-chaperone HscB reveals a tetracysteine metal-binding domain. *The Journal of Biological Chemistry*, *283*(44), 30184–30192. https://doi.org/10.1074/JBC.M804746200

Blamowska, M., Neupert, W., & Hell, K. (2012). Biogenesis of the mitochondrial Hsp70 chaperone. *The Journal of Cell Biology*, *199*(1), 125–135. https://doi.org/10.1083/JCB.201205012

Blamowska, M., Sichting, M., Mapa, K., Mokranjac, D., Neupert, W., & Hell, K. (2010). ATPase domain and interdomain linker play a key role in aggregation of mitochondrial Hsp70 chaperone Ssc1. *Journal of Biological Chemistry*, *285*(7), 4423–4431. https://doi.org/10.1074/JBC.M109.061697

Bohnert, M., Pfanner, N., & van der Laan, M. (2007). A dynamic machinery for import of mitochondrial precursor proteins. *FEBS Letters*, *581*(15), 2802–2810. https://doi.org/10.1016/J.FEBSLET.2007.03.004

Bolender, N., Sickmann, A., Wagner, R., Meisinger, C., & Pfanner, N. (2008). Multiple pathways for sorting mitochondrial precursor proteins. *EMBO Reports*, *9*(1), 42–49. https://doi.org/10.1038/SJ.EMBOR.7401126

Botha, M., Pesce, E. R., & Blatch, G. L. (2007). The Hsp40 proteins of *Plasmodium falciparum* and other apicomplexa: regulating chaperone power in the parasite and the host. *The International Journal of Biochemistry & Cell Biology*, *39*(10), 1781–1803. https://doi.org/10.1016/J.BIOCEL.2007.02.011

Böttinger, L., Oeljeklaus, S., Guiard, B., Rospert, S., Warscheid, B., & Becker, T. (2015). Mitochondrial heat shock protein (Hsp) 70 and Hsp10 cooperate in the formation of Hsp60 complexes. *The Journal of Biological Chemistry*, *290*(18), 11611–11622. https://doi.org/10.1074/JBC.M115.642017

Bouteille, B., & Buguet, A. (2012). The detection and treatment of human African trypanosomiasis. *Research and Reports in Tropical Medicine*, *3*, 35. https://doi.org/10.2147/RRTM.S24751

Bracher, A., & Verghese, J. (2015). The nucleotide exchange factors of Hsp70 molecular chaperones. *Frontiers in Molecular Biosciences*, *2*(APR), 10. https://doi.org/10.3389/FMOLB.2015.00010/BIBTEX

Bradford, M.M. (1976). A rapid and sensitive method for the quantitation of microgram quantities of protein utilizing the principle of protein-dye binding. *Analytical Biochemistry*, *72*(1–2), 248–254. https://doi.org/10.1006/ABIO.1976.9999

Brehmer, D., Rüdiger, S., Gässler, C. S., Klostermeier, D., Packschies, L., Reinstein, J., Mayer, M. P., & Bukau, B. (2001). Tuning of chaperone activity of Hsp70 proteins by modulation of nucleotide exchange. *Nature Structural Biology*, *8*(5), 427–432. https://doi.org/10.1038/87588

Brun, R., Blum, J., Chappuis, F., & Burri, C. (2010). Human African trypanosomiasis. *Lancet*, *375*, 148–159.

Buchberger, A., Theyssen, H., Schroder, H., McCarty, J. S., Virgallita, G., Milkereit, P., Reinstein, J., & Bukau, B. (1995). Nucleotide-induced conformational changes in the ATPase and substrate binding domains of the DnaK chaperone provide evidence for interdomain communication. *Journal of Biological Chemistry*, *270*(28), 16903–16910. https://doi.org/10.1074/JBC.270.28.16903

Bukau, B., Deuerling, E., Pfund, C., & Craig, E. A. (2000). Getting newly synthesized proteins into shape. *Cell*, *101*(2), 119–122. https://doi.org/10.1016/S0092-8674(00)80806-5

Bukau, B., & Horwich, A. L. (1998). The Hsp70 and Hsp60 Chaperone Machines. *Cell*, *92*(3), 351–366. https://doi.org/10.1016/S0092-8674(00)80928-9

Burger, A., (2014). Purification and characterization of TbHsp70.c, a novel Hsp70 from Trypanosoma brucei. Rhodes University, South Africa

Burri, L., Vascotto, K., Fredersdorf, S., Tiedt, R., Hall, M. N., & Lithgow, T. (2004). Zim17, a novel zinc finger protein essential for protein import into mitochondria. *The Journal of Biological Chemistry*, *279*(48), 50243–50249. https://doi.org/10.1074/JBC.M409194200

Büscher, P., Cecchi, G., Jamonneau, V., & Priotto, G. (2017). Human African trypanosomiasis. *Lancet (London, England)*, *390*(10110), 2397–2409. https://doi.org/10.1016/S0140-6736(17)31510-6

Calvillo, M., Diaz, A., Limon, D. I., Mayoral, M. A., Chánez-Cárdenas, M. E., Zenteno, E., Montaño, L. F., Guevara, J., & Espinosa, B. (2013). Amyloid-β(25-35) induces a permanent phosphorylation of HSF-1, but a transitory and inflammation-independent overexpression of Hsp-70 in C6 astrocytoma cells. *Neuropeptides*, *47*(5), 339–346. https://doi.org/10.1016/J.NPEP.2013.06.002

Caro, F., Ahyong, V., Betegon, M., & DeRisi, J. L. (2014). Genome-wide regulatory dynamics of translation in the Plasmodium falciparum asexual blood stages. *ELife*, *3*. https://doi.org/10.7554/ELIFE.04106

Charney, W., Rose, L., & Quinlan, P. (2022). Pentamidine. Handbook of Modern Hospital Safety, Second Edition, 15-1-15–24. https://doi.org/10.2165/00128415-201113760-00075

Cheetham, M. E., & Caplan, A. J. (1998). Structure, function and evolution of DnaJ: conservation and adaptation of chaperone function. *Cell Stress & Chaperones*, *3*(1), 28. https://doi.org/10.1379/1466-1268(1998)003<0028:sfaeod>2.3.co;2

Craig, E. A., & Schlesinger, M. J. (1985). The heat shock response. *Http://Dx.Doi.Org/10.3109/10409238509085135*, *18*(3), 239–280. https://doi.org/10.3109/10409238509085135

Cuff, J. A., & Barton, G. J. (2000). Application of multiple sequence alignment profiles to improve protein secondary structure prediction. Proteins. 2000 Aug 15;40(3):502-511. https://doi.org/10.1002/1097-0134

Czarnecka, A. M., Campanella, C., Zummo, G., & Cappello, F. (2006). Mitochondrial chaperones in cancer: from molecular biology to clinical diagnostics. *Cancer Biology & Therapy*, *5*(7), 714–720. https://doi.org/10.4161/CBT.5.7.2975

Daugaard, M., Rohde, M., & Jäättelä, M. (2007). The heat shock protein 70 family: Highly homologous proteins with overlapping and distinct functions. *FEBS Letters*, *581*(19), 3702–3710. https://doi.org/10.1016/J.FEBSLET.2007.05.039

de Marco, A., Deuerling, E., Mogk, A., Tomoyasu, T., & Bukau, B. (2007). Chaperone-based procedure to increase yields of soluble recombinant proteins produced in *E. coli*. *BMC Biotechnology*, *7*(1), 1–9. https://doi.org/10.1186/1472-6750-7-32/TABLES/2

Dekker, S. L., Kampinga, H. H., & Bergink, S. (2015). DNAJs: More than substrate delivery to HSPA. *Frontiers in Molecular Biosciences*, *2*(JUN), 35. https://doi.org/10.3389/FMOLB.2015.00035/BIBTEX

Deocaris, C. C., Kaul, S. C., & Wadhwa, R. (2006). On the brotherhood of the mitochondrial chaperones mortalin and heat shock protein 60. *Cell Stress & Chaperones*, *11*(2), 116–128. https://doi.org/10.1379/CSC-144R.1

Deocaris, C. C., Yamasaki, K., Kaul, S. C., & Wadhwa, R. (2006). Structural and functional differences between mouse Mot-1 and Mot-2 proteins that differ in two amino acids. *Annals of the New York Academy of Sciences*, *1067*(1), 220–223. https://doi.org/10.1196/ANNALS.1354.027

Dierks, T., Klappa, P., Wiech, H., & Zimmermann, R. (1993). The role of molecular chaperones in protein transport into the endoplasmic reticulum. *Philosophical Transactions of the Royal Society of London. Series B, Biological Sciences*, *339*(1289), 335–341. https://doi.org/10.1098/RSTB.1993.0032

Dores-Silva, P. R., Barbosa, L. R. S., Ramos, C. H. I., & Borges, J. C. (2015). Human Mitochondrial Hsp70 (Mortalin): Shedding light on ATPase activity, interaction with adenosine nucleotides, solution structure and domain organization. *PLoS ONE*, *10*(1). https://doi.org/10.1371/JOURNAL.PONE.0117170

Dores-Silva, P. R., Kiraly, V. T. R., Moritz, M. N. de O., Serrão, V. H. B., dos Passos, P. M. S., Spagnol, V., Teixeira, F. R., Gava, L. M., Cauvi, D. M., Ramos, C. H. I., de Maio, A., & Borges, J. C. (2021). New insights on human Hsp70-escort protein 1: Chaperone activity, interaction with liposomes, cellular localizations and HSPA's self-assemblies remodeling. *International Journal of Biological Macromolecules*, *182*, 772–784. https://doi.org/10.1016/J.IJBIOMAC.2021.04.048

Dores-Silva, P. R., Minari, K., Ramos, C. H. I., Barbosa, L. R. S., & Borges, J. C. (2013). Structural and stability studies of the human mtHsp70-escort protein 1: An essential mortalin co-chaperone. *International Journal of Biological Macromolecules*, *56*, 140–148. https://doi.org/10.1016/J.IJBIOMAC.2013.02.009

Dores-Silva, P. R., Nishimura, L. S., Kiraly, V. T. R., & Borges, J. C. (2017). Structural and functional studies of the *Leishmania braziliensis* mitochondrial Hsp70: Similarities and dissimilarities to human orthologues. *Archives of Biochemistry and Biophysics*, *613*, 43–52. https://doi.org/10.1016/J.ABB.2016.11.004

Dragicevic, N., Mamcarz, M., Zhu, Y., Buzzeo, R., Tan, J., Arendash, G. W., & Bradshaw, P. C. (2010). Mitochondrial amyloid-beta levels are associated with the extent of mitochondrial dysfunction in different brain regions and the degree of cognitive impairment in Alzheimer's transgenic mice. *Journal of Alzheimer's Disease : JAD*, *20 Suppl 2*(SUPPL.2). https://doi.org/10.3233/JAD-2010-100342

Dric Notredame, C. Â., Higgins, D. G., & Heringa, J. (2000). T-Coffee: A novel method for fast and accurate multiple sequence alignment. *J. Mol. Biol*, *302*, 205–217. https://doi.org/10.1006/jmbi.2000.4042

Drini, S., Criscuolo, A., Lechat, P., Imamura, H., Skalický, T., Rachidi, N., Lukeš, J., Dujardin, J. C., & Späth, G. F. (2016). Species- and strain-specific adaptation of the HSP70 super family in pathogenic Trypanosomatids. *Genome Biology and Evolution*, *8*(6), 1980–1995. https://doi.org/10.1093/GBE/EVW140

Drozdetskiy, A., Cole, C., Procter, J., & Barton, G. J. (2015). JPred4: a protein secondary structure prediction server. *Nucleic Acids Research*, *43*(W1), W389–W394. https://doi.org/10.1093/NAR/GKV332

D'Silva, P. R., Schilke, B., Hayashi, M., & Craig, E. A. (2008). Interaction of the J-protein heterodimer Pam18/Pam16 of the mitochondrial import motor with the translocon of the inner membrane. *Molecular Biology of the Cell*, *19*(1), 424. https://doi.org/10.1091/MBC.E07-08-0748

Dutkiewicz, R., Schilke, B., Knieszner, H., Walter, W., Craig, E. A., & Marszalek, J. (2003). Ssq1, a mitochondrial Hsp70 involved in iron-sulfur (Fe/S) center biogenesis. Similarities to and differences from its bacterial counterpart. *The Journal of Biological Chemistry*, *278*(32), 29719–29727. https://doi.org/10.1074/JBC.M303527200

Ellis, J. (1987). Proteins as molecular chaperones. *Nature 1987 328:6129*, *328*(6129), 378–379. https://doi.org/10.1038/328378a0

Ellis, R. J. (2001). Macromolecular crowding: obvious but underappreciated. *Trends in Biochemical Sciences*, *26*(10), 597–604. https://doi.org/10.1016/S0968-0004(01)01938-7

Emadi, S., & Behzadi, M. (2014). A comparative study on the aggregating effects of guanidine thiocyanate, guanidine hydrochloride and urea on lysozyme aggregation. *Biochemical and*

*Biophysical Research Communications*, *450*(4), 1339–1344. https://doi.org/10.1016/J.BBRC.2014.06.133

Fairlamb, A. H., & Horn, D. (2018). Melarsoprol resistance in African Trypanosomiasis. *Trends in Parasitology*, *34*(6), 481–492. https://doi.org/10.1016/j.pt.2018.04.002

Falah, M., & Gupta, R. S. (1994). Cloning of the hsp70 (dnaK) genes from *Rhizobium meliloti* and *Pseudomonas cepacia*: phylogenetic analyses of mitochondrial origin based on a highly conserved protein sequence. *Journal of Bacteriology*, *176*(24), 7748–7753. https://doi.org/10.1128/JB.176.24.7748-7753.1994

Fan, C. Y., Lee, S., Ren, H. Y., & Cyr, D. M. (2004). Exchangeable chaperone modules contribute to specification of type I and type II Hsp40 cellular function. *Molecular Biology of the Cell*, *15*(2), 761–773. https://doi.org/10.1091/MBC.E03-03-0146/ASSET/IMAGES/LARGE/ZMK0020425230009.JPEG

Fenn, K., & Matthews, K. R. (2007). The cell biology of *Trypanosoma brucei* differentiation. *Current Opinion in Microbiology*, *10*(6), 539. https://doi.org/10.1016/J.MIB.2007.09.014

Field, M. C., Sergeenko, T., Wang, Y. N., Böhm, S., & Carrington, M. (2010). Chaperone requirements for biosynthesis of the trypanosome variant surface glycoprotein. *PloS One*, *5*(1). https://doi.org/10.1371/JOURNAL.PONE.0008468

Fishelson, Z., & Kirschfink, M. (2019). Complement C5b-9 and cancer: Mechanisms of cell damage, cancer counteractions, and approaches for intervention. *Frontiers in Immunology*, *10*(APR), 752. https://doi.org/10.3389/FIMMU.2019.00752/BIBTEX

Flaherty, K. M., DeLuca-Flaherty, C., & McKay, D. B. (1990). Three-dimensional structure of the ATPase fragment of a 70K heat-shock cognate protein. *Nature*, *346*(6285), 623–628. https://doi.org/10.1038/346623A0

Folgueira, C., Requena, J. M., de Biología Molecular, C., & Ochoa, S. (2007). A postgenomic view of the heat shock proteins in kinetoplastids. *FEMS Microbiology Reviews*, *31*(4), 359–377. https://doi.org/10.1111/J.1574-6976.2007.00069.X

Fraga, H., Papaleo, E., Vega, S., Velazquez-Campoy, A., & Ventura, S. (2012). Zinc induced folding is essential for TIM15 activity as an mtHsp70 chaperone. https://doi.org/10.1016/j.bbagen.2012.10.002

Fraga, J., Fernández-Calienes, A., Montalvo, A. M., Maes, I., Deborggraeve, S., Büscher, P., Dujardin, J. C., & van der Auwera, G. (2016). Phylogenetic analysis of the Trypanosoma genus based on the heat-shock protein 70 gene. *Infection, Genetics and Evolution*, *43*, 165–172. https://doi.org/10.1016/J.MEEGID.2016.05.016

Francis, D. M., & Page, R. (2010). Strategies to optimize protein expression in *E. coli*. *Current Protocols in Protein Science*, *61*(1), 5.24.1-5.24.29. https://doi.org/10.1002/0471140864.PS0524S61

Frankowska, N., Lisowska, K., & Witkowski, J. M. (2022). Proteolysis dysfunction in the process of aging and age-related diseases. *Frontiers in Aging*, *3*. https://doi.org/10.3389/FRAGI.2022.927630

Frazer, H. E., & Wisdom, G. B. (1985). Detection of autoantigens by immunoblotting using a peroxidase-anti-peroxidase complex. *Journal of Immunological Methods*, *80*(2), 221–225. https://doi.org/10.1016/0022-1759(85)90023-7

Freeman, B. C., Myers, M. P., Schumacher, R., & Morimoto, R. I. (1995). Identification of a regulatory motif in Hsp70 that affects ATPase activity, substrate binding and interaction with HDJ-1. *The EMBO Journal*, *14*(10), 2281–2292. https://doi.org/10.1002/J.1460-2075.1995.TB07222.X

Gabler, F., Nam, S. Z., Till, S., Mirdita, M., Steinegger, M., Söding, J., Lupas, A. N., & Alva, V. (2020). Protein sequence analysis using the MPI bioinformatics toolkit. *Current Protocols in Bioinformatics*, *72*(1), e108. https://doi.org/10.1002/CPBI.108

General, I. J., Liu, Y., Blackburn, M. E., Mao, W., Gierasch, L. M., & Bahar, I. (2014). ATPase subdomain IA is a mediator of interdomain allostery in Hsp70 molecular chaperones. *PLOS Computational Biology*, *10*(5), e1003624. https://doi.org/10.1371/JOURNAL.PCBI.1003624

Goloubinoff, P., Mogk, A., ben Zvi, A. P., Tomoyasu, T., & Bukau, B. (1999). Sequential mechanism of solubilization and refolding of stable protein aggregates by a bichaperone network. *Proceedings of the National Academy of Sciences*, *96*(24), 13732–13737. https://doi.org/10.1073/PNAS.96.24.13732

Goody, R. S., & Hofmann-Goody, W. (2002). Exchange factors, effectors, GAPs and motor proteins: common thermodynamic and kinetic principles for different functions. *European Biophysics Journal : EBJ*, *31*(4), 268–274. https://doi.org/10.1007/S00249-002-0225-3

Goswami, A. V., Chittoor, B., & D'Silva, P. (2010). Understanding the functional interplay between mammalian mitochondrial Hsp70 chaperone machine components. *Journal of Biological Chemistry*, *285*(25), 19472–19482. https://doi.org/10.1074/JBC.M110.105957

Grindle, M. P., Carter, B., Alao, J. P., Connors, K., Tehver, R., & Kravats, A. N. (2021). Structural communication between the *E. coli* chaperones DnaK and hsp90. *International Journal of Molecular Sciences*, *22*(4), 1–21. https://doi.org/10.3390/IJMS22042200

Groemping, Y., & Reinstein, J. (2001). Folding properties of the nucleotide exchange factor GrpE from *Thermus thermophilus*: GrpE is a thermosensor that mediates heat shock response. *Journal of Molecular Biology*, *314*(1), 167–178. https://doi.org/10.1006/jmbi.2001.5116

Guler, J. L., Kriegova, E., Smith, T. K., Lukeš, J., & Englund, P. T. (2008). Mitochondrial fatty acid synthesis is required for normal mitochondrial morphology and function in *Trypanosoma brucei*. *Molecular Microbiology*, *67*(5), 1125–1142. https://doi.org/10.1111/J.1365-2958.2008.06112.X

Güther, M. L. S., Urbaniak, M. D., Tavendale, A., Prescott, A., & Ferguson, M. A. J. (2014). High-confidence glycosome proteome for procyclic form *trypanosoma brucei* by epitope-tag organelle

enrichment and SILAC proteomics. *Journal of Proteome Research*, *13*(6), 2796–2806. https://doi.org/10.1021/PR401209W/SUPPL_FILE/PR401209W_SI_005.XLSX

Hanson, J., Yang, Y., Paliwal, K., & Zhou, Y. (2017). Improving protein disorder prediction by deep bidirectional long short-term memory recurrent neural networks. *Bioinformatics*, *33*(5), 685–692. https://doi.org/10.1093/BIOINFORMATICS/BTW678

Harrison, C. (2003). GrpE, a nucleotide exchange factor for DnaK. *Cell Stress & Chaperones*, *8*(3), 218. https://doi.org/10.1379/1466-1268(2003)008<0218:ganeff>2.0.co;2

Harrison, C. J., Hayer-Hartl, M., di Liberto, M., Hartl, F. U., & Kuriyan, J. (1997). Crystal structure of the nucleotide exchange factor GrpE bound to the ATPase domain of the molecular chaperone DnaK. *Science*, *276*(5311), 431–435. https://doi.org/10.1126/SCIENCE.276.5311.431/ASSET/FA0BB855-1D73-4ACD-B06C-3F2B803A3883/ASSETS/GRAPHIC/SE1775064004.JPEG

Hartl, F. U. (1996). Molecular chaperones in cellular protein folding. *Nature 1996 381:6583*, *381*(6583), 571–580. https://doi.org/10.1038/381571a0

Hartley, J. L. (2006). Cloning technologies for protein expression and purification. *Current Opinion in Biotechnology*, *17*(4), 359–366. https://doi.org/10.1016/J.COPBIO.2006.06.011

Havalová, H., Ondrovičová, G., Keresztesová, B., Bauer, J. A., Pevala, V., Kutejová, E., & Kunová, N. (2021). Mitochondrial HSP70 chaperone system—the influence of post-translational modifications and involvement in human diseases. *International Journal of Molecular Sciences 2021, Vol. 22, Page 8077*, *22*(15), 8077. https://doi.org/10.3390/IJMS22158077

Heffernan, R., Yang, Y., Paliwal, K., & Zhou, Y. (2017). Capturing non-local interactions by long short-term memory bidirectional recurrent neural networks for improving prediction of protein secondary structure, backbone angles, contact numbers and solvent accessibility. *Bioinformatics*, *33*(18), 2842–2849. https://doi.org/10.1093/BIOINFORMATICS/BTX218

Hennessy, F., Nicoll, W. S., Zimmermann, R., Cheetham, M. E., & Blatch, G. L. (2005). Not all J domains are created equal: Implications for the specificity of Hsp40–Hsp70 interactions. *Protein Science : A Publication of the Protein Society*, *14*(7), 1697. https://doi.org/10.1110/PS.051406805

Herrmann, J. M., Stuart, R. A., Craig, E. A., & Neupert, W. (1994). Mitochondrial heat shock protein 70, a molecular chaperone for proteins encoded by mitochondrial DNA. *The Journal of Cell Biology*, *127*(4), 893–902. https://doi.org/10.1083/JCB.127.4.893

Hidalgo, J., Ortiz, J. F., Fabara, S. P., Eissa-Garcés, A., Reddy, D., Collins, K. D., & Tirupathi, R. (2021). Efficacy and toxicity of Fexinidazole and Nifurtimox plus Eflornithine in the treatment of African trypanosomiasis: A Systematic Review. *Cureus*, *13*(8). https://doi.org/10.7759/CUREUS.16881

Honrath, B., Metz, I., Bendridi, N., Rieusset, J., Culmsee, C., & Dolga, A. M. (2017). Glucose-regulated protein 75 determines ER–mitochondrial coupling and sensitivity to oxidative stress in

neuronal cells. *Cell Death Discovery 2017 3:1*, *3*(1), 1–13. https://doi.org/10.1038/cddiscovery.2017.76

Hugenholtz, P. (2002). Exploring prokaryotic diversity in the genomic era. *Genome Biology*, *3*(2), 1–8. https://doi.org/10.1186/GB-2002-3-2-REVIEWS0003/TABLES/1

Imran, M., Khan, S. A., Alshammari, M. K., Alqahtani, A. M., Alanazi, T. A., Kamal, M., Jawaid, T., Ghoneim, M. M., Alshehri, S., & Shakeel, F. (2022). Discovery, development, inventions and patent review of Fexinidazole: The first all-oral therapy for human African trypanosomiasis. *Pharmaceuticals 2022, Vol. 15, Page 128*, *15*(2), 128. https://doi.org/10.3390/PH15020128

Jankovic, J. (2008). Parkinson's disease: clinical features and diagnosis. *Journal of Neurology, Neurosurgery & Psychiatry*, *79*(4), 368–376. https://doi.org/10.1136/JNNP.2007.131045

Jia, K., & Du, H. (2021). Mitochondrial permeability transition: a pore intertwines brain aging and Alzheimer's Disease. *Cells*, *10*(3), 1–14. https://doi.org/10.3390/CELLS10030649

Jin, J., Hulette, C., Wang, Y., Zhang, T., Pan, C., Wadhwa, R., & Zhang, J. (2006). Proteomic identification of a stress protein, mortalin/mthsp70/GRP75: Relevance to Parkinson disease. *Molecular and Cellular Proteomics*, *5*(7), 1193–1204. https://doi.org/10.1074/MCP.M500382-MCP200/ATTACHMENT/F59B96F5-C525-4371-85E8-DC679482C859/MMC1.ZIP

Jobanputra, K., Rajpal, A., & Nagpur, N. (2007). Eflornithine. *Indian Journal of Dermatology, Venereology and Leprology*, *73*(5), 365–366. https://doi.org/10.4103/0378-6323.35752

Jones, D. T. (1999). Protein secondary structure prediction based on position-specific scoring matrices. *Journal of Molecular Biology*, *292*(2), 195–202. https://doi.org/10.1006/JMBI.1999.3091

Jumper, J., Evans, R., Pritzel, A., Green, T., Figurnov, M., Ronneberger, O., Tunyasuvunakool, K., Bates, R., Žídek, A., Potapenko, A., Bridgland, A., Meyer, C., Kohl, S. A. A., Ballard, A. J., Cowie, A., Romera-Paredes, B., Nikolov, S., Jain, R., Adler, J., Hassabis, D. (2021). Highly accurate protein structure prediction with AlphaFold. *Nature 2021 596:7873*, *596*(7873), 583–589. https://doi.org/10.1038/s41586-021-03819-2

Kampinga, H. H., & Craig, E. A. (2010). The HSP70 chaperone machinery: J proteins as drivers of functional specificity. *Nature Reviews. Molecular Cell Biology*, *11*(8), 579–592. https://doi.org/10.1038/NRM2941

Kampinga, H. H., Hageman, J., Vos, M. J., Kubota, H., Tanguay, R. M., Bruford, E. A., Cheetham, M. E., Chen, B., & Hightower, L. E. (2009). Guidelines for the nomenclature of the human heat shock proteins. *Cell Stress & Chaperones*, *14*(1), 105–111. https://doi.org/10.1007/S12192-008-0068-7

Kang, P. J., Ostermann, J., Shilling, J., Neupert, W., Craig, E. A., & Pfanner, N. (1990). Requirement for hsp70 in the mitochondrial matrix for translocation and folding of precursor proteins. *Nature 1990 348:6297*, *348*(6297), 137–143. https://doi.org/10.1038/348137a0

Karzai, A. W., & McMacken, R. (1996). A bipartite signaling mechanism involved in DnaJ-mediated activation of the *Escherichia coli* DnaK protein. *The Journal of Biological Chemistry*, *271*(19), 11236–11246. https://doi.org/10.1074/JBC.271.19.11236

Katoh, K., Misawa, K., Kuma, K. I., & Miyata, T. (2002). MAFFT: a novel method for rapid multiple sequence alignment based on fast Fourier transform. *Nucleic Acids Research*, *30*(14), 3059–3066. https://doi.org/10.1093/NAR/GKF436

Kaul, S. C., Deocaris, C. C., & Wadhwa, R. (2007). Three faces of mortalin: A housekeeper, guardian and killer. *Experimental Gerontology*, *42*(4), 263–274. https://doi.org/10.1016/J.EXGER.2006.10.020

Kaul, S. C., Duncan, E. L., Englezou, A., Takano, S., Reddel, R. R., Mitsui, Y., & Wadhwa, R. (1998). Malignant transformation of NIH3T3 cells by overexpression of mot-2 protein. *Oncogene 1998 17:7*, *17*(7), 907–911. https://doi.org/10.1038/sj.onc.1202017

Kennedy, P. G. E. (2013). Clinical features, diagnosis, and treatment of human African trypanosomiasis (sleeping sickness). *The Lancet Neurology*, *12*(2), 186–194. https://doi.org/10.1016/S1474-4422(12)70296-X

Kennedy, P. G. E. (2019). Update on human African trypanosomiasis (sleeping sickness). *Journal of Neurology*, *266*(9), 2334–2337. https://doi.org/10.1007/S00415-019-09425-7

Khabiri, M., Minofar, B., Brezovský, J., Damborský, J., & Ettrich, R. (2013). Interaction of organic solvents with protein structures at protein-solvent interface. *Journal of Molecular Modeling*, *19*(11), 4701–4711. https://doi.org/10.1007/S00894-012-1507-Z

Kityk, R., Kopp, J., & Mayer, M. P. (2018). Molecular mechanism of J-domain-triggered ATP hydrolysis by Hsp70 chaperones. *Molecular Cell*, *69*(2), 227-237.e4. https://doi.org/10.1016/J.MOLCEL.2017.12.003

Kityk, R., Kopp, J., Sinning, I., & Mayer, M. P. (2012). Structure and dynamics of the ATP-bound open conformation of Hsp70 chaperones. *Molecular Cell*, *48*(6), 863–874. https://doi.org/10.1016/J.MOLCEL.2012.09.023

Kityk, R., Vogel, M., Schlecht, R., Bukau, B., & Mayer, M. P. (2015). Pathways of allosteric regulation in Hsp70 chaperones. *Nature Communications 2015 6:1*, *6*(1), 1–11. https://doi.org/10.1038/ncomms9308

Klausen, M. S., Jespersen, M. C., Nielsen, H., Jensen, K. K., Jurtz, V. I., Sønderby, C. K., Sommer, M. O. A., Winther, O., Nielsen, M., Petersen, B., & Marcatili, P. (2019). NetSurfP-2.0: Improved prediction of protein structural features by integrated deep learning. *Proteins: Structure, Function, and Bioinformatics*, *87*(6), 520–527. https://doi.org/10.1002/PROT.25674

Kleczewska, M., Grabinska, A., Jelen, M., Stolarska, M., Schilke, B., Marszalek, J., Craig, E. A., & Dutkiewicz, R. (2020). Biochemical convergence of mitochondrial HSP70 system specialized in

iron–sulfur cluster biogenesis. *International Journal of Molecular Sciences*, *21*(9). https://doi.org/10.3390/IJMS21093326

Kluth, J., Schmidt, A., März, M., Krupinska, K., & Lorbiecke, R. (2012). Arabidopsis Zinc Ribbon 3 is the ortholog of yeast mitochondrial HSP70 escort protein HEP1 and belongs to an ancient protein family in mitochondria and plastids. *FEBS Letters*, *586*(19), 3071–3076. https://doi.org/10.1016/J.FEBSLET.2012.07.052

Krogh, A., Larsson, B., von Heijne, G., & Sonnhammer, E. L. L. (2001). Predicting transmembrane protein topology with a hidden Markov model: application to complete genomes. *Journal of Molecular Biology*, *305*(3), 567–580. https://doi.org/10.1006/JMBI.2000.4315

Laemmli, U. K. (1970). Cleavage of structural proteins during the assembly of the head of bacteriophage T4. *Nature 1970 227:5259*, *227*(5259), 680–685. https://doi.org/10.1038/227680a0

Langer, T., Lu, C., Echols, H., Flanagan, J., Hayer, M. K., & Hartl, F. U. (1992). Successive action of DnaK, DnaJ and GroEL along the pathway of chaperone-mediated protein folding. *Nature 1992 356:6371*, *356*(6371), 683–689. https://doi.org/10.1038/356683a0

Letunic, I., Copley, R. R., Pils, B., Pinkert, S., Schultz, J., & Bork, P. (2006). SMART 5: domains in the context of genomes and networks. *Nucleic Acids Research*, *34*, D257-D260. https://doi.org/10.1093/NAR/GKJ079

Letunic, I., Khedkar, S., & Bork, P. (2021). SMART: recent updates, new developments and status in 2020. *Nucleic Acids Research*, *49*(D1), D458–D460. https://doi.org/10.1093/NAR/GKAA937

Liberek, K., Marszalek, J., Ang, D., Georgopoulos, C., & Zylicz, M. (1991). Escherichia coli DnaJ and GrpE heat shock proteins jointly stimulate ATPase activity of DnaK. *Proceedings of the National Academy of Sciences of the United States of America*, *88*(7), 2874–2878. https://doi.org/10.1073/PNAS.88.7.2874

Liu, Y., Gierasch, L. M., & Bahar, I. (2010). Role of Hsp70 ATPase domain intrinsic dynamics and sequence evolution in enabling its functional interactions with NEFs. *PLOS Computational Biology*, *6*(9), e1000931. https://doi.org/10.1371/JOURNAL.PCBI.1000931

Liu, Y., Liu, W., Song, X. D., & Zuo, J. (2005). Effect of GRP75/mthsp70/PBP74/mortalin overexpression on intracellular ATP level, mitochondrial membrane potential and ROS accumulation following glucose deprivation in PC12 cells. *Molecular and Cellular Biochemistry*, *268*(1–2), 45–51. https://doi.org/10.1007/S11010-005-2996-1

Lopes, A. H., Souto-Padrón, T., Dias, F. A., Gomes, M. T., Rodrigues, G. C., Zimmermann, L. T., Alves e Silva, T. L., & Vermelho, A. B. (2010). Trypanosomatids: Odd organisms, devastating diseases. *Open Parasitology Journal*, *4*(SPEC. ISS.1), 30–59. https://doi.org/10.2174/1874421401004010030

Louw, C. A., Ludewig, M. H., Mayer, J., & Blatch, G. L. (2010). The Hsp70 chaperones of the Tritryps are characterized by unusual features and novel members. *Parasitology International*, *59*(4), 497–505. https://doi.org/10.1016/J.PARINT.2010.08.008

Lu, Z., & Cyr, D. M. (1998). Protein folding activity of Hsp70 is modified differentially by the hsp40 co-chaperones Sis1 and Ydj1. *The Journal of Biological Chemistry*, *273*(43), 27824–27830. https://doi.org/10.1074/JBC.273.43.27824

Ludewig, M. H., Boshoff, A., Horn, D., & Blatch, G. L. (2015). Trypanosoma brucei J protein 2 is a stress inducible and essential Hsp40. *The International Journal of Biochemistry & Cell Biology*, *60*, 93–98. https://doi.org/10.1016/J.BIOCEL.2014.12.016

Lumry, R., & Eyring, H. (1954). Conformation changes of proteins. *Journal of Physical Chemistry*, *58*(2), 110–120. https://doi.org/10.1021/J150512A005

Ma, Z., Izumi, H., Kanai, M., Kabuyama, Y., Ahn, N. G., & Fukasawa, K. (2006). Mortalin controls centrosome duplication via modulating centrosomal localization of p53. *Oncogene 2006 25:39*, *25*(39), 5377–5390. https://doi.org/10.1038/sj.onc.1209543

Macario, A. J. L., & de Macario, E. C. (2002). Sick chaperones and ageing: a perspective. *Ageing Research Reviews*, *1*(2), 295–311. https://doi.org/10.1016/S1568-1637(01)00005-8

Manczak, M., Mao, P., Calkins, M. J., Cornea, A., Reddy, A. P., Murphy, M. P., Szeto, H. H., Park, B., & Reddy, P. H. (2010). Mitochondria-targeted antioxidants protect against amyloid-beta toxicity in Alzheimer's disease neurons. *Journal of Alzheimer's Disease : JAD*, *20 Suppl 2*(Suppl 2). https://doi.org/10.3233/JAD-2010-100564

Manichaikul, A., Mychaleckyj, J. C., Rich, S. S., Daly, K., Sale, M., & Chen, W. M. (2010). Robust relationship inference in genome-wide association studies. *Bioinformatics*, *26*(22), 2867–2873. https://doi.org/10.1093/BIOINFORMATICS/BTQ559

Margulis, B., Tsimokha, A., Zubova, S., & Guzhova, I. (2020). Molecular chaperones and proteolytic machineries regulate protein homeostasis in aging cells. *Cells*, *9*(5). https://doi.org/10.3390/cells9051308

Matthews, K. R. (2021). Trypanosome signaling-quorum sensing. *Annual Review of Microbiology*, *75*, 495–514. https://doi.org/10.1146/ANNUREV-MICRO-020321-115246

Mayer, M. P., & Bukau, B. (2005). Hsp70 chaperones: cellular functions and molecular mechanism. *Cellular and Molecular Life Sciences : CMLS*, *62*(6), 670–684. https://doi.org/10.1007/S00018-004-4464-6

McCarty, J. S., Buchberger, A., Reinstein, J., & Bukau, B. (1995). The Role of ATP in the Functional Cycle of the DnaK Chaperone System. *Journal of Molecular Biology*, *249*(1), 126–137. https://doi.org/10.1006/JMBI.1995.0284

Meriin, A. B., & Sherman, M. Y. (2005). Role of molecular chaperones in neurodegenerative disorders. *International Journal of Hyperthermia : The Official Journal of European Society for Hyperthermic Oncology, North American Hyperthermia Group*, *21*(5), 403–419. https://doi.org/10.1080/02656730500041871

Mesu, V. K. B. K., Kalonji, W. M., Bardonneau, C., Mordt, O. V., Blesson, S., Simon, F., Delhomme, S., Bernhard, S., Kuziena, W., Lubaki, J. P. F., Vuvu, S. L., Ngima, P. N., Mbembo, H. M., Ilunga, M., Bonama, A. K., Heradi, J. A., Solomo, J. L. L., Mandula, G., Badibabi, L. K., … Tarral, A. (2018). Oral fexinidazole for late-stage African Trypanosoma brucei gambiense trypanosomiasis: a pivotal multicentre, randomised, non-inferiority trial. *The Lancet*, *391*(10116), 144–154. https://doi.org/10.1016/S0140-6736(17)32758-7

Mokranjac, D. (2020). How to get to the other side of the mitochondrial inner membrane - the protein import motor. *Biological Chemistry*, *401*(6–7), 723–736. https://doi.org/10.1515/HSZ-2020-0106

Momose, T., Ohshima, C., Maeda, M., & Endo, T. (2007). Structural basis of functional cooperation of Tim15/Zim17 with yeast mitochondrial Hsp70. *EMBO Reports*, *8*(7), 664. https://doi.org/10.1038/SJ.EMBOR.7400990

Moro, F., Fernández, V., & Muga, A. (2003). Interdomain interaction through helices A and B of DnaK peptide binding domain. *FEBS Letters*, *533*(1), 119–123. https://doi.org/10.1016/S0014-5793(02)03752-3

Moro, F., Fernández-Sáiz, V., Slutsky, O., Azem, A., & Muga, A. (2005). Conformational properties of bacterial DnaK and yeast mitochondrial Hsp70. Role of the divergent C-terminal alpha-helical subdomain. *The FEBS Journal*, *272*(12), 3184–3196. https://doi.org/10.1111/J.1742-4658.2005.04737.X

Mudeppa, D. G., & Rathod, P. K. (2013). Expression of functional *Plasmodium falciparum* enzymes using a wheat germ cell-free system. *Eukaryotic Cell*, *12*(12), 1653–1663. https://doi.org/10.1128/EC.00222-13

Neupert, W., & Brunner, M. (2002). The protein import motor of mitochondria. *Nature Reviews. Molecular Cell Biology*, *3*(8), 555–565. https://doi.org/10.1038/NRM878

Niemann, M., Wiese, S., Mani, J., Chanfon, A., Jackson, C., Meisinger, C., Warscheid, B., & Schneider, A. (2013). Mitochondrial outer membrane proteome of *Trypanosoma brucei* reveals novel factors required to maintain mitochondrial morphology. *Molecular & Cellular Proteomics : MCP*, *12*(2), 515–528. https://doi.org/10.1074/MCP.M112.023093

Njiokou, F., Laveissière, C., Simo, G., Nkinin, S., Grébaut, P., Cuny, G., & Herder, S. (2006). Wild fauna as a probable animal reservoir for *Trypanosoma brucei gambiense* in Cameroon. *Infection, Genetics and Evolution : Journal of Molecular Epidemiology and Evolutionary Genetics in Infectious Diseases*, *6*(2), 147–153. https://doi.org/10.1016/J.MEEGID.2005.04.003

Njiokou, F., Nimpaye, H., Simo, G., Njitchouang, G. R., Asonganyi, T., Cuny, G., & Herder, S. (2010). Domestic animals as potential reservoir hosts of *Trypanosoma brucei gambiense* in sleeping

sickness foci in Cameroon. *Parasite (Paris, France)*, *17*(1), 61–66. https://doi.org/10.1051/PARASITE/2010171061

Nyakundi, D. O., Bentley, S. J., & Boshoff, A. (2018). Hsp70 escort protein: more than a regulator of mitochondrial Hsp70. *Current Proteomics*, *16*(1), 64–73. https://doi.org/10.2174/1570164615666180713104919

Nyakundi, D. O., Vuko, L. A. M., Bentley, S. J., Hoppe, H., Blatch, G. L., & Boshoff, A. (2016). Plasmodium falciparum Hep1 Is Required to Prevent the Self Aggregation of PfHsp70-3. *PLOS ONE*, *11*(6), e0156446. https://doi.org/10.1371/JOURNAL.PONE.0156446

Orsini, F., Migliaccio, E., Moroni, M., Contursi, C., Raker, V. A., Piccini, D., Martin-Padura, I., Pelliccia, G., Trinei, M., Bono, M., Puri, C., Tacchetti, C., Ferrini, M., Mannucci, R., Nicoletti, I., Lanfrancone, L., Giorgio, M., & Pelicci, P. G. (2004). The life span determinant p66Shc localizes to mitochondria where it associates with mitochondrial heat shock protein 70 and regulates trans-membrane potential. *The Journal of Biological Chemistry*, *279*(24), 25689–25695. https://doi.org/10.1074/JBC.M401844200

Packschies, L., Theyssen, H., Buchberger, A., Bukau, B., Goody, R. S., & Reinstein, J. (1997). GrpE accelerates nucleotide exchange of the molecular chaperone DnaK with an associative displacement mechanism. *Biochemistry*, *36*(12), 3417–3422. https://doi.org/10.1021/BI962835L

Palleros, D. R., Raid, K. L., Shi, L., Welch, W. J., & Fink, A. L. (1993). ATP-induced protein Hsp70 complex dissociation requires K+ but not ATP hydrolysis. *Nature 1993 365:6447*, *365*(6447), 664–666. https://doi.org/10.1038/365664a0

Pandey, S., & Singh, S. P. (2012). Organic solvent tolerance of an α-amylase from haloalkaliphilic bacteria as a function of pH, temperature, and salt concentrations. *Applied Biochemistry and Biotechnology*, *166*(7), 1747–1757. https://doi.org/10.1007/S12010-012-9580-4

Panigrahi, A. K., Ogata, Y., Zíková, A., Anupama, A., Dalley, R. A., Acestor, N., Myler, P. J., & Stuart, K. D. (2009). A comprehensive analysis of *Trypanosoma brucei* mitochondrial proteome. *Proteomics*, *9*(2), 434–450. https://doi.org/10.1002/PMIC.200800477

Pareek, G., Samaddar, M., & D'Silva, P. (2011). Primary sequence that determines the functional overlap between mitochondrial heat shock protein 70 Ssc1 and Ssc3 of *Saccharomyces cerevisiae*. Journal of Biological Chemistry, 286(21), 19001–19013. https://doi.org/10.1074/jbc.M110.197434

Pearson, W. R. (2013). Selecting the right similarity-scoring matrix. *Current Protocols in Bioinformatics*, *43*(1), 3.5.1-3.5.9. https://doi.org/10.1002/0471250953.BI0305S43

Pellecchia, M., Szyperski, T., Wall, D., Georgopoulos, C., & Wüthrich, K. (1996). NMR structure of the J-domain and the Gly/Phe-rich region of the *Escherichia coli* DnaJ chaperone. *Journal of Molecular Biology*, *260*(2), 236–250. https://doi.org/10.1006/JMBI.1996.0395

Pettersen, E. F., Goddard, T. D., Huang, C. C., Meng, E. C., Couch, G. S., Croll, T. I., Morris, J. H., & Ferrin, T. E. (2021). UCSF ChimeraX: Structure visualization for researchers, educators, and

developers. *Protein Science : A Publication of the Protein Society*, *30*(1), 70–82. https://doi.org/10.1002/PRO.3943

Petty, K. J. (2001). Metal-chelate affinity chromatography. *Current Protocols in Molecular Biology*, *Chapter 10*(1). https://doi.org/10.1002/0471142727.MB1011BS36

Pfanner, N., & Geissler, A. (2001). Versatility of the mitochondrial protein import machinery. *Nature Reviews. Molecular Cell Biology*, *2*(5), 339–349. https://doi.org/10.1038/35073006

Pilzer, D., & Fishelson, Z. (2005). Mortalin/GRP75 promotes release of membrane vesicles from immune attacked cells and protection from complement-mediated lysis. *International Immunology*, *17*(9), 1239–1248. https://doi.org/10.1093/INTIMM/DXH300

Powers, E. T., Morimoto, R. I., Dillin, A., Kelly, J. W., & Balch, W. E. (2009). Biological and chemical approaches to diseases of proteostasis deficiency. *Annual Review of Biochemistry*, *78*, 959–991. https://doi.org/10.1146/ANNUREV.BIOCHEM.052308.114844

Priyanka, & Seth, P. (2022). Insights into the role of mortalin in Alzheimer's Disease, Parkinson's Disease, and HIV-1-associated neurocognitive disorders. *Frontiers in Cell and Developmental Biology*, *10*, 1139. https://doi.org/10.3389/FCELL.2022.903031/XML/NLM

Priyanka, Wadhwa, R., Chaudhuri, R., Nag, T. C., & Seth, P. (2020). Novel role of mortalin in attenuating HIV-1 Tat-mediated astrogliosis. *Journal of Neuroinflammation*, *17*(1), 1–20. https://doi.org/10.1186/S12974-020-01912-3/FIGURES/9

Qi, R., Sarbeng, E. B., Liu, Q., Le, K. Q., Xu, X., Xu, H., Yang, J., Wong, J. L., Vorvis, C., Hendrickson, W. A., Zhou, L., & Liu, Q. (2013). Allosteric opening of the polypeptide-binding site when an Hsp70 binds ATP. *Nature Structural & Molecular Biology*, *20*(7), 900. https://doi.org/10.1038/NSMB.2583

Quintana, J. F., Zoltner, M., & Field, M. C. (2021). Evolving differentiation in african trypanosomes. *Trends in Parasitology*, *37*(4), 296–303. https://doi.org/10.1016/j.pt.2020.11.003

Raeisossadati, R., & Ferrari, M. F. R. (2020). Mitochondria-ER tethering in neurodegenerative diseases. *Cellular and Molecular Neurobiology 2020 42:4*, *42*(4), 917–930. https://doi.org/10.1007/S10571-020-01008-9

Ran, Q., Wadhwa, R., Kawai, R., Kaul, S. C., Sifers, R. N., Bick, R. J., Smith, J. R., & Pereira-Smith, O. M. (2000). Extramitochondrial localization of mortalin/mthsp70/PBP74/GRP75. *Biochemical and Biophysical Research Communications*, *275*(1), 174–179. https://doi.org/10.1006/BBRC.2000.3237

Ray, M. S., Moskovich, O., Iosefson, O., & Fishelson, Z. (2014). Mortalin/GRP75 binds to complement C9 and plays a role in resistance to complement-dependent cytotoxicity. *The Journal of Biological Chemistry*, *289*(21), 15014. https://doi.org/10.1074/JBC.M114.552406

Rios, L. E., Vázquez-Chagoyán, J. C., Pacheco, A. O., Zago, M. P., & Garg, N. J. (2019). Immunity and vaccine development efforts against *Trypanosoma cruzi*. *Acta Tropica*, *200*, 105168. https://doi.org/10.1016/J.ACTATROPICA.2019.105168

Ritossa, F. (1962). A new puffing pattern induced by temperature shock and DNP in drosophila. *Experientia 1962 18:12*, *18*(12), 571–573. https://doi.org/10.1007/BF02172188

Rohde, M., Daugaard, M., Jensen, M. H., Helin, K., Nylandsted, J., & Jäättelä, M. (2005). Members of the heat-shock protein 70 family promote cancer cell growth by distinct mechanisms. *Genes & Development*, *19*(5), 570–582. https://doi.org/10.1101/GAD.305405

Rojas, F., Silvester, E., Young, J., Milne, R., Tettey, M., Houston, D. R., Walkinshaw, M. D., Pérez-Pi, I., Auer, M., Denton, H., Smith, T. K., Thompson, J., & Matthews, K. R. (2019). Oligopeptide signaling through TbGPR89 drives trypanosome quorum sensing. *Cell*, *176*(1–2), 306-317.e16. https://doi.org/10.1016/J.CELL.2018.10.041

Romero-Meza, G., & Mugnier, M. R. (2020). *Trypanosoma brucei*. *Trends in Parasitology*, *36*(6), 571–572. https://doi.org/10.1016/j.pt.2019.10.007

Rosano, G. L., & Ceccarelli, E. A. (2014). Recombinant protein expression in *Escherichia coli*: advances and challenges. *Frontiers in Microbiology*, *5*(APR). https://doi.org/10.3389/FMICB.2014.00172

Rüdiger, S., Germeroth, L., Schneider-Mergener, J., & Bukau, B. (1997). Substrate specificity of the DnaK chaperone determined by screening cellulose-bound peptide libraries. *The EMBO Journal*, *16*(7), 1501–1507. https://doi.org/10.1093/EMBOJ/16.7.1501

Santra, M., Dill, K. A., & de Graff, A. M. R. (2019). Proteostasis collapse is a driver of cell aging and death. *Proceedings of the National Academy of Sciences of the United States of America*, *116*(44), 22173–22178. https://doi.org/10.1073/PNAS.1906592116/SUPPL_FILE/PNAS.1906592116.SAPP.PDF

Schilke, B., Williams, B., Knieszner, H., Pukszta, S., D'Silva, P., Craig, E. A., & Marszalek, J. (2006). Evolution of mitochondrial chaperones utilized in Fe-S cluster biogenesis. *Current Biology : CB*, *16*(16), 1660–1665. https://doi.org/10.1016/J.CUB.2006.06.069

Schmid, D., Baici, A., Gehring, H., & Christen, P. (1994). Kinetics of molecular chaperone action. *Science*, *263*(5149), 971–973. https://doi.org/10.1126/SCIENCE.8310296

Shiloach, J., & Fass, R. (2005). Growing E. coli to high cell density--a historical perspective on method development. *Biotechnology Advances*, *23*(5), 345–357. https://doi.org/10.1016/J.BIOTECHADV.2005.04.004

Shonhai, A., Botha, M., De Beer, Tjaart A.P., Boshoff, A., Blatch, G. (2008). Structure-Function Study of a Plasmodium falciparum Hsp70 Using Three Dimensional Modelling and in Vitro Analyses. *Protein & Peptide Letters*, 15(10), 1117-1125. 10.2174/092986608786071067

Sichting, M., Mokranjac, D., Azem, A., Neupert, W., & Hell, K. (2005). Maintenance of structure and function of mitochondrial Hsp70 chaperones requires the chaperone Hep1. *EMBO Journal*, *24*(5), 1046–1056. https://doi.org/10.1038/sj.emboj.7600580

Sievers, F., Wilm, A., Dineen, D., Gibson, T. J., Karplus, K., Li, W., Lopez, R., McWilliam, H., Remmert, M., Söding, J., Thompson, J. D., & Higgins, D. G. (2011). Fast, scalable generation of high-quality protein multiple sequence alignments using Clustal Omega. *Molecular Systems Biology*, *7*, 539. https://doi.org/10.1038/MSB.2011.75

Sigrist, C. J. A., Cerutti, L., de Castro, E., Langendijk-Genevaux, P. S., Bulliard, V., Bairoch, A., & Hulo, N. (2009). PROSITE, a protein domain database for functional characterization and annotation. *Nucleic Acids Research*, *38*(SUPPL.1). https://doi.org/10.1093/nar/gkp885

Simarro, P. P., Jannin, J., & Cattand, P. (2008). Eliminating human african trypanosomiasis: where do we stand and what comes next? *PLOS Medicine*, *5*(2), e55. https://doi.org/10.1371/JOURNAL.PMED.0050055

Singh, A. P., Bajaj, T., Gupta, D., Singh, S. B., Chakrawarty, A., Goyal, V., Dey, A. B., & Dey, S. (2018). Serum mortalin correlated with α-synuclein as serum markers in parkinson's disease: A Pilot Study. *Neuromolecular Medicine*, *20*(1), 83–89. https://doi.org/10.1007/S12017-017-8475-5

Singh, S. M., & Panda, A. K. (2005). Solubilization and refolding of bacterial inclusion body proteins. *Journal of Bioscience and Bioengineering*, *99*(4), 303–310. https://doi.org/10.1263/JBB.99.303

Singh, S. M., Sharma, A., Upadhyay, A. K., Singh, A., Garg, L. C., & Panda, A. K. (2012). Solubilization of inclusion body proteins using n-propanol and its refolding into bioactive form. *Protein Expression and Purification*, *81*(1), 75–82. https://doi.org/10.1016/J.PEP.2011.09.004

Sinha, D., & D'Silva, P. (2014). Chaperoning mitochondrial permeability transition: regulation of transition pore complex by a J-protein, DnaJC15. *Cell Death & Disease*, *5*(3), e1101. https://doi.org/10.1038/CDDIS.2014.72

Soares, M. J., & de Souza, W. (1988). Cytoplasmic organelles of trypanosomatids: a cytochemical and stereological study. *Journal of Submicroscopic Cytology and Pathology*, *20*(2), 349–361. https://europepmc.org/article/med/3135113

Stephenson, J. D., & Freeland, S. J. (2013). Unearthing the root of amino acid similarity. *Journal of Molecular Evolution*, *77*(4), 159–169. https://doi.org/10.1007/S00239-013-9565-0/FIGURES/6

Stott, D. I. (1989). Immunoblotting and dot blotting. *Journal of Immunological Methods*, *119*(2), 153. https://doi.org/10.1016/0022-1759(89)90394-3

Studier, F. W. (2005). Protein production by auto-induction in high density shaking cultures. *Protein Expression and Purification*, *41*(1), 207–234. https://doi.org/10.1016/J.PEP.2005.01.016

Subramaniam, C., Veazey, P., Redmond, S., Hayes-Sinclair, J., Chambers, E., Carrington, M., Gull, K., Matthews, K., Horn, D., & Field, M. C. (2006). Chromosome-wide analysis of gene function by

RNA interference in the african trypanosome. *Eukaryotic Cell*, *5*(9), 1539–1549. https://doi.org/10.1128/EC.00141-06

Szklarczyk, D., Gable, A. L., Nastou, K. C., Lyon, D., Kirsch, R., Pyysalo, S., Doncheva, N. T., Legeay, M., Fang, T., Bork, P., Jensen, L. J., & von Mering, C. (2021). The STRING database in 2021: customizable protein-protein networks, and functional characterization of user-uploaded gene/measurement sets. *Nucleic Acids Research*, *49*(D1), D605–D612. https://doi.org/10.1093/NAR/GKAA1074

Szklarz, S., L. K., Guiard, B., Rissler, M., Wiedemann, N., Kozjak, V., van der Laan, M., Lohaus, C., Marcus, K., Meyer, H. E., Chacinska, A., Pfanner, N., & Meisinger, C. (2005). Inactivation of the mitochondrial heat shock protein Zim17 leads to aggregation of matrix Hsp70s followed by pleiotropic effects on morphology and protein biogenesis. Journal of Molecular Biology, 351(1), 206–218. https://doi.org/10.1016/J.JMB.2005.05.068

Tamura, K., Stecher, G., & Kumar, S. (2021). MEGA11: Molecular evolutionary genetics analysis version 11. *Molecular Biology and Evolution*, *38*(7), 3022–3027. https://doi.org/10.1093/MOLBEV/MSAB120

Tatusov, R. L., Fedorova, N. D., Jackson, J. D., Jacobs, A. R., Kiryutin, B., Koonin, E. v., Krylov, D. M., Mazumder, R., Smirnov, S., Nikolskaya, A. N., Rao, B. S., Mekhedov, S. L., Sverlov, A. v., Vasudevan, S., Wolf, Y. I., Yin, J. J., & Natale, D. A. (2003). The COG database: An updated vesion includes eukaryotes. *BMC Bioinformatics*, *4*. https://doi.org/10.1186/1471-2105-4-41

Tissiéres, A., Mitchell, H. K., & Tracy, U. M. (1974). Protein synthesis in salivary glands of Drosophila melanogaster: relation to chromosome puffs. *Journal of Molecular Biology*, *84*(3). https://doi.org/10.1016/0022-2836(74)90447-1

Tsai, J., & Douglas, M. G. (1996). A Conserved HPD Sequence of the J-domain is necessary for YDJ1 stimulation of Hsp70 ATPase activity at a site distinct from substrate binding. *Journal of Biological Chemistry*, *271*(16), 9347–9354. https://doi.org/10.1074/JBC.271.16.9347

Uzarska, M. A., Dutkiewicz, R., Freibert, S. A., Lill, R., & Mühlenhoff, U. (2013). The mitochondrial Hsp70 chaperone Ssq1 facilitates Fe/S cluster transfer from Isu1 to Grx5 by complex formation. *Molecular Biology of the Cell*, *24*(12), 1830. https://doi.org/10.1091/MBC.E12-09-0644

van den Ussel, P., Norman, D. G., & Quinlan, R. A. (1999). Molecular chaperones: small heat shock proteins in the limelight. *Current Biology*, *9*(3), R103–R105. https://doi.org/10.1016/S0960-9822(99)80061-X

van der Laan, M., Hutu, D. P., & Rehling, P. (2010). On the mechanism of preprotein import by the mitochondrial presequence translocase. *Biochimica et Biophysica Acta - Molecular Cell Research*, *1803*(6), 732–739. https://doi.org/10.1016/j.bbamcr.2010.01.013

Vera, A., González-Montalbán, N., Arís, A., & Villaverde, A. (2007). The conformational quality of insoluble recombinant proteins is enhanced at low growth temperatures. *Biotechnology and Bioengineering*, *96*(6), 1101–1106. https://doi.org/10.1002/BIT.21218

Vickerman, K. (1965). Polymorphism and mitochondrial activity in sleeping sickness trypanosomes. *Nature*, *208*(5012), 762–766. https://doi.org/10.1038/208762A0

Volobouéva, L. A., Emery, J. F., Sun, X., & Giffard, R. G. (2013). Inflammatory response of microglial BV-2 cells includes a glycolytic shift and is modulated by mitochondrial glucose-regulated protein 75/mortalin. *FEBS Letters*, *587*(6), 756–762. https://doi.org/10.1016/J.FEBSLET.2013.01.067

von Känel, C., Muñoz-Gómez, S. A., Oeljeklaus, S., Wenger, C., Warscheid, B., Wideman, J. G., Harsman, A., & Schneider, A. (2020). Homologue replacement in the import motor of the mitochondrial inner membrane of trypanosomes. *ELife*, *9*. https://doi.org/10.7554/ELIFE.52560

Wadhwa, R., Kaul, S. C., Ikawa, Y., & Sugimoto, Y. (1993). Identification of a novel member of mouse hsp70 family. Its association with cellular mortal phenotype. *Journal of Biological Chemistry*, *268*(9), 6615–6621. https://doi.org/10.1016/S0021-9258(18)53295-6

Wadhwa, R., Takano, S., Kaur, K., Aida, S., Yaguchi, T., Kaul, Z., Hirano, T., Taira, K., & Kaul, S. C. (2005). Identification and characterization of molecular interactions between mortalin/mtHsp70 and HSP60. *Biochemical Journal*, *391*(Pt 2), 185. https://doi.org/10.1042/BJ20050861

Wadhwa, R., Takano, S., Mitsui, Y., & Kaul, S. C. (1999). NIH 3T3 cells malignantly transformed by mot-2 show inactivation and cytoplasmic sequestration of the p53 protein. *Cell Research*, *9*(4), 261–269. https://doi.org/10.1038/SJ.CR.7290025

Wadhwa, R., Yaguchi, T., Hasan, M. K., Mitsui, Y., Reddel, R. R., & Kaul, S. C. (2002). Hsp70 family member, mot-2/mthsp70/GRP75, binds to the cytoplasmic sequestration domain of the p53 protein. *Experimental Cell Research*, *274*(2), 246–253. https://doi.org/10.1006/EXCR.2002.5468

Wadhwa, Renu., Kaul, S. C., Mitsui, Y., & Sugimoto, Y. (1993). Differential subcellular distribution of mortalin in mortal and immortal mouse and human fibroblasts. *Experimental Cell Research*, *207*(2), 442–448. https://doi.org/10.1006/EXCR.1993.1213

Wakula, M., Balcerak, A., Rubel, T., Chmielarczyk, M., Konopinski, R., Lyczek, F., & Grzybowska, E. A. (2020). The interactome of multifunctional HAX1 protein suggests its role in the regulation of energy metabolism, de-aggregation, cytoskeleton organization and RNA-processing. *Bioscience Reports*, *40*(11). https://doi.org/10.1042/BSR20203094/226900

Walsh, P., Bursać, D., Law, Y. C., Cyr, D., & Lithgow, T. (2004). The J-protein family: modulating protein assembly, disassembly and translocation. *EMBO Reports*, *5*(6), 567–571. https://doi.org/10.1038/SJ.EMBOR.7400172

Wang, S., Peng, J., Ma, J., & Xu, J. (2016). Protein secondary structure prediction using deep convolutional neural fields. *Scientific Reports 2016 6:1*, *6*(1), 1–11. https://doi.org/10.1038/srep18962

Wang, W., Liu, Q., Liu, Q., & Hendrickson, W. A. (2021). Conformational equilibria in allosteric control of Hsp70 chaperones. *Molecular Cell*, *81*(19), 3919-3933.e7. https://doi.org/10.1016/J.MOLCEL.2021.07.039

Wang, Y., Wang, Y., Lin, J., Chen, Q. Z., Zhu, N., Jiang, D. Q., & Li, M. X. (2015). Overexpression of mitochondrial Hsp75 protects neural stem cells against microglia-derived soluble factor-induced neurotoxicity by regulating mitochondrial permeability transition pore opening in vitro. *International Journal of Molecular Medicine*, *36*(6), 1487–1496. https://doi.org/10.3892/IJMM.2015.2380/HTML

Waterhouse, A., Bertoni, M., Bienert, S., Studer, G., Tauriello, G., Gumienny, R., Heer, F. T., de Beer, T. A. P., Rempfer, C., Bordoli, L., Lepore, R., & Schwede, T. (2018). SWISS-MODEL: homology modelling of protein structures and complexes. *Nucleic Acids Research*, *46*(W1), W296–W303. https://doi.org/10.1093/NAR/GKY427

Waterhouse, A. M., Procter, J. B., Martin, D. M. A., Clamp, M., & Barton, G. J. (2009). Jalview version 2—a multiple sequence alignment editor and analysis workbench. *Bioinformatics*, *25*(9), 1189–1191. https://doi.org/10.1093/BIOINFORMATICS/BTP033

Wiedemann, N., & Pfanner, N. (2017). Mitochondrial machineries for protein import and assembly. *Annual Review of Biochemistry*, *86*, 685–714. https://doi.org/10.1146/annurev-biochem-060815-014352

Wiedemar, N., Hauser, D. A., & Mäser, P. (2020). 100 Years of Suramin. *Antimicrobial Agents and Chemotherapy*, *64*(3). https://doi.org/10.1128/AAC.01168-19

Williamson, C. L., Dabkowski, E. R., Dillmann, W. H., Hollander, J. M., Cl, W., Er, D., Wh, D., & Hollander, J. M. (2008). Mitochondria protection from hypoxia/reoxygenation injury with mitochondria heat shock protein 70 overexpression. *Am J Physiol Heart Circ Physiol*, *294*, 249–256. https://doi.org/10.1152/ajpheart.00775.2007.-The

Willmund, F., Hinnenberger, M., Nick, S., Schulz-Raffelt, M., Mühlhaus, T., & Schroda, M. (2008). Assistance for a Chaperone: Chlamydomonas Hep2 activates plastidic Hsp70b for cochaperone binding. *Journal of Biological Chemistry*, *283*(24), 16363–16373. https://doi.org/10.1074/JBC.M708431200

Wu, B., Wawrzynow, A., Zylicz, M., & Georgopoulos, C. (1996). Structure-function analysis of the *Escherichia coli* GrpE heat shock protein. *The EMBO Journal*, *15*(18), 4806. https://doi.org/10.1002/j.1460-2075.1996.tb00861.x

Wu, C. C., Naveen, V., Chien, C. H., Chang, Y. W., & Hsiaos, C. D. (2012). Crystal structure of DnaK protein complexed with nucleotide exchange factor GrpE in DnaK chaperone system: Insight into intermolecular communication*. *The Journal of Biological Chemistry*, *287*(25), 21461. https://doi.org/10.1074/JBC.M112.344358

Xie, H., Guan, J. S., Borrelli, L. A., Xu, J., Serrano-Pozo, A., & Bacskai, B. J. (2013). Mitochondrial alterations near amyloid plaques in an Alzheimer's disease mouse model. *The Journal of Neuroscience : The Official Journal of the Society for Neuroscience*, *33*(43), 17042–17051. https://doi.org/10.1523/JNEUROSCI.1836-13.2013

Yamamoto, H., Momose, T., Yatsukawa, Y. I., Ohshima, C., Ishikawa, D., Sato, T., Tamura, Y., Ohwa, Y., & Endo, T. (2005). Identification of a novel member of yeast mitochondrial Hsp70-associated motor and chaperone proteins that facilitates protein translocation across the inner membrane. *FEBS Letters*, *579*(2), 507–511. https://doi.org/10.1016/j.febslet.2004.12.018

Yan, R., Xu, D., Yang, J., Walker, S., & Zhang, Y. (2013). A comparative assessment and analysis of 20 representative sequence alignment methods for protein structure prediction. *Scientific Reports 2013 3:1*, *3*(1), 1–9. https://doi.org/10.1038/srep02619

Yang, Y., Jin, M., Dai, Y., Shan, W., Chen, S., Cai, R., Yang, H., Tang, L., & Li, L. (2021). Involvement and targeted intervention of mortalin-regulated proteome phosphorylated-modification in hepatocellular carcinoma. *Frontiers in Oncology*, *11*, 3013. https://doi.org/10.3389/FONC.2021.687871/BIBTEX

Young, J. C., Moarefi, I., & Ulrich Hartl, F. (2001). Hsp90: a specialized but essential protein-folding tool. *The Journal of Cell Biology*, *154*(2), 267–273. https://doi.org/10.1083/JCB.200104079

Zhai, P., Stanworth, C., Liu, S., & Silberg, J. J. (2008). The human escort protein Hep binds to the ATPase domain of mitochondrial hsp70 and regulates ATP hydrolysis. *The Journal of Biological Chemistry*, *283*(38), 26098–26106. https://doi.org/10.1074/JBC.M803475200

Zhai, P., Stanworth, C., Nguyen, P., Liu, S., & Silberg, J. (2008). Saccharomyces cerevisiae hep1 promotes the solubility of non-cognate chaperones and requires bound zinc for solubility. *The FASEB Journal*, *22*(S1), 1032.4-1032.4. https://doi.org/10.1096/FASEBJ.22.1_SUPPLEMENT.1032.4

Zhai, P., Vu, M. T., Hoff, K. G., & Silberg, J. J. (2011). A conserved histidine in human DNLZ/HEP is required for stimulation of HSPA9 ATPase activity. *Biochemical and Biophysical Research Communications*, *408*(4), 589–594. https://doi.org/10.1016/J.BBRC.2011.04.066

Zhang, P., Leu, J. I. J., Murphy, M. E., George, D. L., & Marmorstein, R. (2014). Crystal structure of the stress-inducible human heat shock protein 70 substrate-binding domain in complex with peptide substrate. *PLoS ONE*, *9*(7). https://doi.org/10.1371/JOURNAL.PONE.0103518

Zhu, X., Zhao, X., Burkholder, W. F., Gragerov, A., Ogata, C. M., Gottesman, M. E., & Hendrickson, W. A. (1996). Structural analysis of substrate binding by the molecular chaperone DnaK. *Science (New York, N.Y.)*, *272*(5268), 1606–1614. https://doi.org/10.1126/SCIENCE.272.5268.1606

Zimmermann, L., Stephens, A., Nam, S. Z., Rau, D., Kübler, J., Lozajic, M., Gabler, F., Söding, J., Lupas, A. N., & Alva, V. (2018). A completely reimplemented MPI bioinformatics toolkit with a new HHpred server at its Core. *Journal of Molecular Biology*, *430*(15), 2237–2243. https://doi.org/10.1016/J.JMB.2017.12.007

Zininga, T., Makumire, S., Gitau, G. W., Njunge, J. M., Pooe, O. J., Klimek, H., Scheurr, R., Raifer, H., Prinsloo, E., Przyborski, J. M., Hoppe, H., & Shonhai, A. (2015). Plasmodium falciparum Hop (PfHop) interacts with the Hsp70 chaperone in a nucleotide-dependent Fashion and Exhibits Ligand Selectivity. *PloS One*, *10*(8). https://doi.org/10.1371/JOURNAL.PONE.0135326

Zininga, T., Pooe, O. J., Makhado, P. B., Ramatsui, L., Prinsloo, E., Achilonu, I., Dirr, H., & Shonhai, A. (2017). Polymyxin B inhibits the chaperone activity of *Plasmodium falciparum* Hsp70. *Cell Stress and Chaperones*, *22*(5), 707–715. https://doi.org/10.1007/S12192-017-0797-6/FIGURES/5

# A Appendices

## A.1 Bioinformatic sequence data

### A.1.1 Genomic and amino acid sequences

Homo Sapien:

HsHep1 (NP_001074318.1):

CDS:

ATGCTGCGGACTGCGCTGCGCGGCGCGCCGAGGTTGCTGAGTCGCGTGCAGCCCCGG
GCGCCCTGCCTGAGGCGGCTGTGGGGCCGCGGGGCCCGTCCAGAGGTCGCGGGGAGG
CGGCGGGCCTGGGCCTGGGGCTGGCGGCGCTCAAGCTCCGAGCAGGGGCCGGGGCCC
GCGGCGGCTCTGGGGCGCGTGGAGGCGGCGCACTACCAGCTCGTCTACACCTGCAAG
GTCTGCGGGACTAGGTCCTCCAAGCGCATCTCCAAGCTGGCCTATCACCAAGGCGTGG
TCATTGTGACCTGCCCCGGCTGCCAGAACCACCATATCATCGCTGACAACCTGGGCTG
GTTCTCGGACCTGAATGGGAAGAGAAATATCGAAGAGATCCTGACGGCCAGAGGCGA
GCAGGTGCACCGTGTGGCGGGCGAGGGGGCCCTGGAACTGGTTCTGGAGGCTGCAGG
GGCCCCCACATCCACTGCAGCTCCGGAAGCGGGTGAGGATGAGGGTCCCCCCAGCCC
TGGCAAGACGGAGCCGAGCTGA

Amino acid sequence:

MLRTALRGAPRLLSRVQPRAPCLRRLWGRGARPEVAGRRRAWAWGWRRSSSEQGPGPA
AALGRVEAAHYQLVYTCKVCGTRSSKRISKLAYHQGVVIVTCPGCQNHHIIADNLGWFS
DLNGKRNIEEILTARGEQVHRVAGEGALELVLEAAGAPTSTAAPEAGEDEGPPSPGKTEPS

Mortalin (AAH00478.1)

CDS:

GGAGCGCTTGTTTGCTGCCTCGTACTCCTCCATTTATCCGCCATGATAAGTGCCAGCCG
AGCTGCAGCAGCCCGTCTCGTGGGCGCCGCAGCCTCCCGGGGCCCTACGGCCGCCCG
CCACCAGGATAGCTGGAATGGCCTTAGTCATGAGGCTTTTAGACTTGTTTCAAGGCGG
GATTATGCATCAGAAGCAATCAAGGGAGCAGTTGTTGGTATTGATTTGGGTACTACCA
ACTCCTGCGTGGCAGTTATGGAAGGTAAACGAGCAAAGGTGCTGGAGAATGCCGAAG
GTGCCAGAACCACCCCTTCAGTTGTGGCCTTTACAGCAGATGGTGAGCGACTTGTTGG
AATGCCGGCCAAGCGACAGGCTGTCACCAACCCAAACAATACATTTTATGCTACCAA
GCGTCTCATTGGCCGGCGATATGATGATCCTGAAGTACAGAAAGACATTAAAAATGTT
CCCTTTAAAATTGTCCGTGCCTCCAATGGTGATGCCTGGGTTGAGGCTCATGGGAAAT
TGTATTCTCCGAGTCAGATTGGAGCATTTGTGTTGATGAAGATGAAAGAGACTGCAGA
AAATTACTTGGGGCGCACAGCAAAAAATGCTGTGATCACAGTCCCAGCTTATTTCAAT
GACTCGCAGAGACAGGCCACTAAAGATGCTGGCCAGATATCTGGACTGAATGTGCTT
CGGGTGATTAATGAGCCCACAGCTGCTGCTCTTGCCTATGGTCTAGACAAATCAGAAG
ACAAAGTCATTGCTGTATATGATTTAGGTGGTGGAACTTTTGATATTTCTATCCTGGAA

ATTCAGAAAGGAGTATTTGAGGTGAAATCCACAAATGGGGATACCTTCTTAGGTGGG
GAAGACTTTGACCAGGCCTTGCTACGGCACATTGTGAAGGAGTTCAAGAGAGAGACA
GGGGTTGATTTGACTAAAGACAACATGGCACTTCAGAGGGTACGGGAAGCTGCTGAA
AAGGCTAAGTGTGAACTCTCCTCATCTGTGCAGACTGACATCAATTTGCCCTATCTTA
CAATGGATTCTTCTGGACCCAAGCATTTGAATATGAAGTTGACCCGTGCTCAATTTGA
AGGGATTGTCACTGATCTAATCAGAAGGACTATCGCTCCATGCCAAAAAGCTATGCA
AGATGCAGAAGTCAGCAAGAGTGACATAGGAGAAGTGATTCTTGTGGGTGGCATGAC
TAGGATGCCCAAGGTTCAGCAGACTGTACAGGATCTTTTTGGCAGAGCCCCAAGTAA
AGCTGTCAATCCTGATGAGGCTGTGGCCATTGGAGCTGCCATTCAGGGAGGTGTGTTG
GCCGGCGATGTCACGGATGTGCTGCTCCTTGATGTCACTCCCCTGTCTCTGGGTATTGA
AACTCTAGGAGGTGTCTTTACCAAACTTATTAATAGGAATACCACTATTCCAACCAAG
AAGAGCCAGGTATTCTCTACTGCCGCTGATGGTCAAACGCAAGTGGAAATTAAAGTG
TGTCAGGGTGAAAGAGAGATGGCTGGAGACAACAAACTCCTTGGACAGTTTACTTTG
ATTGGAATTCCACCAGCCCCTCGTGGAGTTCCTCAGATTGAAGTTACATTTGACATTG
ATGCCAATGGGATAGTACATGTTTCTGCTAAAGATAAAGGCACAGGACGTGAGCAGC
AGATTGTAATCCAGTCTTCTGGTGGATTAAGCAAAGATGATATTGAAAATATGGTTAA
AAATGCAGAGAAATATGCTGAAGAAGACCGGCGAAAGAAGGAACGAGTTGAAGCAG
TTAATATGGCTGAAGGAATCATTCACGACACAGAAACCAAGATGGAAGAATTCAAGG
ACCAATTACCTGCTGATGAGTGCAACAAGCTGAAAGAAGAGATTTCCAAAATGAGGG
AGCTCCTGGCTAGAAAAGACAGCGAAACAGGAGAAAATATTAGACAGGCAGCATCCT
CTCTTCAGCAGGCATCATTGAAGCTGTTCGAAATGGCATACAAAAAGATGGCATCTGA
GCGAGAAGGCTCTGGAAGTTCTGGCACTGGGGAACAAAAGGAAGATCAAAAGGAGG
AAAAACAGTAATAATAGCAGAAATTTTGAAGCCAGAAGGACAACATATGAAGCTTAG
GAGTGAAGAGACTTCCTGAGCAGAAATGGGCGAACTTCAGTCTTTTTACTGTGTTTTT
GCAGTATTCTATATATAATTTCCTTAATTTGTAAATTTAGTGACCATTAGCTAGTGATC
ATTTAATGGACAGTGATTCTAACAGTATAAAGTTCACAATATTCTATGTCCCTAGCCT
GTCATTTTTCAGCTGCATGTAAAAGGAGGTAGGATGAATTGATCATTATAAAGATTTA
ACTATTTTATGCTGAAGTGACCATATTTTCAAGGGGTGAAACCATCTCGCACACAGCA
ATGAAGGTAGTCATCCATAGACTTGAAATGAGACCACATATGGGGATGAGATCCTTCT
AGTTAGCCTAGTACTGCTGTACTGGCCTGTATGTACATGGGGTCCTTCAACTGAGGCC
TTGCAAGTCAAGCTGGCTGTGCCATGTTTGTAGATGGGGCAGAGGAATCTAGAACAA
TGGGAAACTTAGCTATTTATATTAGGTACAGCTATTAAAACAAGGTAGGAATGAGGCT
AGACCTTTAACTTCCCTAAGGCATACTTTTCTAGCTACCTTCTGCCCTGTGTCTGGCAC
CTACATCCTTGATGATTGTTCTCTTACCCATTCTGGAATTTTTTTTTTTTTAAATAAAT
ACAGAAAGCATCTTGAAAAAAAAAAAAAAAAA

Amino Acid:

MISASRAAAARLVGAAASRGPTAARHQDSWNGLSHEAFRLVSRRDYASEAIKGAVVGID
LGTTNSCVAVMEGKRAKVLENAEGARTTPSVVAFTADGERLVGMPAKRQAVTNPNNTF
YATKRLIGRRYDDPEVQKDIKNVPFKIVRASNGDAWVEAHGKLYSPSQIGAFVLMKMKE
TAENYLGRTAKNAVITVPAYFNDSQRQATKDAGQ
ISGLNVLRVINEPTAAALAYGLDKSEDKVIAVYDLGGGTFDISILEIQKGVFEVKSTNGDTF
LGGEDFDQALLRHIVKEFKRETGVDLTKDNMALQRVREAAEKAKCELSSSVQTDINLPYL
TMDSSGPKHLNMKLTRAQFEGIVTDLIRRTIAPCQKAMQDAEVSKSDIGEVILVGGMTRM

PKVQQTVQDLFGRAPSKAVNPDEAVAIGAAIQGGVLAGDVTDVLLLDVTPLSLGIETLGG
VFTKLINRNTTIPTKKSQVFSTAADGQTQVEIKVCQGEREMAGDNKLLGQFTLIGIPPAPR
GVPQIEVTFDIDANGIVHVSAKDKGTGREQQIVIQSSGGLSKDDIENMVKNAEKYAEEDR
RKKERVEAVNMAEGIIHDTETKMEEFKDQLPADECNKLKEEISKMRELLARKDSETGENI
RQAASSLQQASLKLFEMAYKKMASEREGSGSSGTGEQKEDQKEEKQ

*T.brucei*:

TbHep1 (Tb927.3.2300)

CDS:

ATGCTCCACACAGTGAGCGAGTTGGCGATGCGCAGGTGTTTGTGCCTGCGTGGCTTTC
GTCCTCAGGTGGCGGTAAGCGCCCTTGGCATTGATTTACGGAGTTGTGGCGTGCGCTT
TTGCGCATCGAAGCCTCCTGGGATTCATTTGACTCAGCGTACGTCCGAGGGCCCGGTC
AGCGATGACCCCAGGCGGGGTGCTGTGAGGAACAATATCGAGGAGTTGGTAAAGAAT
CTCTCAGAGGAGGACCAAAGATTAATTCTCAGCGCTCTGCAGGATCCAGAGGCGCAA
CCCAGTTCGAAGATGGGTGGCCCTGGAATAGGCACAAAAACAGGTGACATGGTTGCG
GCGTTCACGTGTGGGCAGTGTGAACATCGTATGGTCAAGAGGTTTAGCAAACATGCTT
ACACAAAAGGTATTGTAATTGTTCAGTGTCCCTCTTGTGAAGTGCGACATCTACTCGC
CGACAACCTTGGCTGGTTTGTGGATGGGGCCAAGAACGTTGAAGAAATGCTCCGCGA
AAAAGGCGATTCTTTTATTCGTGTGGGTAATGATTATCAAGTTGAACCGACTAGTGTT
GGGACTGAGCGCGACGGTAATAATAACTGA

Amino acid sequence:

MLHTVSELAMRRCLCLRGFRPQVAVSALGIDLRSCGVRFCASKPPGIHLTQRTSEGPVSDD
PRRGAVRNNIEELVKNLSEEDQRLILSALQDPEAQPSSKMGGPGIGTKTGDMVAAFTCGQ
CEHRMVKRFSKHAYTKGIVIVQCPSCEVRHLLADNLGWFVDGAKNVEEMLREKGDSFIR
VGNDYQVEPTSVGTERDGNNN

TbmtHsp70 (Tb927.6.3740)

CDS:

ATGTTGGCCCGTCGTGTATGCGCACCCATGTGCCTGGCGTCTGCCCCGTTTGCGCGGT
GGCAGTCATCGAAGGTAACTGGTGACGTGATTGGTATTGATTTGGGTACGACATACAG
TTGTGTTGCAGTAATGGAAGGTGACCGGCCACGCGTACTTGAGAATACAGAGGGTTTC
AGGACGACACCGTCTGTGGTTGCGTTCAAAGGACAGGAAAAACTTGTTGGCCTTGCA
GCGAAACGTCAGGCGATTACGAACCCACAGTCGACATTCTTCGCGGTGAAACGGCTG
ATTGGTCGTCGCTTCGATGATGAGCACATCCAACACGACATCAAGAATGTGCCCTACA
AGATTATTCGGAGCAATAATGGTGATGCGTGGGTGCAAGATGGGAATGGGAAGCAAT
ACTCACCTTCACAAGTTGGTGCATTCGTACTTGAGAAGATGAAGGAAACGGCAGAAA
ACTTCCTGGGACGCAAAGTATCTAACGCTGTGGTGACGTGCCCCGCGTACTTCAATGA
CGCGCAACGTCAGGCAACGAAGGATGCCGGTACGATTGCTGGACTGAATGTGATCCG
TGTTGTGAATGAACCGACTGCTGCTGCACTGGCATATGGCTTGGACAAAACGAAGGA
CAGCTTAATTGCCGTGTATGATCTTGGTGGTGGAACATTTGATATCTCCGTACTTGAA

ATTGCCGGAGGTGTTTTTGAGGTAAAGGCAACGAATGGCGACACTCACCTTGGTGGA
GAAGACTTTGATCTCTGCCTCTCTGATCACATTCTGGAGGAATTCCGCAAGACATCTG
GAATTGACTTGAGCAAGGAGCGGATGGCACTGCAGCGTATTCGTGAGGCTGCAGAAA
AGGCGAAGTGTGAACTTTCGACGACGATGGAGACGGAGGTAAACCTTCCGTTTATCA
CAGCTAACCAGGACGGAGCGCAGCACGTGCAGATGATGGTGAGCCGCAGCAAGTTTG
AGTCCCTTGCTGATAAGCTCGTACAACGTTCACTTGGACCGTGCAAGCAATGCATCAA
GGACGCTGCTGTTGACCTGAAGGAAATCTCTGAGGTTGTGCTTGTTGGTGGTATGACG
CGTATGCCAAAGGTTGTGGAGGCTGTGAAGCAGTTCTTCGGTCGCGAACCGTTCCGTG
GTGTGAACCCTGACGAGGCCGTTGCACTGGGTGCTGCAACACTTGGTGGTGTTCTCCG
TGGTGATGTGAAGGGTCTTGTATTGCTTGACGTTACACCACTATCACTTGGAATCGAA
ACACTTGGTGGTGTCTTCACACGTATGATTCCCAAGAACACAACAATCCCGACGAAGA
AGAGTCAAACCTTCTCAACTGCTGCGGACAACCAAACACAGGTCGGAATCAAAGTGT
TCCAAGGGGAACGAGAAATGGCATCTGACAACCAAATGATGGGTCAGTTTGACCTCG
TTGGAATTCCTCCTGCACCACGCGGTGTACCACAAATTGAGGTGACATTTGACATTGA
TGCTAATGGTATTTGTCACGTAACTGCGAAGGACAAGGCAACTGGGAAAACACAGAA
CATCACCATTACTGCTCATGGTGGGTTGACGAAGGAGCAGATCGAGAACATGATCCG
CGACTCTGAGATGCACGCTGAAGCTGACCGTGTGAAGCGGGAGCTTGTGGAAGTGCG
TAACAATGCTGAGACTCAGGCTAACACTGCTGAGCGACAACTGACGGAATGGAAGTA
CGTGACGGACGCTGAGAAGGAGAATGTGCGTACCCTTTTGGCTGAACTTCGCAAGGT
GATGGAGAATCCAAACGTGACGAAGGATGAACTGTCGGCTTCTACTGACAAACTGCA
AAAGGCAGTGATGGAATGTGGTCGCACGGAGTACCAACAGGCGGCAGCAGCGAACA
GCGGTAGCTCTGGTAGCAGCAGCACAGAAGGTCAGGGTGAGCAACAACAGCAGCAG
GCATCTGGTGAAAAGAAGGAGTAA

Amino acid sequence:

MLARRVCAPMCLASAPFARWQSSKVTGDVIGIDLGTTYSCVAVMEGDRPRVLENTEGFR
TTPSVVAFKGQEKLVGLAAKRQAITNPQSTFFAVKRLIGRRFDDEHIQHDIKNVPYKIIRSN
NGDAWVQDGNGKQYSPSQVGAFVLEKMKETAENFLGRKVSNAVVTCPAYFNDAQRQA
TKDAGTIAGLNVIRVVNEPTAAALAYGLDKTKDSLIAVYDLGGGTFDISVLEIAGGVFEVK
ATNGDTHLGGEDFDLCLSDHILEEFRKTSGIDLSKERMALQRIREAAEKAKCELSTTMETE
VNLPFITANQDGAQHVQMMVSRSKFESLADKLVQRSLGPCKQCIKDAAVDLKEISEVVLV
GGMTRMPKVVEAVKQFFGREPFRGVNPDEAVALGAATLGGVLRGDVKGLVLLDVTPLS
LGIETLGGVFTRMIPKNTTIPTKKSQTFSTAADNQTQVGIKVFQGEREMASDNQMMGQFD
LVGIPPAPRGVPQIEVTFDIDANGICHVTAKDKATGKTQNITITAHGGLTKEQIENMIRDSE
MHAEADRVKRELVEVRNNAETQANTAERQLTEWKYVTDAEKENVRTLLAELRKVMEN
PNVTKDELSASTDKLQKAVMECGRTEYQQAAAANSGSSGSSSTEGQGEQQQQQASGEKK
E

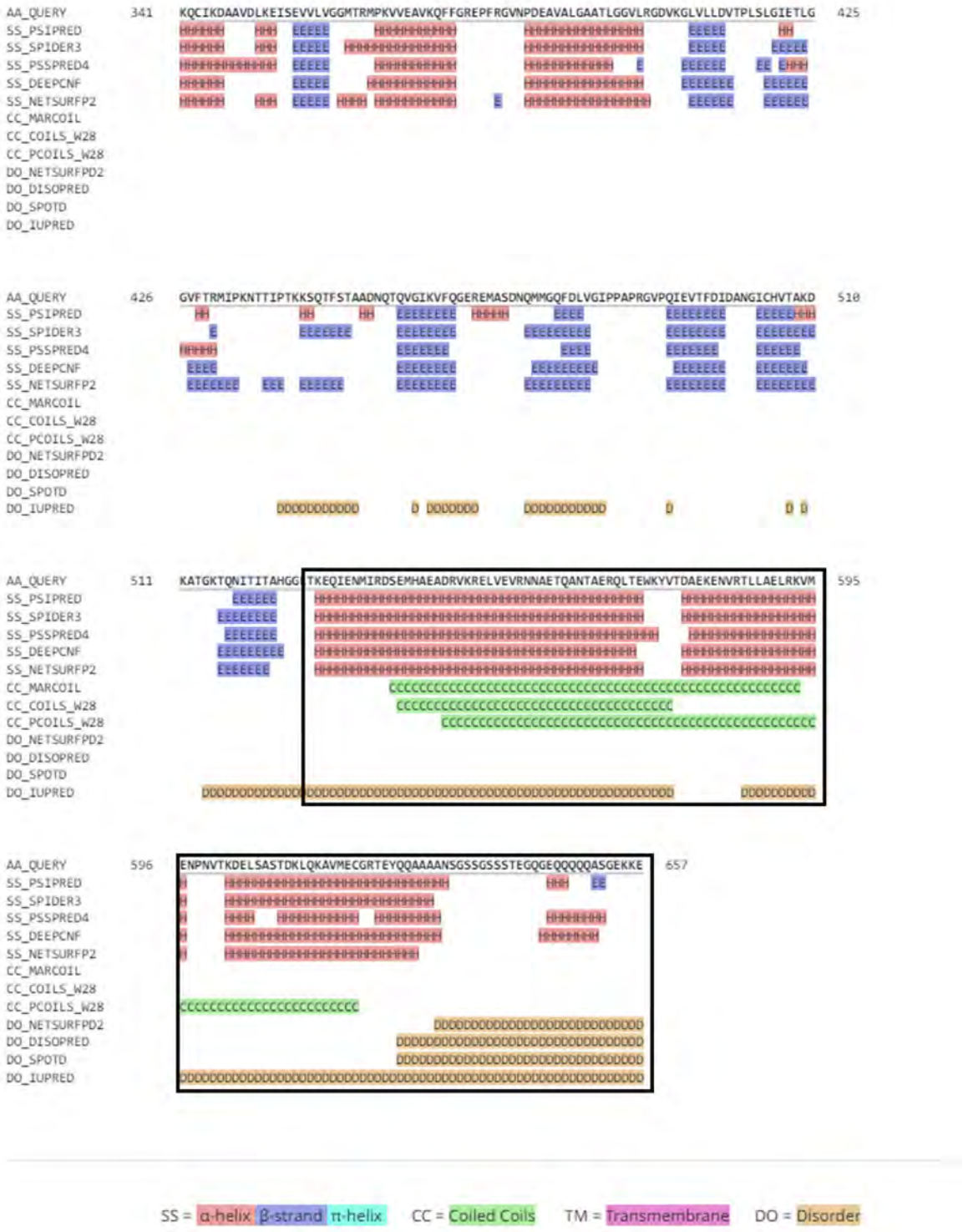


A 1: The secondary structure prediction of the SBD of TbmtHsp70 using Quick2D: Secondary structures are indicated by the key provided with a box used to display the α-helix rich SBDα subdomain.

| | |
|---|---|
| Protein | Chaperone protein DnaK |
| Gene | dnaK |
| Source organism | Escherichia coli (strain K12) go to search |
| UniProt | P0A6Y8 go to UniProt |
| Experimental structures | 61 structures in PDB for P0A6Y8 go to PDBe-KB |
| Biological function | Plays an essential role in the initiation of phage lambda DNA replication, where it acts in an ATP-dependent fashion with the DnaJ protein to release lambda O and P proteins from the preprimosomal complex. DnaK is also involved in chromosomal DNA replication, possibly through an analogous interaction with the DnaA protein. Also participates actively in the response to hyperosmotic shock. go to UniProt |

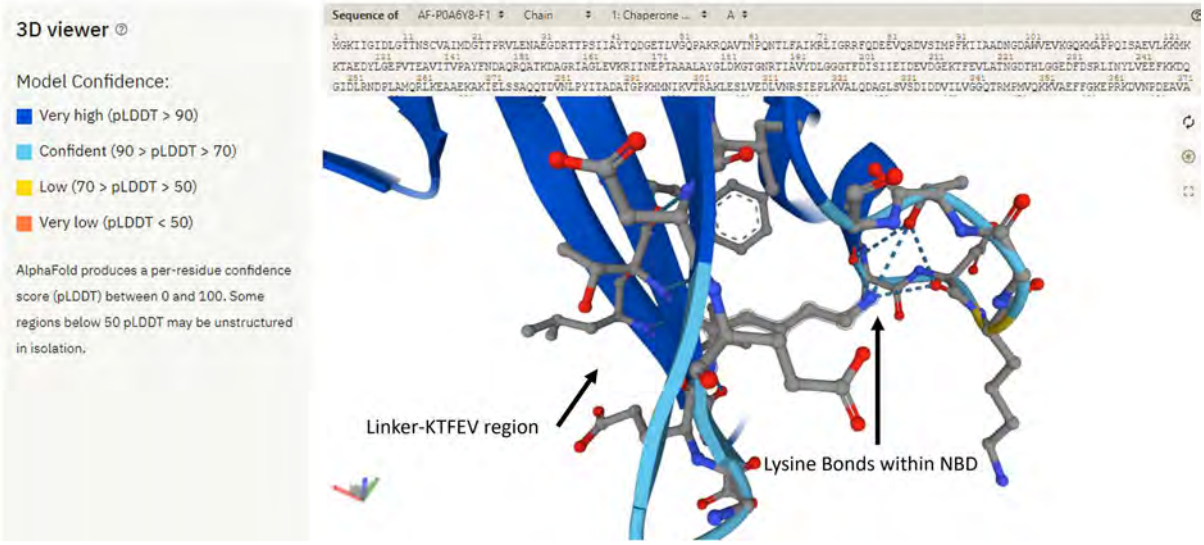


A 2: Lysine bonds to NBD within DnaK: The Alphafold model of DnaK displaying the linker and KTFEV motif region. The network of bonds of interest between the lysine side chain of the KTFEV motif and a region buried within the NBD is indicated by an arrow.

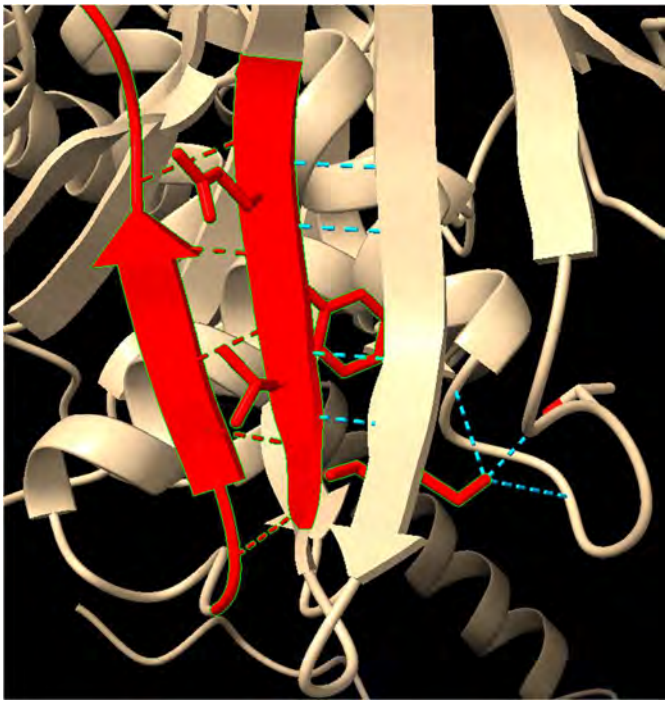

A 3 : Bonds between linker region and KTFEV motif within DnaK with Lysine bonds to NDB present: Pymol imaged model with the linker and KTFEV motif indicated in red with the bonds between the two displayed as dashed red lines. Bonds between the lysine side chain and the NBD region are shown in blue.

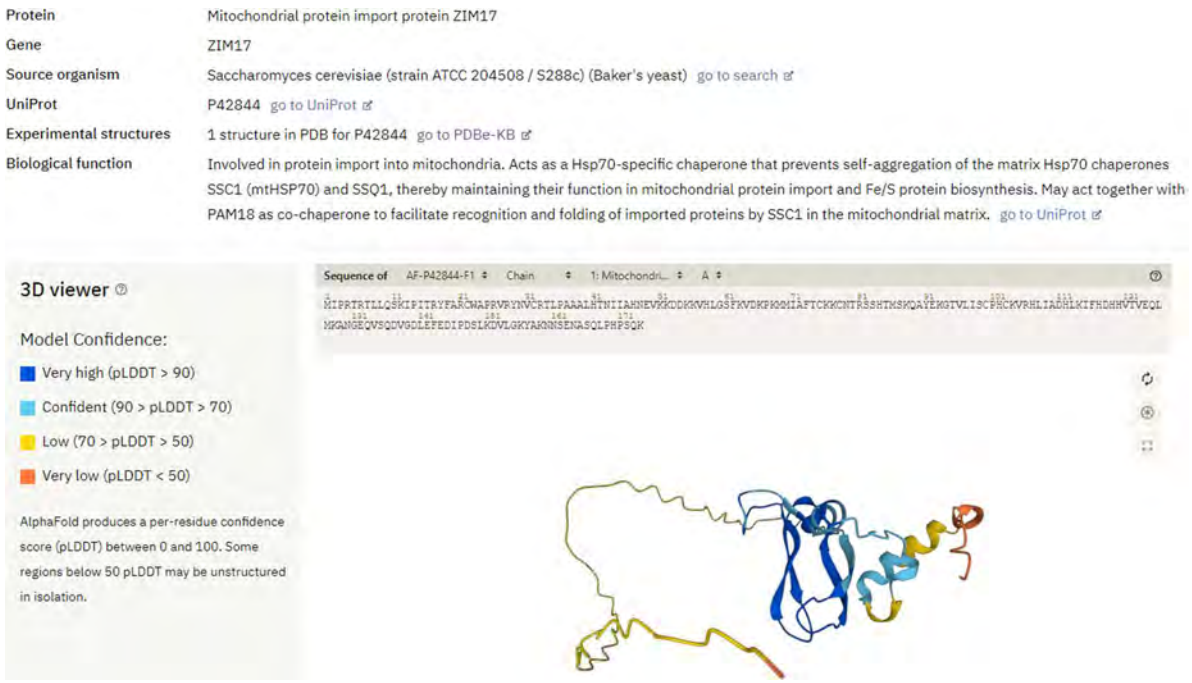


A 4 : Alphafold model of Tim15 (Zim17): Alphafold model of Tim15 created to illustrate the position of zf-DNL α-helical structure displayed above the tetra-cysteine binding pocket described as perpendicular to the tetracysteine area in previous models.

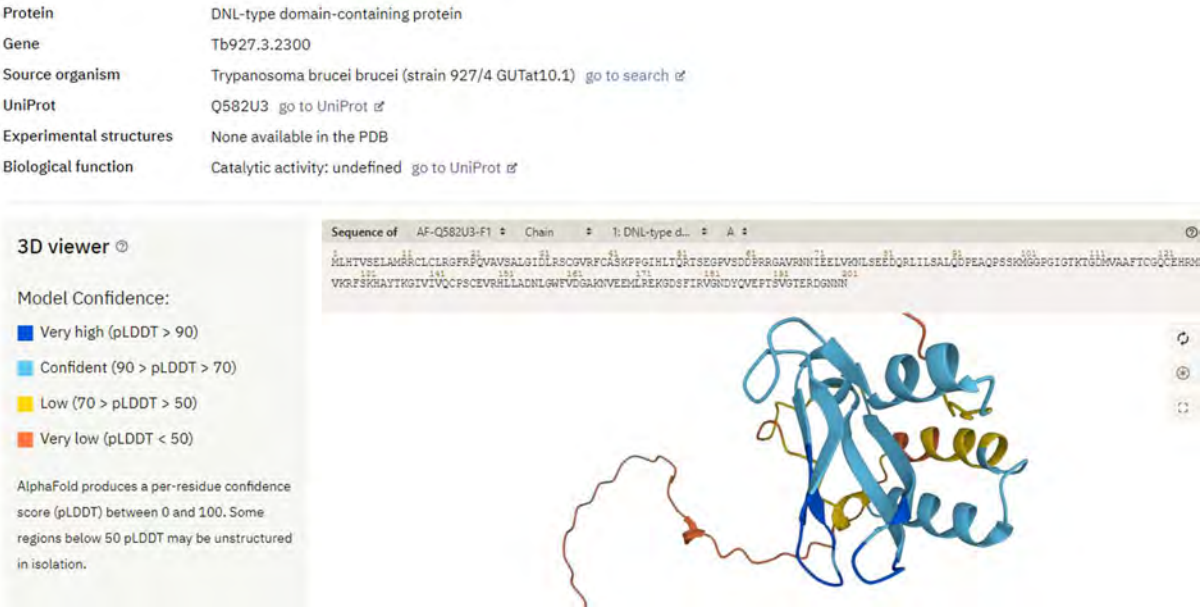


A 5: Alphafold model of TbHep1 indicating confidence ratings of α-helical structures: The confidence ratings are displayed in the key to the right of the figure with one of the α-helical structures represented as confident ( 70 – 90 %) while the second structure is indicated in yellow (50 – 70 %)

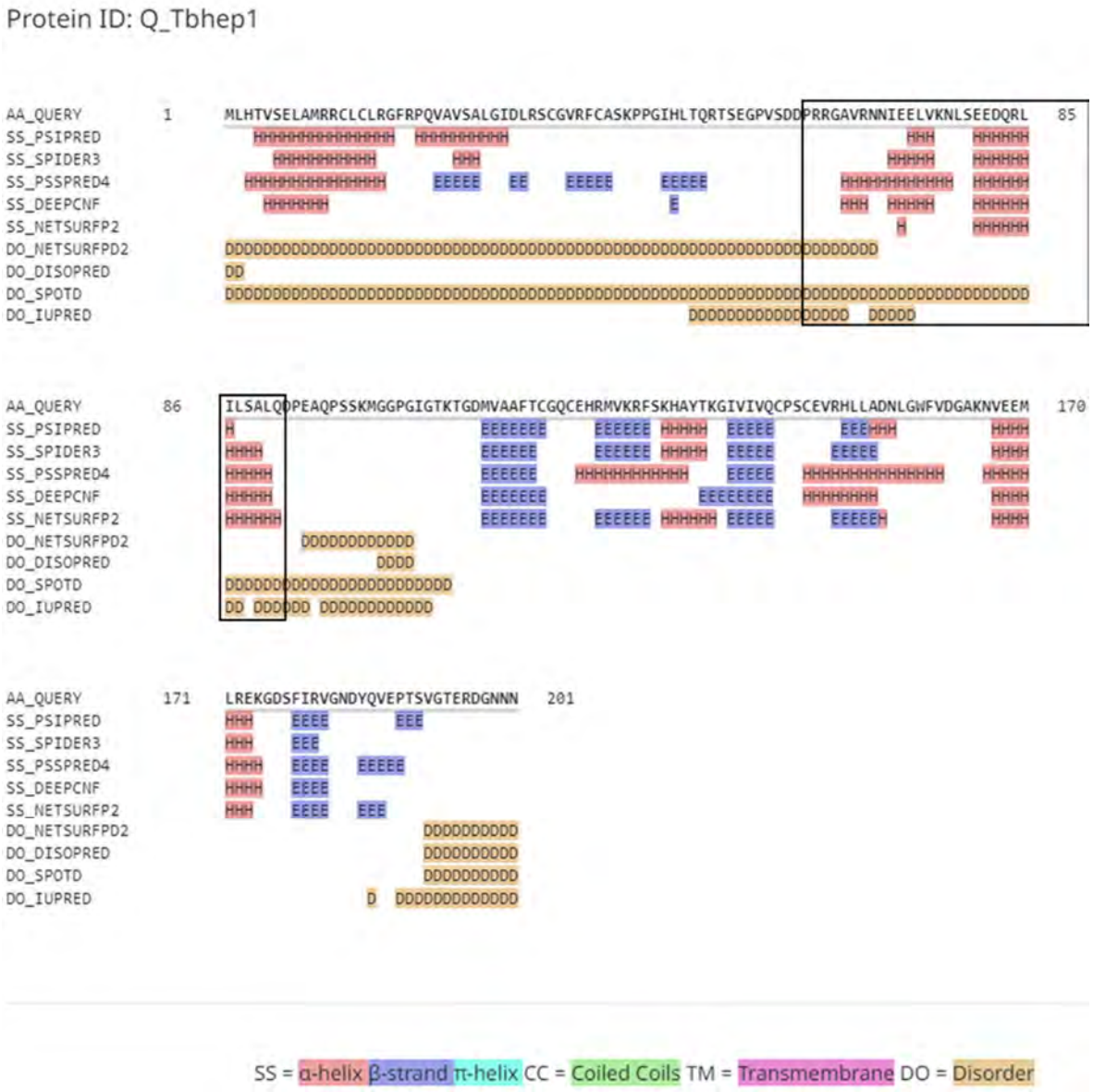


A 6: Secondary structure prediction of TbHep1 using Quick2D: Secondary structures are indicated by the key provided with a box used to display the region of interest where Alphafold suggests α-helical structures may be present

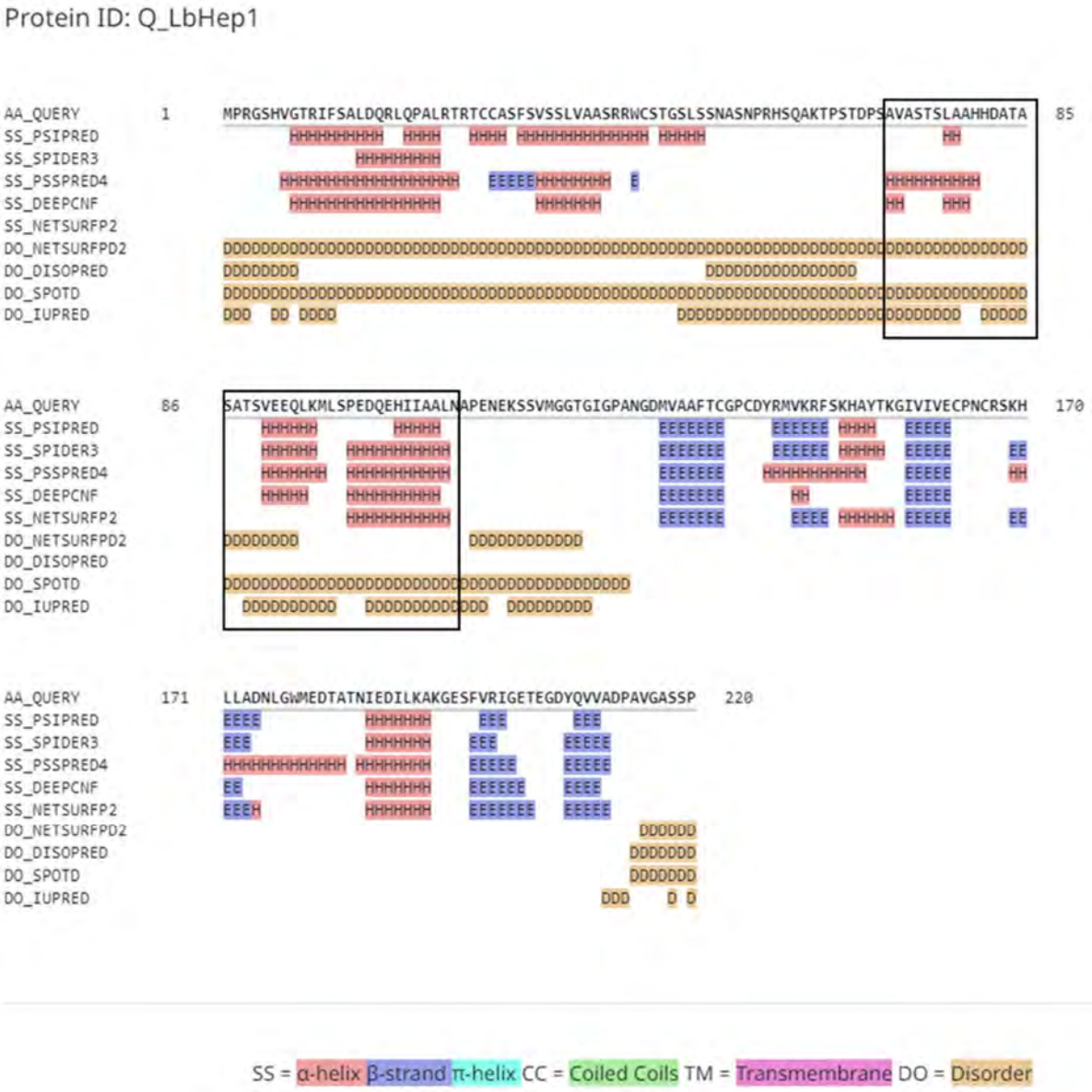


A 7 : Secondary structure prediction of LbHep1 using Quick2D prediction tools: Secondary structures are indicated by the key provided with a box used to display the region of interest where *T. brucei* may have α-helical structures.

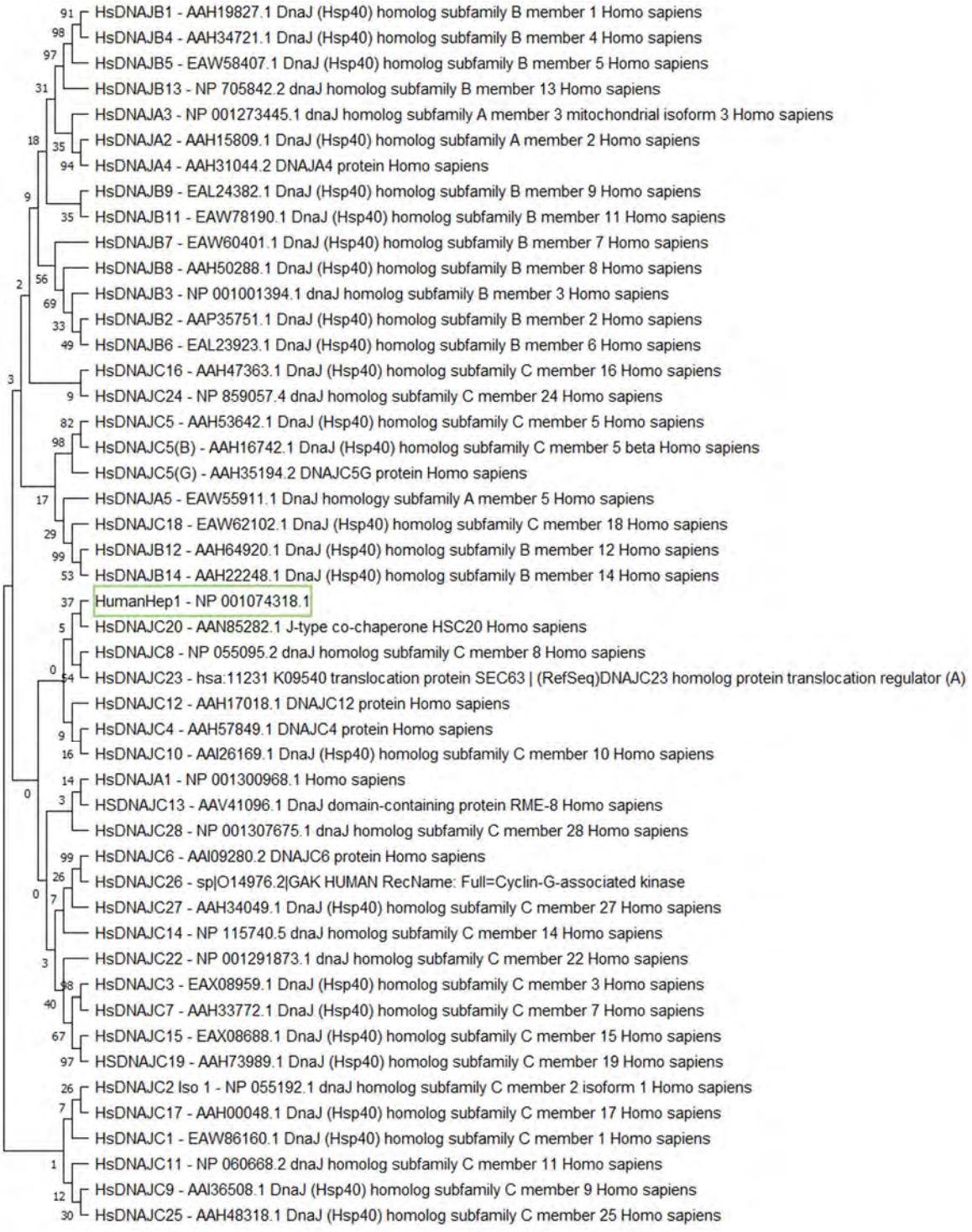


A 8: HsHep1 phylogenetic analysis with *H. sapien* JDPs: The phylogenetic analysis of HsHep1 with *H. sapien* JDPs obtained from NCBI with HsHep1 indicated by a green box. Phylogenetic trees are the result of consensus amongst 1000 bootstrap iterations using a maximum likelihood statistical method following a poission distribution carried out on MEGA11.

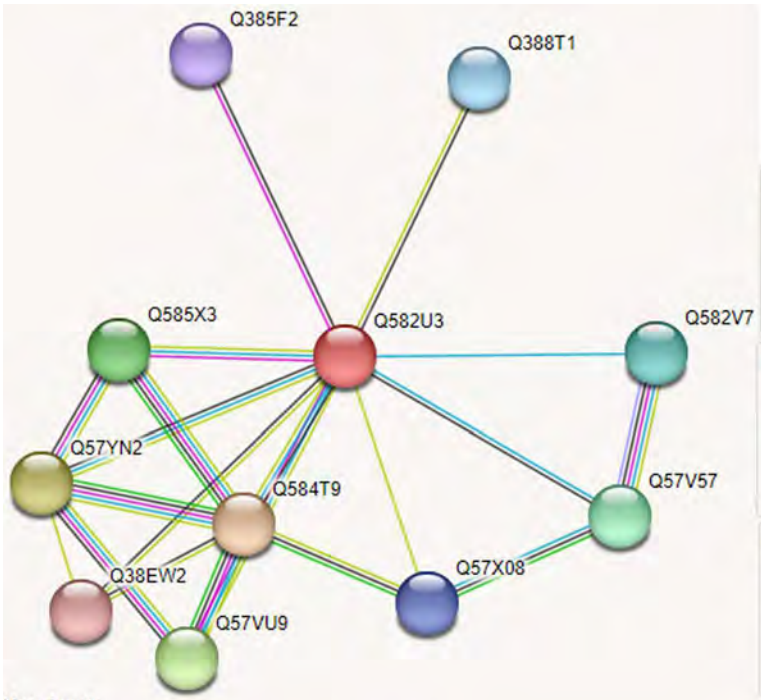


**Your Input:**

| | | Neighborhood | Gene Fusion | Cooccurence | Coexpression | Experiments | Databases | Textmining | [Homology] | Score |
|---|---|---|---|---|---|---|---|---|---|---|
| Q582U3 | DNL-type domain-containing protein (201 aa) | | | | | | | | | |

**Predicted Functional Partners:**

| | | | | | | | | | | |
|---|---|---|---|---|---|---|---|---|---|---|
| Q584T9 | GrpE protein homolog; Essential component of the PAM complex, a complex required for the translocation of transit peptide-c... | | | | • | | • | • | | 0.901 |
| Q57YN2 | Uncharacterized protein | | | | • | | • | • | | 0.850 |
| Q57VU9 | Heat shock 70 kDa protein, putative | | | | | • | • | • | | 0.806 |
| Q585X3 | Heat shock 70 kDa protein, mitochondrial, putative; Belongs to the heat shock protein 70 family. | | | | | • | • | • | | 0.806 |
| Q57V57 | Protein kinase, putative | | | | • | | • | | | 0.661 |
| Q582V7 | Serine/threonine-protein kinase, putative; Belongs to the protein kinase superfamily. | | | | | | • | | | 0.641 |
| Q388T1 | GPI mannosyltransferase 2; Mannosyltransferase involved in glycosylphosphatidylinositol- anchor biosynthesis. | | | | • | | | • | | 0.579 |
| Q57X08 | Proteasome 26S non-ATPase subunit 9, putative | | | | | | | • | | 0.524 |
| Q385F2 | Protein transport protein Sec31, putative | | | | • | • | | | | 0.520 |
| Q38EW2 | Sulfhydryl oxidase | | | | • | | | • | | 0.520 |

A 9: String data indicating the putative interactions of TbHep1 (Q582U3): The evidence for each interaction in indicated by the legend to the right of the String mind map and the proteins represented by each node are listed below, alongside the provided uniprot number. The protein PAM18 is denoted by the Uniprot code Q5YN2 although the protein is described as uncharacterized. All information for the figure was provided by STRING (Szklarczyk et al., 2021).

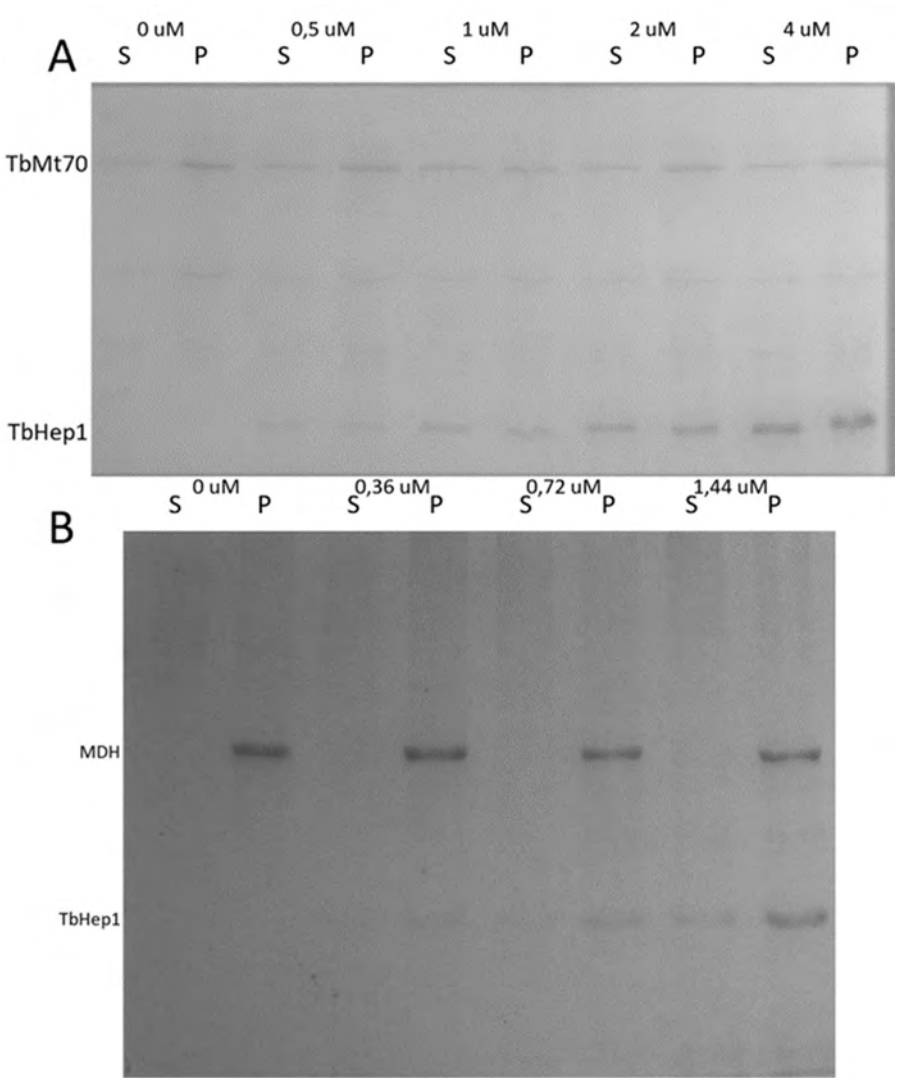


A 10: A comparison of the degree of TbHep1 aggregation in the presence and absence of the TbmtHsp70 client protein: SDS-PAGE displaying the aggregation of TbHep1 in the presence of (A) TbmtHsp70 and (B) MDH with S representing the soluble supernatant fraction and P representing the insoluble pellet fraction and the respective proteins labelled and the concentration of TbHep1 indicated in uM above the appropriate pair of lanes.

| | |
|---|---|
| Protein | Heat shock 70 kDa protein, mitochondrial, putative |
| Gene | Tb927.6.3740 |
| Source organism | Trypanosoma brucei brucei (strain 927/4 GUTat10.1) go to search |
| UniProt | Q585X3 go to UniProt |
| Experimental structures | None available in the PDB |
| Biological function | Not available. go to UniProt |

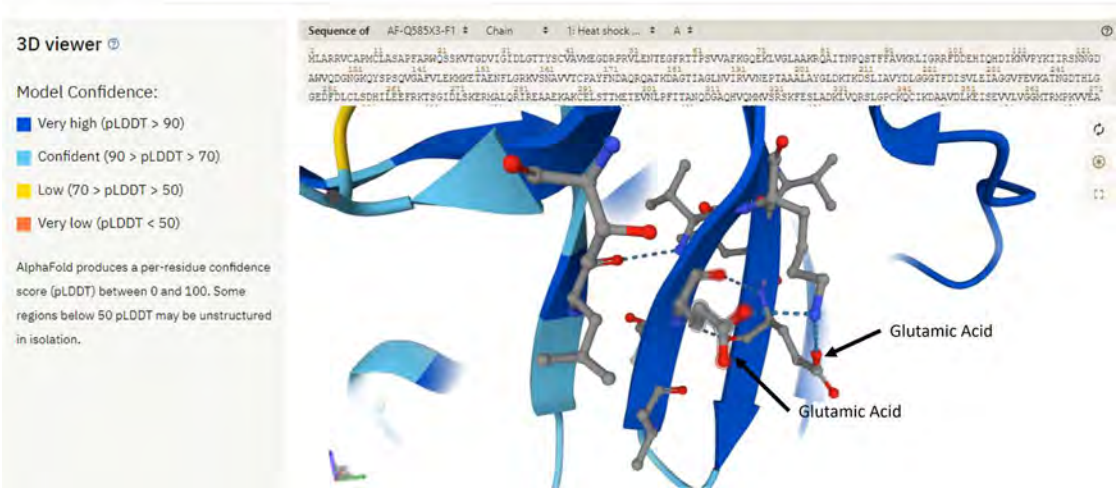


A 11: Bonds between LEI residues and the GVFEV motif within TbmtHsp70: Alphafold model displaying the GVFEV motif and LEI region of TbmtHsp70. The glutamic acid residues interacting between the linker region and the LEI motif of interest are indicated by arrows with the network of bonds displayed in light blue.

| | |
|---|---|
| Protein | Stress-70 protein, mitochondrial |
| Gene | HSPA9 |
| Source organism | Homo sapiens (Human) go to search |
| UniProt | P38646 go to UniProt |
| Experimental structures | 5 structures in PDB for P38646 go to PDBe-KB |
| Biological function | Chaperone protein which plays an important role in mitochondrial iron-sulfur cluster (ISC) biogenesis. Interacts with and stabilizes ISC cluster assembly proteins FXN, NFU1, NFS1 and ISCU (PubMed:26702583). Regulates erythropoiesis via stabilization of ISC assembly (PubMed:21123823, PubMed:26702583). May play a role in the control of cell proliferation and cellular aging (By similarity). go to UniProt |

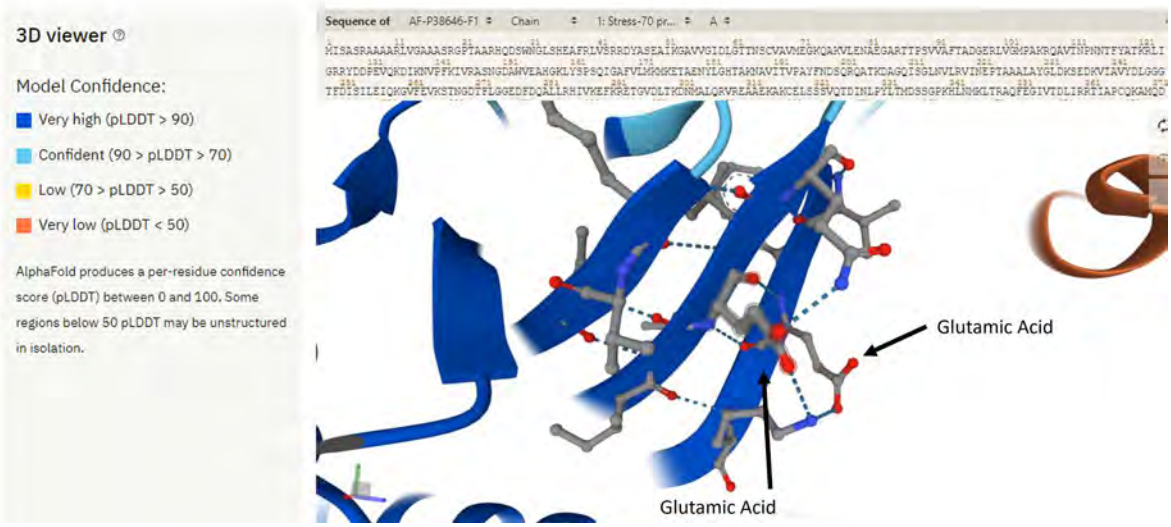


A 12: Bonds between LEI residues and GVFEV motif within Mortalin: Alphafold model displaying the GVFEV motif and LEI region of mortalin. The glutamic acid residues interacting between the linker region and the LEI motif of interest are indicated by arrows with the network of bonds displayed in light blue.

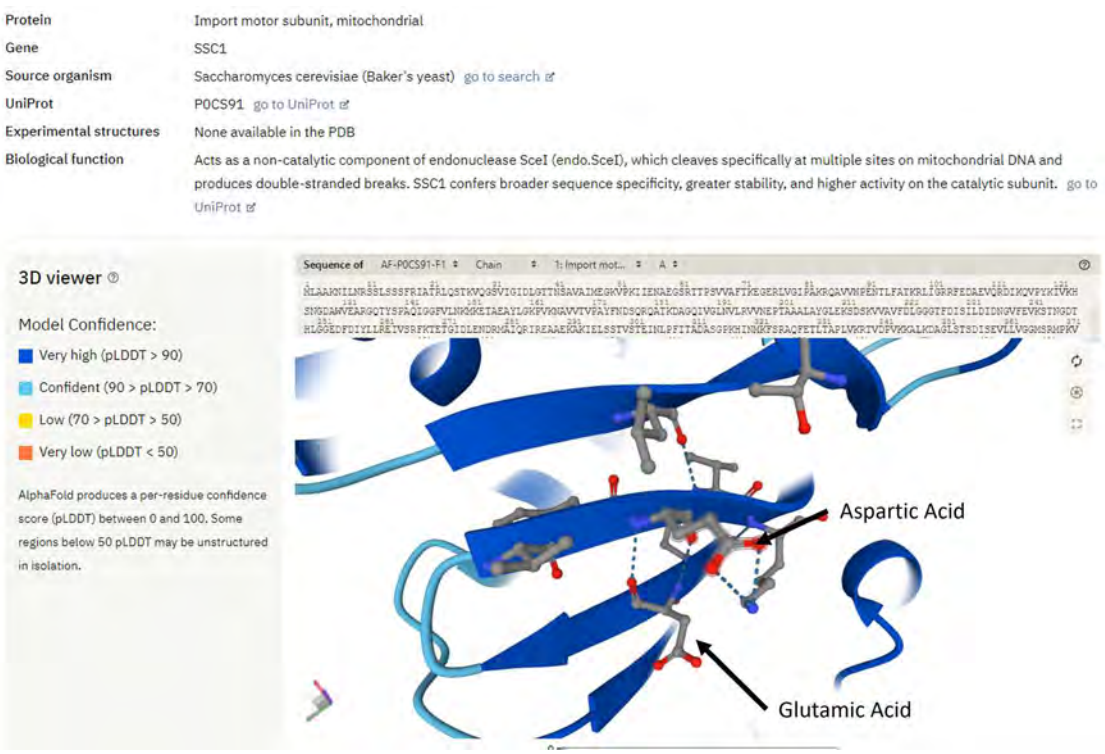


A 13: Bonds between LDI residues and GVFEV motif within Ssc1: Alphafold model displaying the GVFEV motif and LDI region of Ssc1. The glutamic and aspartic acid residues interacting between the linker region and the LDI motif of interest are indicated by arrows with the bond between the two displayed in light blue.